

INVESTIGATION OF PET-DEGRADING ENZYMES AND THEIR IMPLICATIONS ON MICROPLASTICS

DISSERTATION

zur Erlangung des akademischen Grades eines
Doktors der Naturwissenschaften (Dr. rer. nat.)
an der Fakultät für Biologie, Chemie und Geowissenschaften
der Universität Bayreuth

vorgelegt von

Sebastian Valentin Alfons Weigert

aus Burglengenfeld

Bayreuth, 2022

Die vorliegende Arbeit wurde in der Zeit von Januar 2018 bis Januar 2022 in Bayreuth am Lehrstuhl für Biochemie unter Betreuung von Frau Professorin Dr. Birte Höcker angefertigt.

Vollständiger Abdruck der von der Fakultät für Biologie, Chemie und Geowissenschaften der Universität Bayreuth genehmigten Dissertation zur Erlangung des akademischen Grades eines Doktors der Naturwissenschaften (Dr. rer. nat.).

Dissertation eingereicht am: 19.01.2022

Zulassung durch die Promotionskommission: 26.01.2022

Wissenschaftliches Kolloquium: 22.07.2022

Amtierender Dekan: Prof. Dr. Benedikt Westermann

Prüfungsausschuss:

Prof. Dr. Birte Höcker

Prof. Dr. Matthias Ullmann

Prof. Dr. Peter Strohrig

PD Dr. Alfons Weig

Table of Contents

	<u>Page</u>
List of abbreviations.....	II
Figures.....	IV
1 Zusammenfassung	1
2 Summary	3
3 Introduction.....	5
3.1 Nature of polymers.....	5
3.2 History of plastics and rise of plastic pollution	6
3.3 The fate of plastic waste	8
3.4 Plastic degradation, fragmentation, and microplastics.....	9
3.5 Impact of microplastics.....	13
3.6 Discovery of plastic and PET degrading enzymes.....	15
3.7 Cutinases – A class of promiscuous enzymes	17
3.8 PET degrading enzymes.....	19
3.9 Contribution of enzymes for a sustainable plastic economy	26
4 Synopsis.....	29
5 List of Publications and Personal Contribution.....	38
6 Appending Publications	40
7 Acknowledgments	100
8 References	102

List of abbreviations

BHET	Bis-(2-hydroxyethyl) terephthalate	Mt	Million tons
boPET	Biaxially-orientated PET	MTP	Microtiter plates
CBM	Carbohydrate binding module	PAH	Polycyclic aromatic hydrocarbon
DDT	Dichlorodiphenyltrichloroethane	PBAT	Polybutylene adipate terephthalate
DNA	Desoxyribonucleic acid	PBDE	Polybrominated diphenyl ether
DS	Disulfide bond	PBS	Polybutylene succinate
DSC	Differential scanning calorimetry	PCB	Polychlorinated biphenyl
EDC	Endocrine-disrupting chemical	PCL	Polycaprolactone
FCP	Fatigue crack propagation	PCR	Polymerase chain reaction
FsC	<i>Fusarium solani</i> cutinase	PE	Polyethylene
GFP	Green fluorescent protein	PEF	Polyethylene furanoate
GMO	Genetically modified organism	PET	Polyethylene terephthalate
HEMT	1-(2-hydroxyethyl) 4-methyl terephthalate	PLA	Polylactic acid
HOTP	2-hydroxyterephthalate	POP	Persistent organic pollutant
IsPETase	PETase from <i>Ideonella sakaiensis</i>	PP	Polypropylene
kDa	Kilodalton	PS	Polystyrene
LCC	Leaf-compost cutinase	PU	Polyurethane
LD-PE	Low density polyethylene	PVC	Polyvinylchloride
MD	Molecular dynamics	RNA	Ribonucleic acid
MHET	Mono-2-hydroxyethyl terephthalate	SEM	Scanning electron microscopy
		TfCut2	<i>Thermobifida fusca</i> cutinase 2
		TfH	<i>Thermobifida fusca</i> hydrolase

T _g	Glass transition temperature	T _m	Melting temperature
Thc_Cut1	<i>Thermobifida cellulosilytica</i> cutinase 1	TPA	Terephthalic acid
Thc_Cut2	<i>Thermobifida cellulosilytica</i> cutinase 2	UHPLC	Ultra high performance liquid chromatography
		UV	Ultra-violet

Figures

	<u>Page</u>
Figure 1 Structures of common polymers.....	5
Figure 2 Example for mismanaged waste in coastal areas.	8
Figure 3 Simplified schema for common abiotic degradation processes in PET...	10
Figure 4 Typical schema for plastic entering the environment.....	11
Figure 5 Schematic representation of a spherulite	16
Figure 6 Crystal structure of Leaf-branch cutinase (LCC).	18
Figure 7 Structural comparison of polyethylene terephthalate (PET) and Cutin....	19
Figure 8 PET hydrolysis schema for IsPETase.	22
Figure 9 Superimposed crystal structures of known PET degrading cutinases.....	23
Figure 10 Crystal structures of IsPETase.....	24
Figure 11 Overview over the modules of the assay platform.....	30
Figure 12 Solved crystal structure of PET6 in cartoon representation.	32
Figure 13 Visual and mechanical impact of enzymatic PET degradation.....	36

1 Zusammenfassung

Kunststoffe, umgangssprachlich auch Plastik genannt, sind einige der bedeutendsten Materialien unserer modernen Welt. Faktoren, die diesen Siegeszug begünstigten, waren überzeugende Materialeigenschaften wie hohe mechanische Stärke, Widerstandsfähigkeit gegenüber einer Vielzahl von Einflüssen, geringes Gewicht sowie letztlich auch eine kostengünstige Produktion. Ein mangelhaftes Abfallmanagement kombiniert mit einer Jahresproduktion von über 300 Millionen Tonnen bedingt jedoch zwangsläufig in einem massiven Abfluss von Plastikmüll in die Umwelt. Aufgrund der hohen Stabilität kann das Material dort für Jahrzehnte oder sogar Jahrhunderte überdauern. Trotzdem unterliegt das Material dort biotischen und abiotischen Umwelteinflüssen, insbesondere Feuchtigkeit, UV-Strahlung und mechanischem Stress, welche einen stetigen Fragmentierungsprozess in Gang setzen, der letztlich zur Entstehung von Mikro- und Nanoplastik führt. Diese mikroskopischen Kunststoffpartikel trugen zu einer Neubewertung der Dringlichkeit von Plastikverschmutzung bei, da sie allgegenwärtig sind und Studien negative Effekte jener Partikel auf die Vitalität verschiedenster Lebewesen nachweisen konnten. Die Entdeckung von Enzymen, welche in der Lage sind, Kunststoffe abzubauen, eröffnete dabei sowohl neue Perspektiven für die Eliminierung von Plastikverschmutzung in der Umwelt als auch für die Entwicklung neuer Recyclingprozesse.

Polyethylenterephthalat (PET) ist ein Standardkunststoff, der eine Grundgerüst aus Heteroatomen besitzt, welches die enzymatische Hydrolyse begünstigt. Folglich konnten mittlerweile einige PET-abbauende Enzyme identifiziert werden. Die IsPETase nimmt dabei eine prominente Rolle ein, da es seinem Ursprungsorganismus *Ideonella sakaiensis* die Fähigkeit verleiht, PET als Energiequelle zu nutzen. Kürzlich wurde in einer Studie außerdem eine optimierte Variante der PET Hydrolase LCC präsentiert, welche herausragende Abbauraten für PET erreicht. Mit Hilfe dieses Enzyms konnten die Autoren außerdem einen vollständigen Recyclingprozess demonstrieren, was das Potential enzymatischer Anwendungen unterstreicht.

Im Rahmen dieser Dissertation werden drei Forschungsarbeiten präsentiert, welche sich alle im Bereich von PET-abbauenden Enzymen bewegen. In der ersten Studie entwickelten wir eine neue Screening Plattform, die auf dem neuartigen Aufbringen eines PET-Films als Substrat auf Standard-Laborartikeln basiert. In Kombination mit verbesserter Komptabilität hinsichtlich Lysat-basierter Anwendungen ergibt sich ein äußerst nützliches und für Hochdurchsatzanwendungen geeignetes

Werkzeug zur Charakterisierung neuer PET-abbauenden Enzyme. Auf Basis dieser Plattform wurde das Enzym PET6 von *Vibrio gazogenes* untersucht, welches eine bemerkenswerte Anpassung an seine salzhaltige Umgebung zeigt, wobei hohe Salzkonzentrationen das Enzym stabilisieren und den PET-Abbau verbessern. Trotz vergleichsweise geringer Aktivität ist PET6 dabei im Hinblick auf Plastikabbau in der Umwelt von Interesse, da *V. gazogenes* weltweit in salzhaltigen Ökosystemen verbreitet ist, die auch für ihre hohe Mikroplastikbelastung bekannt sind. In einer weiteren Studie konnten wir außerdem zeigen, dass der Einfluss von enzymatischem Abbau auf die Materialeigenschaften von PET einen größeren Einfluss hat als die Quantifizierung löslicher Abbauprodukte vermuten lässt. Eine besondere Rolle schreiben wir hierbei dem wasserunlöslichen BHET-Dimer zu, welches wir in den oberen Schichten des Materials nachweisen konnten. Wir vermuten, dass diese Substanz die innere Struktur von PET schwächt und dadurch die überproportionale Schwächung der mechanischen Eigenschaften von PET auslöst, welche wir nach enzymatischem Kontakt messen konnten. Daher könnte enzymatischer Abbau eine entscheidende Rolle bei der Fragmentierung von PET in der Umwelt spielen.

Die hier gezeigten Arbeiten, und darin entwickelten Methoden, leisten damit einen Beitrag zur weiteren Erforschung PET-abbauender Enzyme und ermöglichen ein besseres Verständnis der Auswirkungen von biotischen Faktoren auf Plastik in der Umwelt.

2 Summary

Plastic is one of the key materials in our modern world. Its inexpensiveness combined with forceful material properties, such as lightweight, high mechanical strength, and resistance to various factors, fired its demand over the last decades. However, insufficient waste management combined with production rates of over 300 million tons result in vast amounts of plastic waste escaping into the environment. Unlike other materials, plastic can persist in the environment for decades or centuries due to its durability. However, biotic and abiotic factors, such as UV radiation, humidity, and mechanical stress, act on the material during its way through various environments, gradually fragmenting it down to microplastic or even nanoplastic particles. These tiny particles raised awareness towards worldwide plastic pollution as they can be found ubiquitously and show severe adverse effects on various organisms. Consequently, plastic, especially micro- and nanoplastic, is seen as a global and urgent threat that requires an immediate answer. In this context, the discovery of enzymes that act on these recalcitrant materials opened a new perspective for the decomposition of plastic in the environment as well as for technical recycling applications.

Polyethylene terephthalate (PET) is a commodity plastic that features a heteroatom backbone that facilitates enzymatic attack. Hence, several enzymes could be identified and characterized to degrade PET efficiently. A prominent enzyme in this context is PETase which enables its host *Ideonella sakaiensis* to use PET as an energy source, demonstrating the materials' breakdown in natural environments. A recent study presented an engineered variant of the PET hydrolase LCC with enhanced PET degradation capability. Its successful application in a large-scale full recycling process further illustrates the potential of those enzymes.

As part of this thesis, three publications are presented in the scope of PET degrading enzymes. For efficient analysis and characterization, we developed a screening platform featuring a new substrate provisioning by applying PET films on lab consumables. In combination with improved capabilities for screening in lysate, the assay features a useful, high-throughput-compatible tool for the characterization of new PET degrading enzyme variants. With this experimental basis, the enzyme PET6 from *Vibrio gazogenes* was investigated, which revealed a remarkable adaptation towards its saline origin. PET6 is stabilized by elevated salt concentrations, which also promotes PET degradation. Despite comparably low degradation rates, PET6 is an interesting candidate for natural PET decomposition due to the ubiquitous prevalence of *V.*

gazogenes, especially in marine environments with typically high plastic concentrations. In another study, we could show that enzymatic activity of IsPETase has an even higher impact on material properties than tracking of soluble degradation suggests. We propose that the presence of the insoluble degradation product BHET dimer, which we found in near-surface layers, weakens the internal composition of the material. This could explain why PET experiences disproportional embrittlement upon enzymatic attack. Hence microbial and enzymatic processes could have a decisive influence on the fragmentation process of PET in natural environments.

The work shown here and the methods developed therein thus contribute to future research on PET-degrading enzymes and provide a better understanding of the effects of biotic factors on plastics in the environment.

3 Introduction

3.1 Nature of polymers

Polymers, a concept also prominently found in nature, describe macromolecules with monomers arranged in repetitive units joining to large molecules. Some of them comprise the most fundamental building blocks of life, including RNA and DNA as genetic information, proteins for manifold functions, polysaccharides for storage and structural purposes, such as starch, cutin, and lignin in plants. Depending on the sequence of these repetitive units, polymers can be characterized as homopolymers when comprised of only identical repetitive units. A prominent example of such a homopolymer is cellulose, where the repetitive unit comprises two $\beta(1\rightarrow4)$ linked D-glucose molecules (Figure 1). Proteins, on the contrary, are heteropolymers as the repetitive units are the single amino acids joined by a peptide bond, which may vary in sequence in a non-periodic fashion.

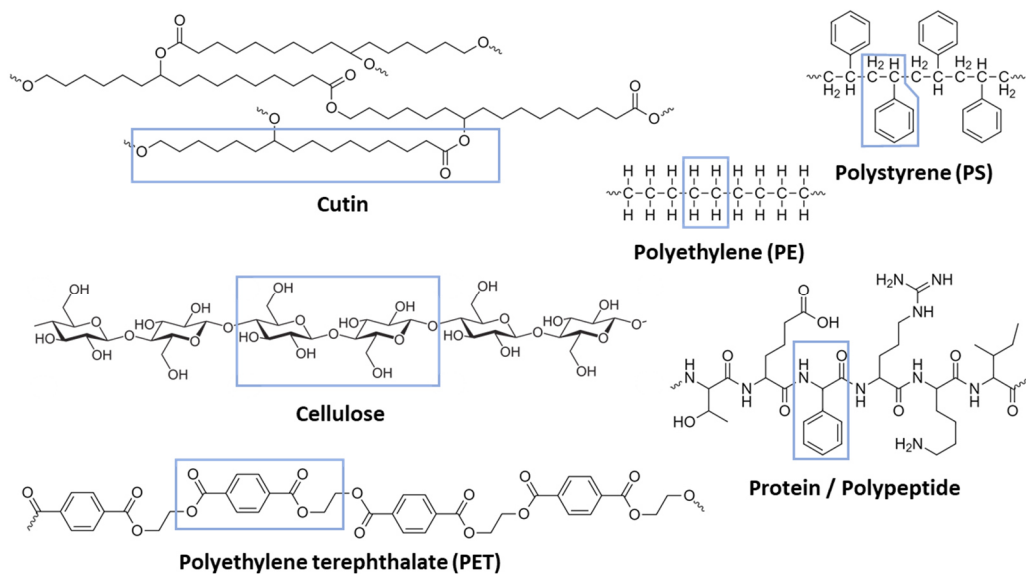


Figure 1 Structures of common polymers, the repetitive units are marked with blue boxes. Cutin is shown as a polyester comprised of 10,16-dihydroxy palmitic acid monomers, while the repetitive unit of cellulose is two glucose moieties connected by a glycosidic $\beta(1\rightarrow4)$ link constituting cellulose as a member of homopolymers. In contrast, proteins are typical heteropolymers, where amino acids, which join to the polypeptide, differ by their side chain; in this example, threonine, glutamic acid, phenylalanine, arginine, lysine, and isoleucine. In contrast to the aforementioned bio-based polymers, PS, PE, and PET are petrol-based commodity plastics.

Other than sequence motifs, there are more general categories for grouping polymers that are not necessarily restricted to natural biopolymers. Another commonly used category is based on the plasticity of the material, discriminating between thermoplastics, which can be reshaped after production (e.g., by heating), thermosetting polymers (thermosets), which on the contrary feature an unalterable and rigid structure, and elastomers with their inherent flexibility. The backbone and thus the bond type of

polymers can also be a distinguishing feature, like a C-C backbone in polyolefins with their prominent members polyethylene (PE) and polypropylene (PP), or heteroatom backbone as in polyurethanes, polyesters, and polyamides also describing the bond type of the polymer. Depending on the origin of the polymer, there is the category of biogenic polymers which are directly produced by organisms, the semi-synthetic polymers made from renewable biomass resources (e.g., cellulose acetate), and synthetic polymers, which are dominantly petroleum-based. This is, to some extent, also related to the category of biodegradability. The often-used term plastics summarizes man-made polymers, thus the categories of semi-synthetic and synthetic polymers.

An integral part of these plastics are additives which are employed in vastly varying concentrations¹. Many of these compounds have been developed to alter material properties according to specific needs², with plasticizer as the most common type. Furthermore, there are dyes, flame retardants, fillers, reinforcements, and stabilizers against physical or chemical influences, e.g., radiation, hydrolysis, and oxidation. Also, some additives are applied for better processing of the final product or as biocides for long-term resistance against biological activity². In many cases, only additives enable a successful application of plastics for a particular purpose or allow for easy adaptation. In this way, they fundamentally define the characteristics of a polymer, thereby making a decisive contribution to the versatility of plastics in general. As such, plastics come in countless shapes and have become an integral part of our modern world, ranging from everyday products to high-tech products. Simply put, our world is inconceivable without plastics. That pervasiveness can be explained by the benefits of plastic being versatile, lightweight, inert, resistant to various influences, and in general, having excellent mechanical properties. As these properties also favor adverse effects like persistence and accumulation in the environment, plastic consumption is now discussed critically, but the advantages of plastics are not neglectable³. Eventually, our continuously heavy reliance on these materials demands an answer for sustainable plastic handling in all regards.

3.2 History of plastics and rise of plastic pollution

Due to the abundance of biogenic polymers in nature, it seems logical that the first commercial plastic invented was a semi-synthetic polymer, thus a modified biopolymer. This first plastic nitrocellulose, also called Celluloid, was developed twice independently between 1850 and 1869⁴. Made from cellulose and nitric acid, it was

intended as a substitute for ivory, and its success likely saved elephants from eradication at that time. Interestingly, even this first commercially successful plastic already contained camphor as a plasticizer, emphasizing the relevance of these compounds for plastics already in these early stages. The first fully synthetic plastic was developed by Baekeland in the 1910s, creating a thermoset made from phenol and formaldehyde named Bakelite⁴. As it could be used for advanced molding application, it became a trend material typical for its time, impacting the general socio-economic development of society^{5,6}. In the same period, polyvinylchloride (PVC) was patented, which in contrast to Bakelite, still has a relevant share in today's plastic production⁷. A first preview of the starting success story of plastics was the hype about DuPont's nylon stockings. Their shortage due to the prioritization of war goods made from nylon as well as the popularity of the stockings themselves, culminated in the nylon riots in 1945-1946⁸. Despite this shortage, Second World War and the post-war period were a turning point for the plastic industry. With the general deprivation of traditional raw materials during the war, industry and research were turning focus towards novel plastics as a substitute or pursuing the idea to create new materials with novel property profiles^{4,8}. Driven by the warfare's financial resources, which fostered innovation and increased production capacities, many innovations in that field entered the civil market during the next years^{4,8}. This is also reflected by the massive increase in plastic production amounts. While the total produced plastic before 1950 was approximately around 4 to 8 million tons (Mt), the annual production increased to 1.5 to 2 Mt in the early 1950s^{4,9,10}. Over the next five centuries, a yearly growth rate of around 10% increased the world production up to 200 Mt in 2002¹⁰. Even in the following years, with soared awareness for reasonable plastic consumption, the average annual growth was still around 3.4 percent, yielding an immense total production mass of around 365 Mt for 2020¹⁰.

Although the widespread use of polymers was on the rise, only in the early 1970s did scientists document the first observation of plastic pollution in the environment by describing plastic particles on the surface of the Sargasso Sea¹¹. By that year, the accumulated plastic production had reached about 331 Mt with a discard rate of probably 100% as recycling and incineration were not common before the 1980s¹². Nevertheless, the topic of plastic pollution got little attention despite slightly more effort in correct plastic waste management with increasing recycling and incineration rates up to 10% each¹². It was Richard Thompson and colleagues in 2004 with their publication analyzing the distribution of plastics in the oceans¹³, who for the first time also considered small

particles and put the fate of discarded plastic into the focus of the scientific community as well as the public. In the context of these findings, they coined the term “microplastics” for plastic particles smaller than 5mm in size¹³.

3.3 The fate of plastic waste

A first step to approach the topic of plastic entering the environment is to identify the main sources of plastic waste itself. In 2015 there was 302 Mt primary plastic waste produced, with the most significant shares from packaging (141 Mt), textiles (42 Mt), consumer & institutional products (37 Mt), and transportation (17 Mt)¹². In order to characterize this influx more precisely, parameters such as the type of polymers, additives contained, size and shape, and the pathway must be taken into account¹⁴. In general, there are three options for plastic end-of-life, namely recycling, incineration, and discarding as the least sustainable option¹⁵. However, despite the efforts in improving plastic waste management to decrease discarding rates, even the members of the European Union plus Swiss and Norway, sharing a high level of development as well as public consciousness for environmental topics, still dumped 25% of their plastic waste into landfills in the year 2018¹⁵. If the total amount of plastic ever produced is considered, about 59% ended up in landfills by 2015, making up for 4900 Mt¹². Discarded plastic is often not left at properly secured dumpsites or landfills, which is why large amounts are leaking into the environment upon wind, rain, and floods¹⁶ (Figure 2).



Figure 2 Example for mismanaged waste in coastal areas (Albania). Subsequent transport of lightweight plastics into the sea by wind and rain is likely. (Photo by Antoine GIRET on Unsplash)

Nevertheless, even plastic sent to recycling may still not reach its destination and contribute to plastic pollution¹⁷, emphasizing that plastic waste management generally

has room for improvement. When considering the pathways of macroplastics (>5mm in size) into the environment, a primary distinction must be made into the ocean-based and land-based entry¹⁸. While littering and systematic failures in waste management are issues in both spheres, there are some specific contributions. For land-based entry, relevant factors are industrial and agricultural waste, the transfer from landfills, and contamination from composting and waste water treatment plants¹⁸⁻²¹. For the ocean-based paths, unique positions are abandoned or lost fishing gear or lost ship cargo^{18,22,23}. Besides transport between land and oceans upon wind and waves, there is an input from land to the sea with riverine systems as a link. As all this plastic waste ends up in different ecosystems, negative effects on the therein living species are inevitable. While pictures of seabirds and turtles and other animals entangled in plastic litter are a present view in media, there are other severe implications, including ingestion and smothering, known for many species^{24,25}. And it is the humans who suffer from a plastic polluted environment at the same time²⁶. However, it is not only the presence of plastic litter or macroplastic in ecosystems that poses a threat but also its ongoing fragmentation into smaller pieces, eventually down to microplastic particles.

3.4 Plastic degradation, fragmentation, and microplastics

Although plastics commonly share high resistance against various factors resulting in high durability and associated subsequent persistence in the environment, there is yet a constant fragmentation process of these materials²⁷. The procedures leading to this fragmentation can be divided into biotic factors and abiotic factors, the latter being either physical or chemical. Biotic factors are diverse, ranging from microbial and enzymatic attack on a molecular level to ingestion or transport along food webs on a macroscopic level, but do not appear until biotic contact has taken place²⁸. Abiotic factors, however, act immediately on the material when it enters an environment in the form of UV radiation, temperature, humidity, chemicals, and mechanical stress like wind or waves²⁹. Some of these factors induce changes in the chemical composition of the polymer, such as humidity, radiation, or elevated temperatures causing hydrolysis, thermal-oxidation, and photo-oxidation, respectively^{27,29}. These processes usually decrease the average molecular mass of the polymer through chain scissions and, for oxidative processes, introduce new, mainly polar chemical groups. Various reaction paths further include the formation of radicals, in some cases even causing crosslinking³⁰. The molecular mass of the polymer is tightly linked with its material

properties. PET, for example, undergoes a massive change from ductility towards massive embrittlement once the critical molecular mass falls below the threshold of around 17kg/mol³¹. The actual degradation mechanism itself depends on the polymer and its chemical structure. For example, only polymers with a heteroatom backbone with hydrolyzable bonds, such as polyesters, polyurethanes, and polyamides, are susceptible to hydrolysis. For other polymers with a C-C backbone, such as polyolefins, sensitivity to UV radiation is more dependent on the presence of potential chromophores (e.g., phenyl-group in polystyrene), while processes like thermal oxidation are influenced by humidity and availability of oxygen^{30,32}. If other substances in the material like additives or remaining monomers from synthesis are considered, even more reactions are possible.

The typical abiotic degradation process for PET are (thermal) hydrolysis, photodissociation, and photo-oxidation. However, diverse reactions are possible, including Norrish reactions of type I and II and radical-based reactions³³. Figure 3 shows the most common abiotic degradation products for PET.

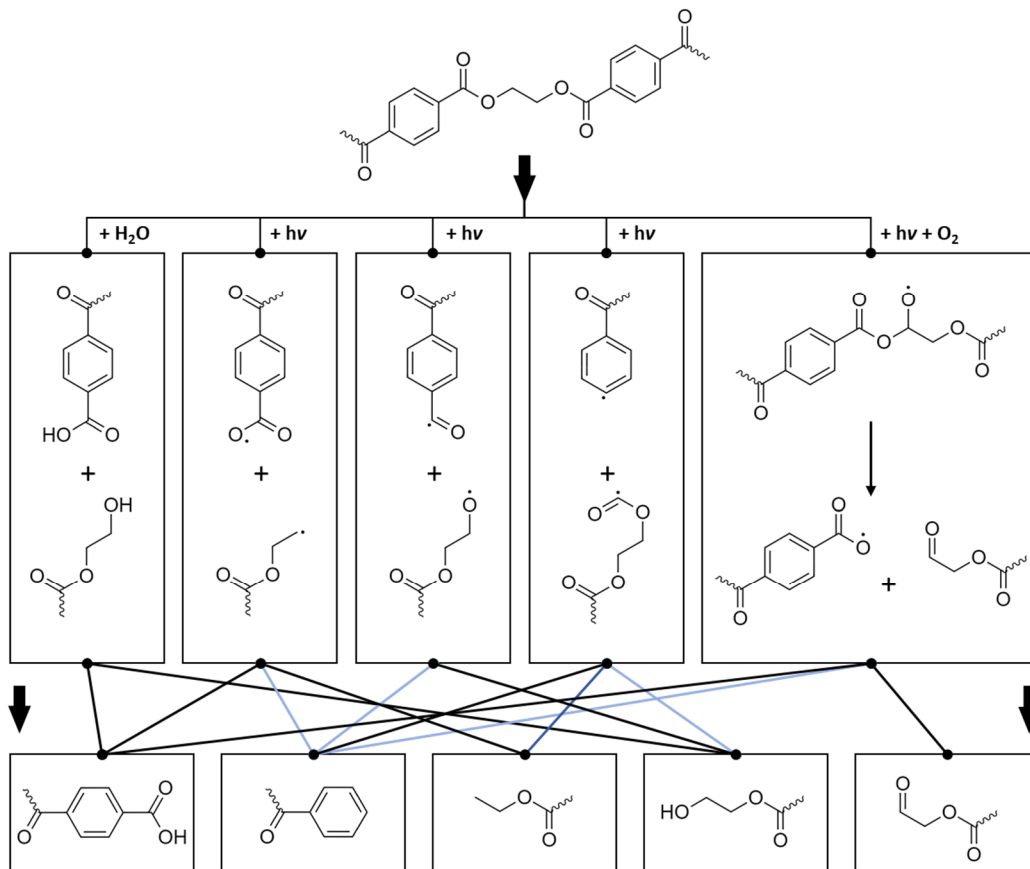


Figure 3 Simplified schema for common abiotic degradation processes in PET. Hydrolysis (left side) requires the presence of water, while the other degradation paths are initiated by radiation causing photodissociation according to a Norrish Type I reaction. A photo-oxidative pathway is shown on the right side. The lines link the intermediates

with the possible products/end groups at the bottom; blue lines indicate the release of CO or CO₂. Any radical transfer to a third partner in this last step is not shown for simplification. The figure is based on the work of Hurley *et al.*³⁴, Sang *et al.*³³, and Day *et al.*³⁵.

The most straightforward possible reaction is the hydrolysis of the ester bond, creating a carboxyl- and hydroxyl- end-group, which comprises the reversed synthesis reaction. An activation by UV radiation can lead to chain scission with the subsequent introduction of aldehyde, vinyl, ethyl, hydroxyl, or carboxyl ends^{33–35}. Depending on the propagation of radicals, different products are possible, including the release of CO₂ and CO^{32,35,36}.

All these processes and factors, biotic and abiotic, may act individually or synergistically and weaken the material by the deterioration of the physiochemical structure, eventually leading to embrittlement. For larger pieces, this usually starts with abiotic degradation according to the available factors in the environment, inflicting first cracks paving the way for fragmentation³⁷. This generates more surface or weak points for an iterative fragmentation process while biotic factors such as biofilm formation and subsequent enzymatic attack mostly but not exclusively intervene later in this process^{38,39}. However, factors may vary over time, for example, when fragments or particles undergo a transition from terrestrial to aquatic environments or through sedimentation. In Figure 4, an overview of the sources of plastic waste and their paths in the environment after the end of use is illustrated.

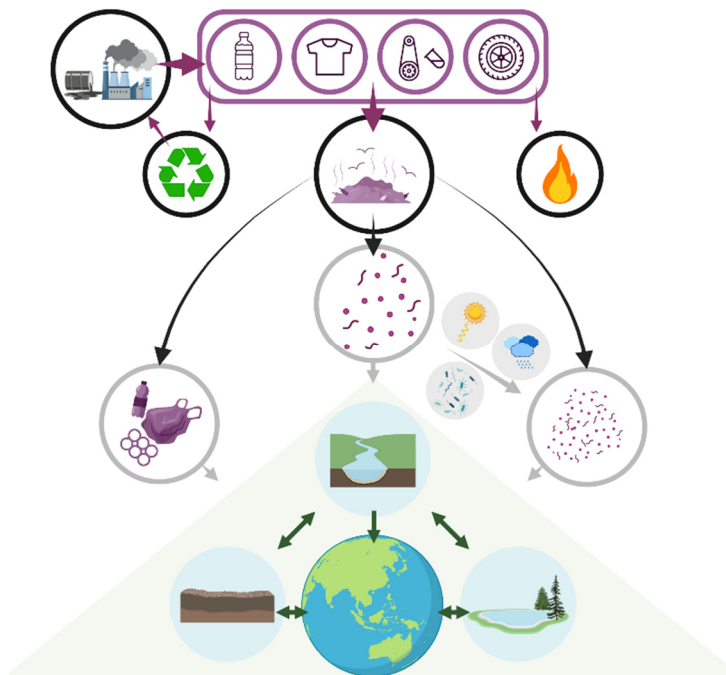


Figure 4 Typical schema for plastic entering the environment. Of all the plastic produced, with the greatest demands from packaging, textiles, institutional products, and transport, only minor shares go to recycling or

incineration. Most mismanaged plastic waste is prone to leak into the environment as large plastic litter or down to microplastic. Abiotic and biotic factors acting on the material promote plastic degradation into smaller pieces. Eventually, plastic of vastly different sizes may enter environmental compartments, including exchange and transfer within them.

There is also a complex interplay of these factors, e.g., where biofilm formation initiates biotic degradation but in return inhibits further photo-degradation by blocking UV transmission⁴⁰. In this way, plastic litter and macroplastic are broken up into what is referred to as secondary microplastics. Primary microplastic, however, does not derive from the fragmentation of larger pieces but enters directly into the environment^{41,42}. It can originate from medical or cosmetic products (e.g., abrasives) or from the polymer production process itself. A significant amount of primary microplastic is generated through wear-off during a product's intended use, such as fibers released from fishing nets and synthetic textiles, or abrasion from tyres^{42,43}. Within primary microplastics, the contribution derives from the laundering of synthetic fibers with 35% and the abrasion of tyres (28%); nevertheless, primary microplastics account for only 15-31% in the ocean⁴⁴. Consequently, the major share of 69-81% arises from secondary microplastics⁴⁴.

This whole system of plastic in the environment must be considered as a highly dynamic and continuous process. There is a constant afflux of litter, macro-, and microplastic into the environment, transported in various ways in and among aerial, aquatic, riverine, and terrestrial systems. While there are accumulation zones for plastic such as garbage patches⁴⁵, there are also temporary sinks for plastic such as peripheral areas, shorelines^{38,46}, floodplains⁴⁷, and estuaries⁴⁸, where material persists for some time before further transport. Eventually, the sea floor comprises the main permanent sink for plastics⁴⁹, but sedimentation processes are not restricted to the oceans. Thus, estuaries and salt-marshes are also seen as a large permanent sink for macro- and microplastics⁵⁰. In parallel degradative processes act on the material leading to fragmentation into smaller and smaller pieces, with the number of particles increasing exponentially. However, even microplastic particles are just an intermediate stage before being ground to nanoplastics, defined as particles below 1 μm . The decreased size also affects the transport behavior of the particles. The transport of macroplastic has many requirements, as the particle's size, shape, and density must be compatible with the strength and density of the transport current. A foil, for example, might be blown away by the wind, while a solid piece of the same polymer would, in contrast, stay put. Especially in riverine or aquatic systems, density is generally a decisive factor as fragments with densities above 1 g cm^{-3} (e.g. PET $\approx 1.35 \text{ g cm}^{-3}$) might sink, unlike those floating with densities below 1 g cm^{-3} (e.g. PP $\approx 0.9 \text{ g cm}^{-3}$)^{51,52}. However, with the

decreasing particles sizes, the physical regime for the transport of these particles changes, and the shape and density as mentioned above become less critical. Therefore, microplastics are readily transported under various conditions in all kinds of environments. Within aquatic systems, this includes the transport in rivers, by waves and tides, and via surface water and flooding, but also along food webs⁵³⁻⁵⁵. In addition, these particles can also migrate in soils and other terrestrial systems, and when small enough, this eventually enables even long-range aerial transport by wind^{53,55}. Thus, the high potential for spreading leads inevitably to microplastic particles in pristine places far off and remote from human civilization, as shown for the Arctic and Antarctic sea and inaccessible alpine areas^{56,57}.

3.5 Impact of microplastics

With their ubiquitous emergence, microplastics have gained much attention since the 2000s. The apparent key question is how these particles would interact with the environment, including flora, fauna, and eventually humans, and if this would implicate severe downstream problems on a global scale. Although countless studies have been published by now, the entire complexity of microplastic interactions is hard to cover. The interaction and reaction of organisms are dramatically dependent on the type of polymer, size, and shape. Weathering, aging, and potential biofilm formation change the surface properties and thereby multiplies the combinations that must be considered. Each species might interact utterly differently with a specific set of particles, and for humans and other higher organisms, even different tissues or cell types must be considered. Another challenge is the tracking of such small particles within these experiments. As a result, studies must unavoidably restrict their scope to very specified subjects. Nevertheless, some conclusions can be drawn for the impacts of plastic particles of different sizes on biota.

Various ecotoxicological effects on organisms have been found⁵⁸⁻⁶⁰ while these adverse impacts can be divided into two categories: (1) physical effects caused by the simple presence of the particle and (2) effects induced by associated substances and organisms of the plastic particle⁶¹. The most common physical interaction is ingestion by an organism, which usually does not cause increased mortality⁵⁸. Often the uptake of microplastic has some kind of filling effect, reducing the capacity to assimilate nutritious food. Thus, the decreased energy intake might lead to changes in the metabolic and behavioral constitutions and viability; furthermore, reproduction efficiency can be

affected disproportionately. This principle was shown in a study on turtles where 25% plastic content in the food reduced reproduction up to 88%⁶². In the context of adverse effects of plastics on organisms, some of the greatest concerns emanate from endocrine-disrupting chemicals (EDCs), which are abundantly present as common additives like phthalates and bisphenols as plasticisers⁶¹. As they are not covalently bound in the material, diffusion upon biological contact and subsequent uptake is possible. This might even be promoted by fragmentation and degradation, which increases the surface area and decreases in hydrophobicity of the material, thus easing the release of those hydrophobic compounds. Due to the hormone-like structure of EDCs, they can mimic or antagonize their function and intervene in hormone synthesis from metabolism to receptor expression⁶¹. With this efficacy spectrum, they threaten not only many organisms and animals but also humans.

For the latter, there are two main uptake mechanisms for plastic particles with ingestion via beverages and contaminated food on the one hand and through inhalation of aerial micro- and nanoplastic on the other⁶³. Interestingly, fibers are in both scenarios the dominant species in particle shapes⁶³. This uptake, particularly by inhalation, can have severe impacts, as shown in a study that nanoplastic particles can harm lung tissue with effects on viability, protein expression, apoptosis, and more⁶⁴. Besides their immediate adverse impacts on the organism, these plastic particles also pose a threat as they may act as a transport vehicle for harmful substances. Their typically hydrophobic nature generates high adsorption and absorption potential that is even increased with rising particle surface upon fragmentation. Eventually, this enables the accumulation of critical compounds. Thus, besides the sorption of heavy metals with subsequent transport^{65,66}, there is a discussion about the role of microplastic particles in the context of persistent organic pollutants (POPs). These POPs are described as hydrophobic compounds such as polycyclic aromatic hydrocarbon (PAH), polychlorinated biphenyl (PCB), polybrominated diphenyl ethers (PBDE), and dichlorodiphenyltrichloroethane (DDT), which are adsorbed by plastic particles unintentionally during transport through different environments⁶⁷. Due to the high sorption potential of plastic particles and their mobility, their risk potential regarding POPs is unclear. Furthermore, processes that might induce disadvantageous desorption processes leading to locally high POP concentrations are hardly studied. However, the threat of microplastic particles loaded with POPs is controversially discussed as they might also act as a beneficial permanent sink for POPs⁶⁷.

Aside from these chemical pollutants, the surface of plastic particles can also carry dangerous pathogens within their biofilm. The elevated levels of fungal pathogens found on microplastic in terrestrial environments⁶⁸ and analogously pathogenic species of the genus *Vibrio* in marine systems⁶⁹ demonstrate that the plastisphere can be a fatal breeding ground for human pathogens. Taken together, it is convincing that microplastic presents a severe danger to organisms in different ways. Nonetheless, more research is needed to gain an overall picture of the risk potential of microplastic and related particles.

3.6 Discovery of plastic and PET degrading enzymes

With the prevalence of biopolymers in nature, the existence of a machinery for synthesis, conversion, and degradation of these molecules is a prerequisite. Enzymes naturally cover these tasks with their catalytic activity involved in virtually every biochemical reaction. While some of these biopolymers feature a C-C backbone, like lignin, the majority features polymer backbones created by condensation reactions, such as amides, glycosides, and esters. Reversely, these polymers resulting from condensation can easily be depolymerized via hydrolysis, with the chemical equilibrium shifted to the side of the monomers, fully recovering the educts of synthesis. On the contrary, C-C bonds are much more stable, demanding an energy-intensive mechanism for synthesis and degradation. For the latter, a form of activation of the C-C bond system is necessary anyway^{70,71}, often requiring radicals, peroxides, or oxidative processes. As many biopolymers, including RNA, DNA, proteins, and polysaccharides, are involved in continuous synthesis, degradation, and resynthesis processes, it seems only reasonable that they rely on the handy dehydrative condensation process. In contrast, polymers with a C-C backbone are more restricted to special applications.

Nevertheless, there are also biopolymers featuring hydrolyzable bonds in theory, which are still hard to depolymerize. Such examples of even global relevance are cellulose and lignocellulose that are particularly recalcitrant to enzymatic degradation, mainly due to the crystalline order of the cellulose fibres⁷². The efficient degradation of the mass polymer lignocellulose, which is crucial for a functioning carbon cycle, is only enabled by different cellulases working in parallel with a specific cleavage profile supported by specialized carbohydrate-binding modules (CBM)^{73,74}. Besides crystalline structures, hydrophobicity of the polymer can also complicate degradation, which is true for cutin. Cuticular tissues act in plants as a protective barrier at the surface made from cutin, waxes, and polysaccharides⁷⁵. Cutin itself can be described as a branched

polyester comprised of hydroxy/epoxy fatty acids with the length of C16 and C18⁷⁵. The group of enzymes dealing with the degradation of this tenacious polymer is accordingly called cutinases.

The degradation of man-made plastics presents similar or even more complex challenges than biopolymers. Commodity plastics often feature a very high degree of crystallinity of up to 45-95% and 50-80% for PE and PP, respectively⁵¹. A high crystallinity content increases the material strength, rigidity, and melting temperature⁷⁶, but the arrangement of the polymer chain in these densely packed lamellar crystalline regions impairs enzymatic attack⁷⁷. These lamellae are arranged in spherical structures called spherulites, whereas amorphous arranged polymer chains are present both between the lamella and outside of the spherulite (Figure 5).

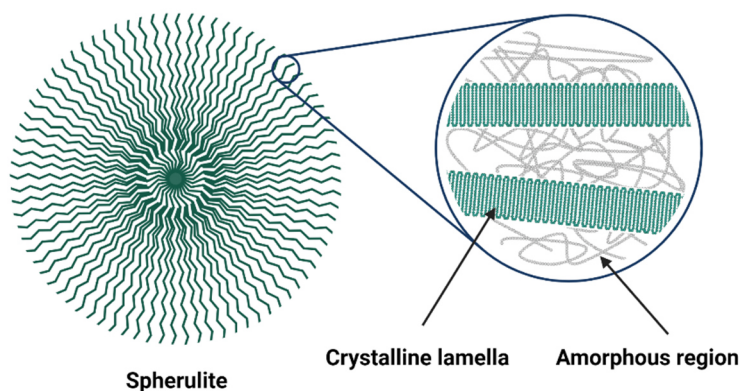


Figure 5 Schematic representation of a spherulite containing the crystalline regions in semi-crystalline materials. The spherical structures are comprised of lamella, where the polymer chains adopt a regular, thus crystalline order. In between and outside of the spherulite, polymer chains adopt an amorphous state.

Furthermore, the plastics with the highest global resin demand, PE, PP, PVC, and PS, summing up to a 65% share in total¹⁵, share a C-C backbone impeding biotic deterioration. The enzymatic degradation of these materials often requires abiotic pre-treatment to introduce chain scission or hydrophilic end groups, as only a few known organisms are actually capable of dismantling virgin material⁷⁷. The organisms involved in the degradation of C-C backbone polymers are algae, fungi, and bacteria⁷⁷ and some invertebrates by virtue of their gut biome mediating the degradation of, e.g., PE or PS^{78,79}. Nevertheless, the difficulty of breaking C-C bonds is also reflected in the known performance of microbial and enzymatic degradation of these individual plastics. Since degradation rates of these plastics are comparably low, they are blended with fast biodegradable polymers such as polycaprolactone (PCL), polylactic acid (PLA), or starch if fast biotic decomposition is desired. These fast degrading polymers attract microbes

inducing biofilm formation and, once decomposed, leave a porous structure within the main polymer, making it vulnerable for subsequent various degradation processes⁷⁷.

The situation is different for the two commodity plastics based on a heteroatom backbone, polyurethane (PU) and PET, where biodegradation is well known. PU undergoes different ways of hydrolysis upon enzymatic attack with esterase activity as the most common option⁸⁰, while also oxidative degradation has been described⁸¹. However, PU plays a minor role in scientific interest in enzymatic plastic degradation, which PET has dominated over the last years. With an 8-10% share, PET is one of the most abundantly produced plastics and is often released in the environment due to the short life cycle of its typical products, including food containers, bottles, and fibers¹². With its moderate crystallinity of commonly around 35%, it represents a good target for enzymatic degradation. Meanwhile, several enzymes with PET activity have been found, most of which can be attributed to the class of cutinases.

3.7 Cutinases – A class of promiscuous enzymes

Cutinases (E.C. 3.1.1.74) act on cutin, which is, as mentioned above, a hydrophobic polyester comprised of linked C16 and C18 ω -hydroxy fatty acids⁸² with additional hydroxyl and epoxy groups enabling cross-linking of the biopolymer. As the main component of the cuticula, besides polysaccharides and waxes, it protects plants' epidermis, preventing evaporation, and comprises a physical barrier for pathogens. Thus, cutinases were first reported in the context of phytopathogens which use this enzyme as a tool to overcome the protective cuticula during infection⁸³⁻⁸⁵. The first cutinase studied in detail, including structural characterization, was the *Fusarium solani* cutinase (FsC)⁸⁶, which confirmed the enzyme as a member of the alpha/beta hydrolase superfamily⁸⁷. Consequently, cutinases share a common structural topology containing eight beta sheets connected by six alpha helices⁸⁷ (Figure 6). The active site features the catalytic triad Ser-His-Asp with the serine being surface exposed due to the missing hydrophobic lid compared to the structurally and chemically closely related true lipases^{86,88}.

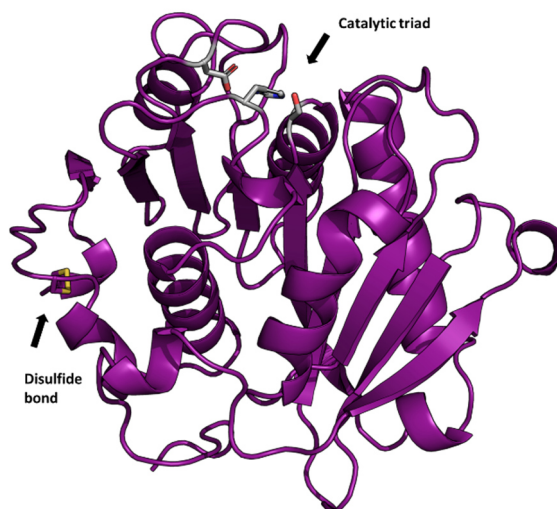


Figure 6 Crystal structure of Leaf-branch cutinase (LCC) (PDB ID 4EB0) in cartoon representation as an example for the alpha/beta hydrolase fold of cutinases. The typical composition of the central beta sheets enclosed by alpha helices is visible; the catalytic triad (grey) within the binding groove and the disulfide bond near the C-terminus are shown as sticks and were labeled accordingly.

This open architecture towards the active site presumably promotes the promiscuity of cutinases, which are active on many substrates, including triglyceride and fatty acid esters, extending their ability to hydrolyse an extensive and solid material like cutin. Apart from the alpha/beta hydrolase fold core, the layout of the enzymes may vary with the molecular weight ranging from around 20 kDa for most fungal cutinases up to 35 kDa for some bacterial variants, yet the latter are usually around 30 kDa⁸⁹. The observed variation stems from differences in decoration at loops and especially at the termini. The optimal working conditions for those enzymes correlate with their origin, and as most bacterial enzymes were found in thermophilic organisms, their optimal temperatures are around 50-60°C, while fungal variants prefer 40-45°C or even below⁸⁹. Numerous disulfide bonds are often related to thermophilic proteins as they have a stabilizing effect even at elevated temperatures. However, it seems unlikely that this rule can be applied to the thermostability of natural cutinases. Though fungal cutinases have two to three of these links, they usually show lower thermostability and activity at high temperatures compared to bacterial variants with mostly just one disulfide bond. Regarding pH, most cutinases have been reported to work optimally in the range of slightly alkaline to neutral pH of around 7-9, yet some variants function in acidic environments down to pH 4⁸⁹. Although PET and cutin have no striking structural resemblance (see Figure 7), they are both polyesters and build a compact polymer with a hydrophobic character containing polar groups.

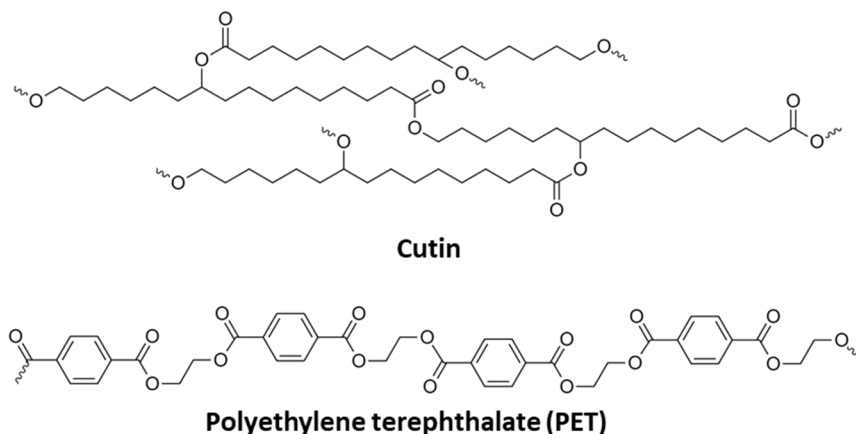


Figure 7 Structural comparison of polyethylene terephthalate (PET) and Cutin. For simplicity, Cutin is depicted as a homopolymer made from 10,16-dihydroxypalmitic acid, neglecting the diverse composition of fatty acids present in natural cutin.

Considering the promiscuity of cutinases mentioned above, activity on PET of these enzymes seems conceivable. And in fact, all PET degrading enzymes known today can be assigned to this enzyme class⁹⁰.

3.8 PET degrading enzymes

To date, many polyester degrading enzymes are known that show activity on PET to some extent. Kawai *et al.* suggested⁹¹ that these enzymes can be grouped into PET surface-modifying enzymes and PET hydrolases or PET-degrading enzymes. On the surface of PET material, single polymer chains are jutting out from the bulk material as loops or chain ends, accounting only for a marginal fraction of the whole material mass. Besides cutinases, many hydrolases have been identified to cleave such exposed PET chains, including members from lipases, carboxylesterases, and even peptidases^{91,92}. Consequently, the degradation of jutting chains leaves either hydroxyl or carboxyl end-groups on the surface leading to hydrophilization. Surface hydrophilicity is linked to several favorable properties of PET during processing, such as dyeability or wettability, why this enzymatic treatment is also used for industrial purposes⁹³. However, the degradation process of these surface-modifying enzymes is naturally limited to the surface itself as these enzymes are missing the ability to degrade the bulk material underneath. This extended competence is limited to the PET hydrolases alias PET degrading enzymes. As criteria for these enzymes, Kawai *et al.* proposed detectable surface erosion with optical imaging and a mass loss of at least 10%⁹¹.

Before individual enzymes and their performance are discussed, the connection between incubation temperature during the reaction and PET's glass transition

temperature (T_g) must be considered. PET is a semi-crystalline material where the polymer chains arrange either in lamellar, crystalline structures or unstructured amorphous regions (compare Figure 5). The content of these crystalline regions, depending among other factors on the material's processing, is measured as percent crystallinity. The T_g describes the temperature at which polymer chains in the amorphous phase experience a rapid increase in mobility. For PET, the T_g is between 67 °C and 81 °C depending on the crystallinity with the lower temperature for fully amorphous PET⁹⁴. However, when PET is in a humid environment, it absorbs water which weakens the interactions within the amorphous phase. Thus T_g is significantly decreased to 60-65 °C, depending on several parameters including initial T_g , relative humidity, and temperature^{95,96}.

Enzymatic degradation primarily occurs on amorphous regions due to the higher mobility and thereby accessibility of polymer chains to the enzyme. Therefore, crystallinity is a decisive factor for studying enzymatic PET degradation. Consequently, the enzymatic degradation profits from incubation temperatures near T_g , where the chains in the amorphous regions gain even more flexibility. However, this requires enzymes with sufficient kinetic and thermal stability. At temperatures above T_g , amorphous regions start to arrange themselves slowly into crystalline structures and thus increase crystallinity, referred to as cold crystallization⁹⁴. Tournier *et al.* reported that this phenomenon is unfavorable for further enzymatic PET degradation⁹⁷, which suggests limiting the incubation temperature to not far above T_g . Considering the connection between activity and T_g , one should generally distinguish between mesophilic and thermophilic enzymes regarding their absolute performance. As mesophilic enzymes cannot act near PET's T_g , they are usually much slower than their thermophilic counterparts but might still show impressive turnover rates useful for specific scenarios.

In the following section, some noteworthy PET degrading enzymes will be introduced, yet there are many more which have been reviewed by several authors^{90,91,98}. In 2005 Müller *et al.* discovered the PET degrading activity of BTA-1 alias TfH, which was found in *Thermobifida fusca* DSM43793⁹⁹. They could show that the enzyme could degrade two low crystalline PET films made from a PET bottle or virgin PET pellets. After incubation at 55°C for three weeks, they measured weight losses between 43 and 54%⁹⁹. Consequently, TfH is considered the first known PET degrading enzyme. The organism *Thermobifida fusca* belongs to the order of *Actinomycetales* associated with the decomposition of plant material¹⁰⁰ where such enzymatic activity of cutinases is

expected. This finding drew attention to enzymes and organisms of similar origin, and several PET degrading enzymes could be identified, especially from the genus *Thermobifida* such as TfCut2 from *T. fusca* KW3^{101,102} or Thc_Cut2 from *T. cellulosilytica* DSM44535¹⁰¹.

TfCut2 showed rapid degradation of an amorphous PET film with a weight loss of 16% in only 50h at 65 °C despite poor kinetic stability causing a 50% activity loss over the incubation period¹⁰³. Furthermore, they tested several mutants of TfCut2 to improve PET degradation rates and found the single mutant G62A, which considerably increased the weight loss to 43% under the same conditions. The single mutant reduced affinity to the degradation product MHET which is only hesitantly further hydrolyzed and thus resolved product inhibition which prevented higher overall degradation rates¹⁰³. The mutations used in their study were inspired by another enzyme previously discovered by Sulaiman *et al.* in 2012¹⁰⁴. By screening a metagenome library from a leaf-branch compost, where *Actinomycetales* are also dominant⁹¹, they discovered another cutinase active on various substrates. This enzyme was named Leaf-compost cutinase (LCC), and when tested on PET as the substrate, it exhibited the highest PET degradation activity known to that time. In a follow-up study, they specified LCC's activity with 20-25% weight loss on a probably amorphous PET film at 70°C in 24h¹⁰⁵, but, similar to TfCut2, the kinetic stability is limited with a half-life of 40 minutes at 70°C. This could be addressed by glycosylation on three sites when expressed in *Pichia pastoris*, promoting stability and thermostability of LCC and increasing the onset for thermal-induced aggregation about 10°C¹⁰⁶. These results emphasize the importance of thermostability and kinetic stability for efficient PET hydrolysis.

The discovery of PETase from *Ideonella sakaiensis* (IsPETase) by Yoshida *et al.* in 2016 had a considerable impact on the research on PET degrading enzymes¹⁰⁷. These bacteria were found on a dumpsite, growing on PET bottles, and excel at using the polymer as their sole energy and carbon source. To achieve this, the organism possesses a two-enzyme system comprised of PETase, a cutinase-like enzyme, and MHETase, which is related to feruloyl esterases. As the PETase is active on PET itself, degrading it to primarily mono-2-hydroxyethyl terephthalate (MHET) with small amounts of terephthalic acid (TPA) and bis(2-hydroxyethyl) terephthalate (BHET), MHETase eventually hydrolyses MHET into TPA and ethylene glycol¹⁰⁷ (Figure 8).

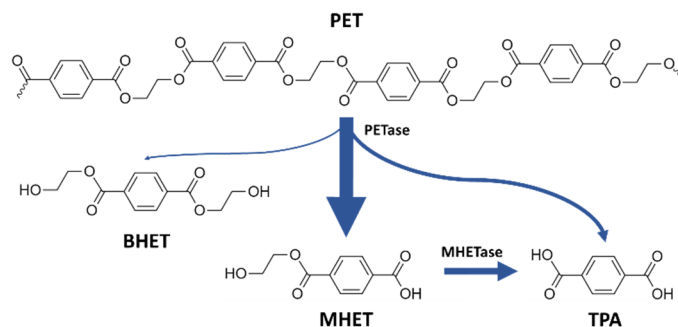


Figure 8 PET hydrolysis schema for IsPETase with the typical products of enzymatic PET hydrolysis BHET, MHET, and TPA. IsPETase produces MHET as the dominant product as indicated by the size of the arrows, which can subsequently be further hydrolyzed into TPA by MHETase.

The novelty of IsPETase was the putative evolutionary adaptation and the activity at ambient temperatures around 30°C. While it is unquestionable that IsPETase outperformed LCC under the given conditions, the thesis of IsPETase's high activity on highly crystalline PET must be questioned critically. The performance on highly crystalline material in the experimental setup presented by Yoshida *et al.*¹⁰⁷ was so low that it was more likely caused by surface-modifying activity or degradation of amorphous regions but of activity on crystalline regions. Furthermore, comparing the PET degradation performance under optimal conditions, IsPETase is orders of magnitude slower than LCC, as also shown by the authors. Nevertheless, IsPETase gained immense attention in public media and the scientific community as a potential savior against plastic pollution and recycling applications. For scientists, the hope was that IsPETase's unusual activity at ambient temperatures could serve as a foundation for future protein engineering approaches. With redesigns towards higher thermostability, exploiting the known benefits for PET degradation near T_g seemed feasible. The popularity of IsPETase as a research topic is also reflected by the variety of nearly simultaneously published IsPETase crystal structures around 2018^{108–113}. Those structures revealed IsPETase as typical cutinase with only minor differences to other PET degrading cutinases shown in Figure 9 A.

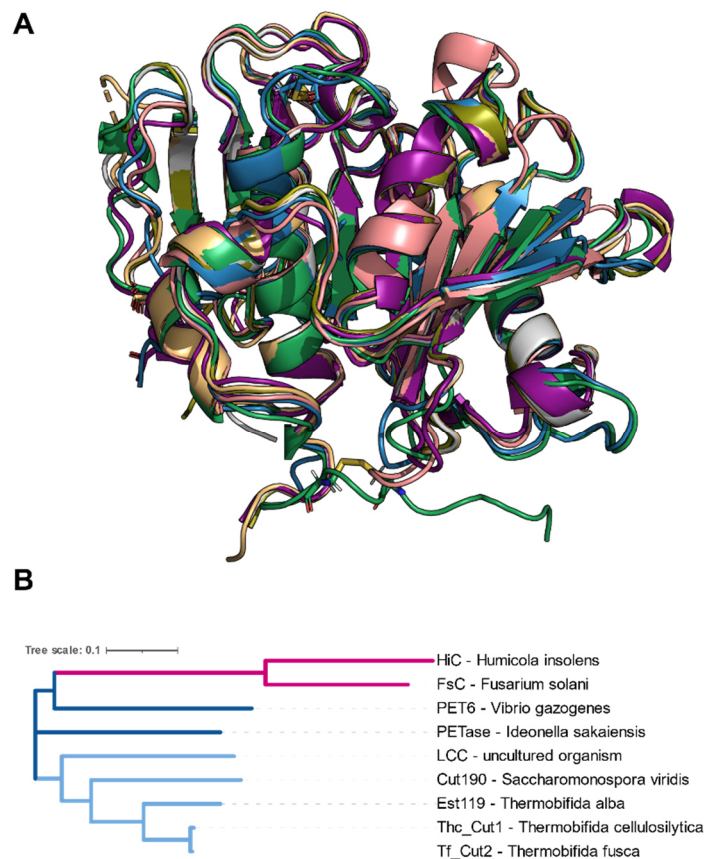


Figure 9 Superimposed crystal structures of known PET degrading cutinases in cartoon representation are shown in **A**. The structures of Thc_Cut1 (PDB 5lui, grey), Cut190(PDB 4wfi, coral), Est119 (PDB 3vis, ochre), Tf_Cut2 (PDB 4cg1, olive), LCC (PDB 4eb0, purple) match well with IsPETase (PDB 5xjh, blue) including PET6 from *Vibrio gazogenes*. **B** shows a phylogenetic tree to visualize relationships within these enzymes based on these sequences complemented by the two fungal cutinases HiC (PDB 4oyy) and FsC (Uniprot ID Q99174). The tree was calculated with Clustal Omega¹¹⁴ using default settings and visualized with iTOL v6¹¹⁵. The analysis shows one cluster for the *Actinomycetales* variants colored in light blue and the fungal cutinases in pink. Thus, IsPETase takes a position between these two clades, which is also true for PET6.

However, some features of IsPETase set it apart from its bacterial peers, such as an additional disulfide bond which is more common for fungal variants. The closer relationship of IsPETase to fungal, mesophilic PET degrading enzymes is also evident from phylogenetic analysis⁹¹ (Figure 9 B). IsPETase features a more open substrate-binding site on the structural level, yet many residues around the active and binding site are conserved throughout all cutinases. An overview of the active and binding site of IsPETase is depicted in Figure 10.

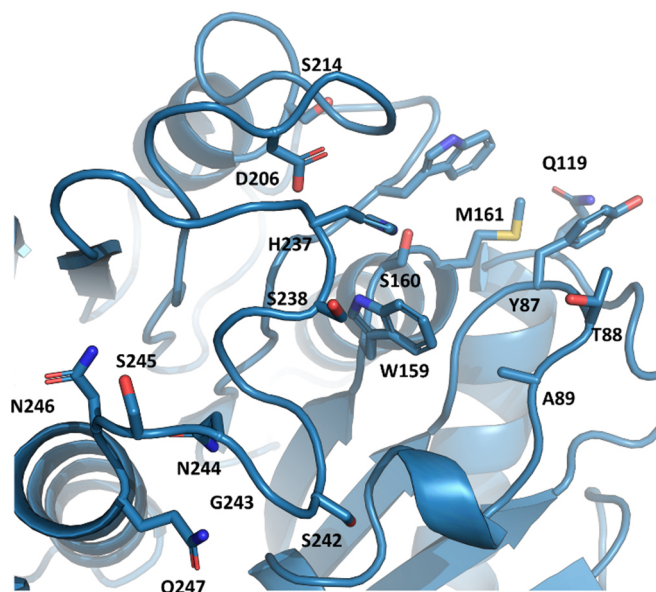


Figure 10 Crystal structures of IsPETase (PDB 5xjh) in cartoon representation. Relevant residues in and around the active- and binding site, as discussed in several studies, are shown in stick representation and labeled accordingly.

To investigate whether this different surrounding of the active site is beneficial for the enzyme, Austin *et al.* created the double mutant S238F/W159H mutating these two residues towards the conserved sequence among *Actinomycetales* cutinases¹⁰⁸. Interestingly activity of the double mutant was slightly increased and realized a higher reduction in measured crystallinity upon incubation, questioning the different architecture as an evolutionary adaptation towards PET as substrate. A similar question arises around the “wobbling” Trp185 and the opposing Ser214 adjacent to the active site^{108,111}. There are hints that this wobbling motion, enabled by the provided space of the relatively small serine, is essential for substrate interaction in IsPETase, in that the increased flexibility of the active site contributes to the activity¹¹². However, this mechanism has not been described for other performant PET degrading enzymes; hence it could be a unique adaptation towards its mesophilic activity profile. The structure of IsPETase further shows no binding sites for divalent cations. In other cutinases like those from *Actinomycetales*, divalent cation binding is a common motif, where the concentration even has a decisive impact on thermostability, activity and may induce even minor structural changes in the enzymes^{91,96}.

However, similar to other PET hydrolases, knowledge of how the substrate interacts with the enzyme on a structural level is limited. Although there are some crystal structures of IsPETase with substrate analogous like 1-(2-hydroxyethyl) 4-methyl terephthalate (HEMT) (PDB-ID 5xh3)¹¹³, no structure of IsPETase or other cutinases

show a complex with a full-length substrate to describe protein-ligand interaction holistically. Thus Joo *et al.* performed docking with 2-HE(MHET)₄, a molecule comprising four repeating units of PET, and divided the calculated binding site into two subsections. The smaller subsite I is comprised of the residues Tyr87, Gln119, Met161, including the wobbling Trp185. The elongated Subsite II contains Thr88, Ala89, Trp159 next to the catalytic serine, Ser238 and Asn241. Hence, the complete binding site resembles an L-shape. Eventually, they proposed that subsite I harbours the first PET repetition unit where the cleavage occurs. This follows the typical serine hydrolase mechanism, where the charge relay system of the catalytic triad deprotonates the serine, which performs a nucleophilic attack on the ester bond, forming an enzyme-acyl-intermediate which is resolved by a final nucleophilic attack of a water molecule to release the product. According to Joo *et al.*, the moiety in Subsite I is cleaved at the terephthalic acid while the resulting OH-terminal points towards subsite II¹¹⁰. The released product depends on the composition of the end groups on both sides of the cleavage site, releasing either MHET, TPA, or BHET. A piece-by-piece sliding of the enzyme on a polymer chain would thereby produce MHET, explaining it as the dominant product of IsPETase¹¹⁰. However, other PET degrading enzymes show different preferences for the released products suggesting differences in the binding behavior¹¹⁶. Considering the reported flexibility of the surrounding of the active site of IsPETase, those rigid docking results must be taken with a pinch of salt. Furthermore, the mechanism was also questioned by Wei *et al.* by asking whether a PET chain could adopt the suggested L-shape conformation¹¹⁷. While the fundamental cleavage mechanism was confirmed by Jerves *et al.* with reliable QM/MM calculations¹¹⁸, the extended substrate-binding pose remained elusive as their modeling was limited to a short PET dimer as substrate.

Regardless of this lack of knowledge, groups have performed protein engineering approaches on IsPETase, ranging from extensive redesigns to effective variants with just a few mutations. An extensive review of PET degrading enzymes and descendant engineered enzymes has been recently presented by Magalhães *et al.*¹¹⁶. In the following, some chosen variants will be presented, starting with an interesting enzyme designed by Son *et al.* They introduced only a few mutations yielding a triple (S121E/D186H/R280A) and a quadruple (S121E/D186H/S242T/N246D) mutant which feature improved thermostability and increased PET degradation at ambient temperatures (37-40°C) by 14- and 58-fold respectively^{119,120}. Remarkably, they achieved this improvement in activity at ambient temperatures without acting even near the PET's

T_g . In contrast, Cui and colleagues took a different approach to achieve higher performance by targeting thermostability¹²¹. They performed an extensive redesign on IsPETase, increasing stability by pushing the melting temperature (T_m) from 31°C to 78°C for their designed DuraPETase, meaning comfortable stability even above T_g . Besides the expected increased activity at elevated temperatures around 60°C, they claimed a 300fold increase in activity at ambient temperatures for their DuraPETase¹²¹, yet the latter could not be confirmed in our experiments.

In the scope of designing potent systems for PET degradation, not only single enzymes have to be considered for protein engineering projects. It was shown that a fusion of PETase and MHETase connected by a linker increased performance about 5fold¹²². This might indicate either a product inhibition similar as seen in TfCut2¹⁰³ or simply a synergistic effect on the activity of these enzymes. Nevertheless, the most potent known PET degrading enzyme by now is not a descendant of IsPETase but from LCC. Tournier *et al.* stabilized LCC by introducing two cysteines to form a disulfide bond at a binding site for divalent cations (D238C and S283C) and combined it with mutation Y127G and either F243I or F243W, yielding the variants LCC-ICCG and LCC-WCCG⁹⁷. With this, they could improve the kinetic stability of the enzyme and achieve depolymerization rates over 90% of PET in a bioreactor at 72°C within 10h. Further, they extracted the TPA gained by the enzymatic degradation and used it to synthesize new PET. The material properties of their resynthesized PET met the standards for petrochemical-based virgin PET⁹⁷. With this reuse of the monomers to synthesize new PET with decent material properties, they achieved a proof of concept for large-scale enzymatic recycling of PET.

3.9 Contribution of enzymes for a sustainable plastic economy

In order to assess how PET-degrading enzymes could contribute to solving the environmental problems caused by the massive use of plastics and subsequent poor waste management in the future, two scenarios need to be considered: One deals with potential enzymatic plastic degradation after entering the environment, thereby lessening adverse effects of plastic pollution. The other scenario is about how enzymes could improve recycling processes, achieving material reuse without a subtle decrease in material properties. However, due to their chemical structure, as discussed previously, only hydrolyzable polymers such as polyesters, polyamides, and polyurethanes are suitable candidates for efficient enzymatic attack. Despite these theoretical

considerations, a practical relevance for enzymatic degradation on a petrochemical commodity plastic is only insight for PET. Now two main research topics in this field suggest themselves: The first is the protein engineering on highly active thermophilic PET degrading enzymes and their integration in large-scale recycling processes. As shown with the improved variants of LCC⁹⁷, this goal is in reach, but many points still need to be addressed. For a successful implementation, low-price production of the enzyme is a prerequisite. Furthermore, conversion rates should be improved to reach 100%, and substrate compatibility with extremely high crystallinity, like biaxially-orientated PET (boPET), must be ensured. Eventually, the recovery and purification for both monomers must be improved. The currently proposed method for TPA extraction produces absurdly large amounts of 0.6kg sodium sulfate per 1 kg of recycled PET⁹⁷.

The other question about PET degrading enzymes or plastic degrading enzymes, in general, is how they contribute to plastic removal in the environment, wherefore primarily mesophilic and naturally occurring enzymes must be considered. Hence, applying protein engineering on mesophilic enzymes with our knowledge today seems unnecessary, except for estimating the immediate evolutionary potential of an enzyme. Those improved enzymes, together with their successfully shown integration in marine organisms like algae¹²³, are only of academic interest, as a release of those modified enzymes in genetically modified organisms (GMO) is simply inconceivable and unrealistic. Therefore, future research should focus on identifying PET or plastic degrading enzymes already present in nature and try to document and quantify their actual contribution to plastic degradation in the environment and not *in-vitro* only.

Tackling plastic pollution requires a whole new approach to how we deal with plastic. Nevertheless, enzymes can contribute to closing the loop for a sustainable plastic economy, even though many actions have to be taken. The first step, of course, would be to avoid or reduce plastic consumption in general and increase efforts for reuse and recycling. As part of efficient waste management, incineration, dumping, and leakage to the environment must be minimized. The inevitable need for new raw material should be covered from biomass or by synthesis with green hydrogen and CO₂ from capturing technologies. Thus, the plastic industry would also reduce its carbon footprint, presenting a necessary contribution to the world's fight against climate change. But even when made from renewable sources, material properties and adverse environmental impacts of Bio-PET, Bio-PE and Bio-PP are identical¹²⁴, emphasizing that bio-based does not implicate biodegradability. Hence, the usage of bio-based plastics with similar benefits

but faster biodegradability must be enforced in the future. And promising candidates are already in the starting blocks: For the low-density PE and PP, polybutylene succinate (PBS) and polybutylene adipate terephthalate (PBAT) are decent substitutes¹²⁵ while polyethylene furanoate (PEF) has similar properties to PET¹²⁶. These materials allow for more rapid biodegradation when intentionally or unintentionally released into the environment.

Enzymes could play an essential role in the future, not only in innovative applications such as pre-incorporation into plastics products to improve degradation after use. But more than that, enzymes are helping decisively with the crucial component of a sustainable circular economy for plastics, namely recycling. With the contribution of enzyme-based recycling, the material properties of circulating plastics materials could be maintained at a high level, complementing traditional thermal recycling. Gradually, plastics will become more biocompatible with their bio-based synthesis from biomass to processing to final degradation. And enzymes do have the potential to contribute and shine in all these disciplines.

4 Synopsis

List of publications in this synopsis:

Weigert, S.; Gagsteiger, A.; Menzel, T.; Höcker, B. A Versatile Assay Platform for Enzymatic Poly(Ethylene-Terephthalate) Degradation. *Protein Engineering, Design and Selection* **2021**, *34*, gzab022. <https://doi.org/10.1093/protein/gzab022>

Menzel, T. and **Weigert, S.**; Gagsteiger, A.; Eich, Y.; Sittl, S.; Papastavrou, G.; Ruckdäschel, H.; Altstädt, V.; Höcker, B. Impact of Enzymatic Degradation on the Material Properties of Poly(Ethylene Terephthalate). *Polymers* **2021**, *13* (22), 3885. <https://doi.org/10.3390/polym13223885>.

Weigert, S.; Perez-Garcia, P.; Chibani, C.; Schmitz, R.; Gagsteiger, A.; Gisdon, F.; Schweinschaut, K.; Ullmann, M.; Chow, J.; Streit, W.; Höcker, B. Investigation of the halophilic PET hydrolyse PET6 from *Vibrio gazogenes*. (DRAFT)

A vital step in investigating PET hydrolyzing enzymes is to establish an experimental setup that allows the assessment of whether and to what extent an enzyme candidate can act on PET. The character of PET as a water-insoluble, massive substrate poses a special challenge that stands out to commonly used soluble substances in biochemical activity assays. Soluble substrate analogs of PET like BHET are available, but as the key feature of PET hydrolases is their ability to act on a massive, hydrophobic substrate, an assay employing a soluble compound can hardly work out these qualities.

As this research project is embedded within the CRC 1357 microplastics, initial trials employing microplastic particles as a substrate for our experiments were logical. However, the hydrophobicity of PET microplastics particles made handling and precise substrate provisioning laborious. And once in solution, particles may either sink due to the higher density than water or float on the surface because of poor wetting properties and air adsorption at the surface. Therefore, varying shares of the substrate were either exposed to air, sticking on the sidewalls of reaction vessels, or accumulating on the bottom, causing differences in the interaction of substrate and enzyme and thereby in the measured activity. In the literature, different approaches have been described for substrate supply in their experiments, including PET films^{96,101,107}, solid pieces from post-consumer plastic^{96,99,107}, or nanoparticles¹²⁷. While the latter are easy to handle and provision, thus suited for high-throughput applications, massive substrates, such as films, demand manual substrate handling, limiting upscaling for high-throughput.

However, nanoplastic particles also have drawbacks as they are fully amorphous, while realistic PET commonly has a high crystallinity known for diminishing enzymatic hydrolysis. Therefore, a fully amorphous nanoplastic substrate might be partially misleading. In our paper “A versatile assay platform for enzymatic poly(ethylene-terephthalate) degradation”, we present a new approach for substrate provisioning with the application of a PET film onto standard lab consumables like microtiter plates (MTP) and PCR tubes. For this purpose, PET is dissolved in trifluoroacetic acid and applied to each well, ensuring equal wetting. By choosing the temperature in the subsequent drying step, the crystallinity of the resulting coating can be adjusted between 10-18%; other values might be possible with drying temperatures outside the tested range. Activity tests with PET degrading enzymes showed successful provisioning of the substrate with decent standard deviations, while differences within the different formats must be considered. The offered options within the assay platform are summarized in the following Figure 11.

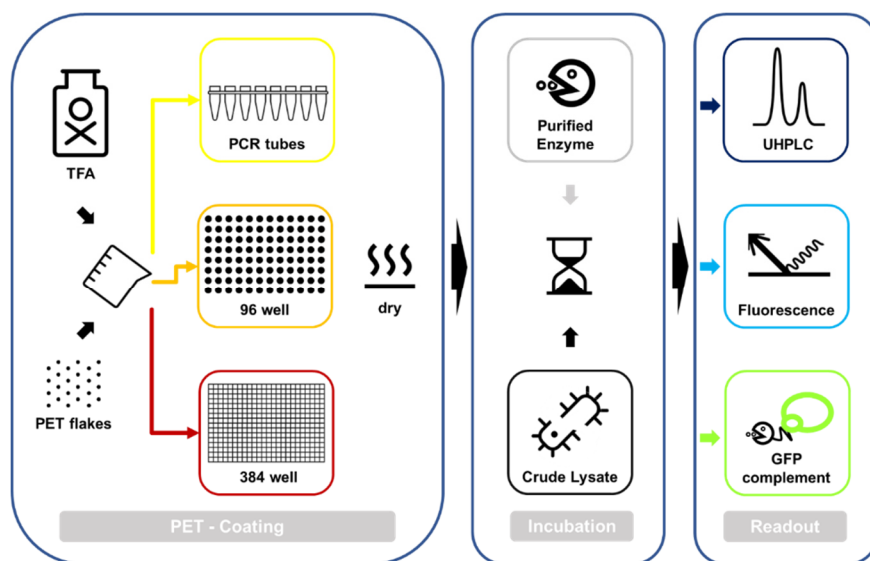


Figure 11 Overview of the modules to choose from within the assay platform. The PET coating can be applied to different lab consumables, including PCR tubes and microtiter plates, while crystallinity is controlled in the drying step. For incubation, the enzyme is either added purified or as lysate. The activity is quantified with either UHPLC or fluorescence readout. Within lysate experiments, the actual enzyme concentration can be determined by a split-GFP system to normalize the measured activity. (Figure taken from Weigert et al., PEDS, 2021, Oxford University Press¹²⁶)

The most consistent results could be achieved at the core wells of a 96-MTP yielding a standard deviation of only 4% therefore suited for analytical experiments, while other formats like PCR tubes show a much higher standard deviation of 15%. However, this PCR format perfectly fits fast and convenient temperature screening by virtue of a thermocycler. This coating approach offers myriad options for the PET starting material such as virgin or recycled PET grades, pre-weathered material (UV radiation, humidity,

et cetera.), and options for supplementation with different additives. In this way, the system can reflect the complexity of PET material types, especially the relevant degradation processes in nature, and their influence and interplay with enzymatic degradation can be systematically investigated. The enzyme can either be added purified or as crude lysate suitable for high throughput applications. The use of crude lysate is complemented by a split green fluorescent protein (split-GFP) system allowing for quantification of expressed enzyme in the cell extract to rank the enzyme's performance relative to their expression level. While developing the crude lysate part of the assay, we encountered problems with an unexpected activity loss of IsPETase and its engineered offspring DuraPETase in lysate. The phenomena could be reproduced with purified enzyme, which also lost activity when lysate was added, indicating an inhibition by lysate compounds. However, LCC-WCCG was unaffected by lysate, suggesting a specific adverse interaction with IsPETase. As demonstrated, this could be resolved by adding Tween20 as detergent enabling the successful use of IsPETase analogs in the crude lysate screening experiments. Nevertheless, the underlying effect remains elusive, and whether this lysate has similar effects on other enzymes and the solution in the form of detergent is also universally working is yet to be found out.

The generation of a fluorescent chromophore for fast readout is based on TPA conversion into the fluorescent chromophore 2-hydroxy terephthalate (HOTP) adopted from Wei *et al.*¹²⁹, but we enhanced this method with the addition of MHETase before the conversion of TPA to HOTP. MHET can present a significant share of the degradation products of PET, depending on the enzyme and reaction conditions. When MHETase further hydrolyzes MHET into TPA, the former share of MHET can also be integrated into the fluorescent readout. In this way, enzymatic degradation is more comprehensively depicted, and the readout method further profits from a higher signal in general. We further developed a speedy method for UHPLC detection of the degradation products with a total runtime of only 4 minutes for low to medium throughput. In summary, this whole assay platform offers many options and adaptations regarding the choice of substrate, incubation, and readout. Thus, it offers a suitable experimental setup for all kinds of questions regarding the activity of PET degrading enzymes.

Consequently, it was the experimental basis for the characterization of a new PET degrading enzyme shown in our work "Investigation of the halophilic PET hydrolase PET6 from *Vibrio gazogenes*". PET6 is an enzyme from the halophile organism *Vibrio gazogenes* and had been previously discovered by Danso *et al.*¹²⁷ using a bioinformatic

search approach to identify new potential PET hydrolases in metagenomic data. However, the choice to investigate PET6 in detail within this project happened by chance. Our underlying idea was to expand the structural knowledge about PET degrading enzymes and find enzymes with novel properties. For this purpose, some enzyme candidates were selected from the work of Danso *et al.*, which stood out for their low sequence identity compared to IsPETase. Under these considerations, PET2, PET6, PET12, PET38, and PET42 were selected and could be successfully purified but for PET42. However, crystallization trials of these enzymes were only successful for PET6 why it was picked for the following study. The crystal structure of PET6 showed, as expected, the typical alpha/beta hydrolase fold but revealed an interesting binding of sodium and chloride ions (Figure 12).

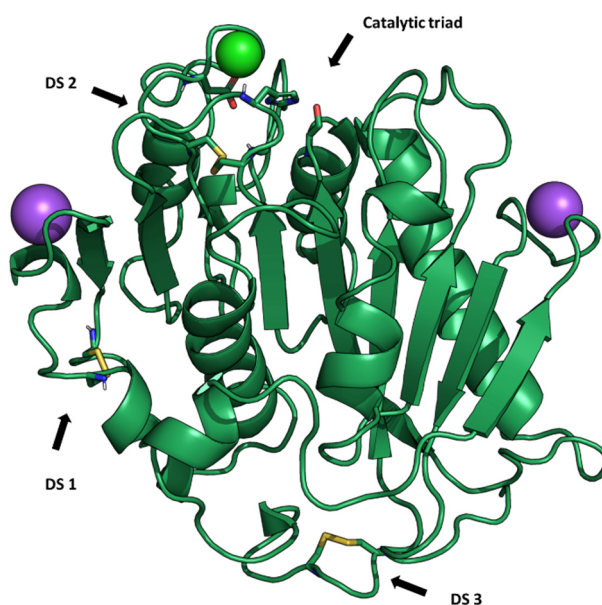


Figure 12 Solved crystal structure of PET6 in cartoon representation. The catalytic triad and the disulfide bonds (DS 1-3) are shown in sticks and are labeled accordingly. The sodium (purple) and chloride (green) ions are depicted as spheres.

In principle, these ion species are no novelty, known for being bound in other cutinase structures. But for those the sodium chloride combination is not that emphasized or is escorted by divalent cations like Ca^{2+} or Mg^{2+} (see Thc_cut1 PDB-ID 5LUI, Cut190 PDB-ID 4WFK, Ta_cut PDB ID 6AID). Many cutinases are specifically enhanced by divalent ions in terms of thermostability and activity, while the activity of PET6 remains unchanged upon the addition of different divalent cations. This indicates an adaptation of PET6 towards an environment with high sodium chloride concentrations stabilizing the enzyme, which seems logical considering its saline origin. Consequently, we could show that sodium chloride has a similar function for PET6 as divalent cations

have for other cutinases regarding stability and activity. The optimal salt concentration is surprisingly high, about 1 to 1.5 M, although higher salt concentrations are also well tolerated.

Interestingly, this is the opposite behavior of IsPETase, which severely suffers in activity from even low salt concentrations. When high salt is combined with its optimal temperature of 50°C, the enzyme can realize decent PET degradation, which outcompetes IsPETase at similar conditions. Nevertheless, this is still below what potent enzymes like IsPETase or LCC can do at optimal conditions. This question of activity was also considered within the study from the perspective of evolutionary potential, i.e., how mutations that may already occur in nature could positively influence the PET degradation capacity of PET6. For this purpose, some residues common in other functional PET hydrolases were introduced. Of these, especially the variant PET6-VSTA shows a substantial increase in activity with only two amino acids being exchanged. This highlights that even minor evolutionary adaptations could significantly improve PET6-mediated PET degradation. MD simulations of this double mutant with a PET tetramer also provided clues on how these mutations might contribute to increased activity. The analysis revealed a more stable and better-coordinated interaction of the substrate around the active site for PET6-VSTA, which might explain the higher turnover compared to the wild type.

Eventually, this raises the typical question of whether these PET degrading enzymes found in nature contribute to PET degradation in the environment. In general, this is hard to answer as PET activity *in vitro* does not necessarily mean similar activity in nature given the complex surrounding. Nevertheless, some theoretical aspects can be used to approach an answer to this question. As a starting point, the organism hosting the enzyme should get in proximity to the corresponding plastic particles. Though, even if this is the case, it is still unclear whether the protein is expressed and exported to contact the material and whether it remains there, considering possible diffusion to the periphery. In addition, the general activity of the specific enzyme under the given environment, including temperature, pH, salinity, and potential naturally occurring inhibitors, must be considered.

For PET6, some facts qualify this enzyme as a worthy candidate. The host organism *Vibrio gazogenes* is like the whole genus of *Vibrio* ubiquitous and abundant in marine systems, including estuaries and salt marshes, as part of the bacterioplankton^{69,130–132}. Additionally, the halophilic character of PET6 qualifies it to be

active under those conditions, though actual activity in seawater is yet to be determined. Within the study, we were also searching for homologs of PET6 in the *Vibrio* genus and successfully found those in three other *Vibrio* species. In addition, nine other members of the genus have homologs for MHETase that may be useful for PET degradation in microbial communities, which is a widespread concept. The proximity of those organisms to plastic is evident as high concentrations of plastic and microplastic particles are documented for estuaries and salt marshes and as oceans are considered a sink for plastics anyway. This coincidence is emphasized by the finding of the *Vibrio* species as part of the plastisphere, which describes the ecosystems naturally forming around plastic particles released into the environment. Nevertheless, the low activity of PET6 at typical ocean surface temperatures well below 30°C must be considered despite the enormous potential biomass of *Vibrios* carrying genes for PET degradation. Though, there is a need for further experiments particularly focusing on actual degradation rates in nature, to assess the actual contribution of PET6 or *Vibrio* species in general.

But as we demonstrated in our publication “Impact of Enzymatic Degradation on the Material Properties of Poly(Ethylene Terephthalate)”, the fate of these plastic particles can also be significantly changed by even subtle degradation events caused by enzymes. Material properties define a material’s behavior during its intended use, but in the same way, they influence its destiny after the end of use when not disposed of properly. For polymers, these properties are tightly linked with the chemical composition of the individual chains, including additives and how these can interact among themselves. Upon degradation, new chemical groups may be introduced, and chain scissions may decrease the average chain length or resolve crosslinks. In this way, these interactions that contribute to the integrity and define characteristics are altered, which in most cases means weakening. We often encounter this phenomenon for the abiotic degradation process when, e.g., a plastic foil becomes so brittle after being exposed to UV light and humidity for years that it falls into pieces upon minimum mechanical force. While the underlying mechanism has also been described for PET, the impact of enzymatic activity on the material properties of the remaining plastic is poorly investigated. As an experimental method to monitor these changes in the material properties, we chose fatigue crack propagation (FCP) which features high sensitivity for even slight changes. This technique applies a dynamic, periodical force to a specimen while the crack growth speed is measured. When certain factors or events weaken the material, this manifests in the measurements as the crack grows faster through the specimen. For the incubation of those specimen, we constructed sample holders that

restrict the contact of solution during incubation to the area of the designated crack growth.

The concept of the experiment was to identify and quantify differences in the crack propagation after the specimen were either incubated in enzymatic solution or buffer only as control after 96 hours. Additionally, after 24 and 48 hours, samples were taken for scanning electron microscopy (SEM) and ultra high performance liquid chromatography (UHPLC) to analyze the timeline of degradation on an optical level and the emergence of soluble products. Without enzyme present, no degradation processes can be detected, but in the other case, a progressing surface erosion in the SEM images is visible backed by increasing concentrations of the soluble degradation products TPA, MHET, and BHET. With increasing incubation time, the roughness of the surface increased, which is observable in the atomic force microscopy measurements and particularly in the SEM images showing the rise of colloidal structures. The latter could result from uneven surface erosion or an accumulation of non-soluble degradation products. Such insoluble degradation products could be identified in differential scanning calorimetry (DSC) measurements of near-surface layers after enzymatic incubation, where a distinct peak for a BHET dimer was detectable. This substance could explain why specimens treated with enzymes show lower tolerance towards mechanical stress. We hypothesized that the BHET dimer diffuses into the material inducing the embrittlement, as seen in the FCP analysis. Moreover, this diffusion of BHET dimers may explain why crack propagation is strongly affected in these samples, while actual enzymatic degradation is limited to an insignificant depth (probably a few μm) at the surface compared to the whole sample material. (4mm) (see Figure 13).

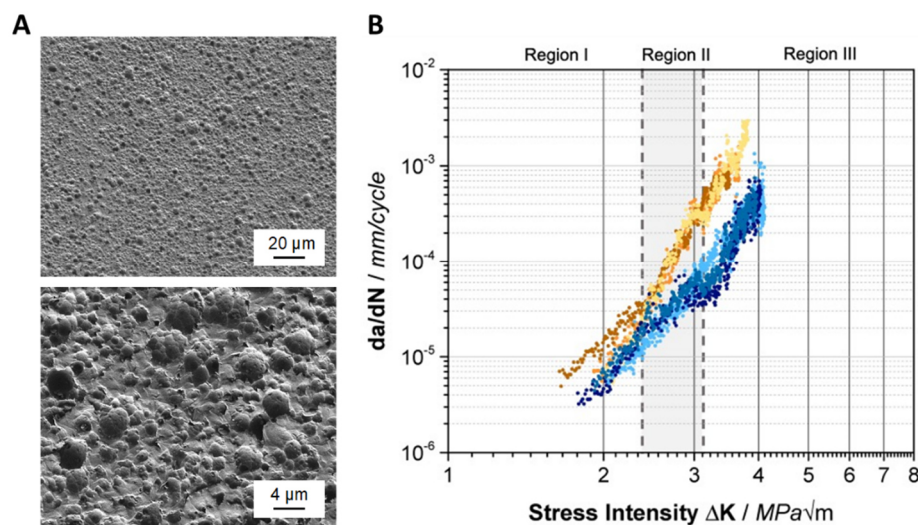


Figure 13 Surface of PET after incubation with IsPETase for 96 hours (A). The resulting rough surface, including colloidal structures, possibly composed of BHET dimer, are shown in two magnifications. The results of the subsequent mechanical analysis of the specimen (figure B) revealed faster crack propagation and thus material failure after enzymatic incubation (orange tones) compared to blank samples without enzymatic treatment (blue tones). (Figure taken from Menzel *et al.*, MDPI Polymers, 2021¹³³)

Similarly, the BHET dimer might also influence the measured crystallinity after incubation. Theoretically, an increased crystallinity would be expected as amorphous regions are easier to be attacked by the PET degrading enzymes and should therefore be preferentially hydrolyzed. However, the crystallinity decreased from 22% to 18% upon enzymatic incubation. This indicates either a direct enzymatic attack on the crystalline regions or again a BHET dimer mediated disruption of those crystalline arrangements. However, apart from the possible effects of the BHET dimer, it is interesting to speculate why this substance is accumulating in the first place. Presented on the surface, one could assume that the enzyme preferably processes this short substrate as it might easily bind in the enzyme's active site due to higher degrees of freedom compared to a more rigid polymer chain. However, efficient binding of the substrate to IsPETase might require more than two repetitive units of PET which could explain the accumulation of the BHET dimer. Future studies must explore whether this behavior is valid for all PET degrading enzymes and further investigate the exact impact of the BHET dimer and the nature of the colloidal structures.

In conclusion, enzymatic activity and its impact might be underrated if only weight loss or soluble degradation products are tracked. Especially in the scope of PET degradation in the environment, enzymatic activity accelerating fragmentation due to the impact on material properties should be considered. Furthermore, as the surface grows exponentially with advancing fragmentation, this creates even more space accessible for

microbial activity. Thus, although the absolute hydrolysis rates on the initial particles might be limited, the enzymatic degradation could have significant downstream effects.

5 List of Publications and Personal Contribution

List of publications as part of this thesis:

Weigert, S.; Gagsteiger, A.; Menzel, T.; Höcker, B. A Versatile Assay Platform for Enzymatic Poly(Ethylene-Terephthalate) Degradation. *Protein Engineering, Design and Selection* **2021**, *34*, gzab022. <https://doi.org/10.1093/protein/gzab022>

The design of this study was led by myself with assistance from Birte Höcker. I further conducted the experiments partially supported by Andreas Gagsteiger, while Teresa Menzel took over the differential scanning calorimetry (DSC) measurements. The analysis of the data, including graphical representation and writing the manuscript, was performed by myself, while all authors contributed to editing the manuscript and provided feedback during the whole study.

Menzel, T. and **Weigert, S.;** Gagsteiger, A.; Eich, Y.; Sittl, S.; Papastavrou, G.; Ruckdäschel, H.; Altstädt, V.; Höcker, B. Impact of Enzymatic Degradation on the Material Properties of Poly(Ethylene Terephthalate). *Polymers* **2021**, *13* (22), 3885. <https://doi.org/10.3390/polym13223885>.

Teresa Menzel and I contributed equally to this paper. The conceptualization and design of the study were done by the two of us guided by Birte Höcker. While Teresa Menzel and Yannick Eich conducted the optical and mechanical characterization of the specimen, I performed the enzymatic incubation of the samples and analysis of soluble degradation products supported by Andreas Gagsteiger. The AFM measurements and associated analysis were done by Sebastian Sittl, who also added corresponding results to the manuscript. Overall manuscript preparation, including analysis and figures, was again done in equal parts by Teresa Menzel and me. Together with Birte Höcker and Andreas Gagsteiger, we led the manuscript's editing and revision. All other authors contributed with feedback and suggestions.

Weigert, S.; Perez-Garcia, P.; Gagsteiger, A.; Gisdon, F.; Schweinshaut, K.; Chibani, C.; Schmitz, R.; Ullmann, M.; Chow, J.; Streit, W.; Höcker, B. Investigation of the halophilic PET hydrolyse PET6 from *Vibrio gazogenes*. (DRAFT)

The conceptualization and design of this study were done by Pablo Perez-Garcia, Jennifer Chow, and myself, supported by Birte Höcker and Wolfgang Streit. Pablo Perez-Garcia contributed to the metagenomic analysis while I conducted all experiments on the performance of the enzyme variants with support from Andreas Gagsteiger in later experiments. While the first batch of PET6 was purified and successfully crystallized by Kristine Schweinshaut under my supervision, I collected the data and solved the crystal structure. The molecular dynamic simulations were planned by me together with Florian Gisdon, who conducted the calculations

and analysis. Manuscript preparation was led by myself together with Pablo Perez-Garcia, supported by Jennifer Chow, Birte Höcker, and Wolfgang Streit through editing and feedback also over the whole study.

Further publications:

Zhang, H.; Pérez-García, P.; Dierkes, R. F.; Applegate, V.; Schumacher, J.; Chibani, C. M.; Sternangel, S.; Preuss, L.; **Weigert, S.**; Schmeisser, C.; Danso, D.; Pleiss, J.; Almeida, A.; Höcker, B.; Hallam, S. J.; Schmitz-Streit, R. A.; Sander HJ Smits, S. H.J.; Chow, J.; Streit, W. R. The Bacteroidetes *Aequorivita* sp. and *Kaistella jeonii* produce promiscuous esterases with PET-hydrolyzing activity. *Frontiers in Microbiology and Microbiotechnology* **2021**. <https://doi.org/10.3389/fmicb.2021.803896>

Muller, Y. A.; Häge, S.; Alkhashrom, S.; Höllriegel, T.; **Weigert, S.**; Dolles, S.; Hof, K.; Walzer, S. A.; Egerer-Sieber, C.; Conrad, M.; Holst, S.; Lösing, J.; Sonntag, E.; Sticht, H.; Eichler, J.; Marschall, M. High-Resolution Crystal Structures of Two Prototypical β - and γ -Herpesviral Nuclear Egress Complexes Unravel the Determinants of Subfamily Specificity. *Journal of Biological Chemistry* **2020**, *295* (10), 3189–3201. <https://doi.org/10.1074/jbc.RA119.011546>.

Bartoschik, T.; Galinec, S.; Kleusch, C.; Walkiewicz, K.; Breitsprecher, D.; **Weigert, S.**; Muller, Y. A.; You, C.; Piehler, J.; Vercruyse, T.; Daelemans, D.; Tschammer, N. Near-Native, Site-Specific and Purification-Free Protein Labeling for Quantitative Protein Interaction Analysis by MicroScale Thermophoresis. *Sci Rep* **2018**, *8* (1), 4977. <https://doi.org/10.1038/s41598-018-23154-3>.

6 Appending Publications

Original Article

A versatile assay platform for enzymatic poly(ethylene-terephthalate) degradation

Sebastian Weigert¹, Andreas Gagsteiger¹, Teresa Menzel², and Birte Höcker^{1,*}

¹Department of Biochemistry, University of Bayreuth, Universitätsstraße 30, 95447 Bayreuth, Germany, and

²Department of Polymer Engineering, University of Bayreuth, Universitätsstraße 30, 95447 Bayreuth, Germany

*To whom correspondence should be addressed. E-mail: birte.hoecker@uni-bayreuth.de

Received 3 June 2021; Revised 29 July 2021; Editorial Decision 5 August 2021; Accepted 5 August 2021

Abstract

Accumulation of plastic and subsequent microplastic is a major environmental challenge. With the discovery of potent polyethylene terephthalate (PET)-degrading enzymes, a new perspective arose for environmental decomposition as well as technical recycling. To explore the enormous diversity of potential PET-degrading enzymes in nature and also to conveniently employ techniques like protein engineering and directed evolution, a fast and reliable assay platform is needed. In this study we present our versatile solution applying a PET coating on standard lab consumables such as polymerase chain reaction tubes, 96- and 384-well microtiter plates, yielding an adjustable crystallinity of the PET. Combining the reaction vessels with either ultra-high performance liquid chromatography (UHPLC) or fluorometric readout and additional enzyme quantification offers a range of advantages. Thereby, the platform can easily be adapted to diverse needs from detailed analysis with high precision to high-throughput (HT) applications including crude lysate analysis.

Key words: assay platform, PET-degrading enzymes, PETase, screening

Introduction

The rise of plastic materials in the 20th century has undoubtedly revolutionised our world. With their novel properties and features they enabled profound progress in nearly every aspect of life making plastic a remarkable success story. But some of these outstanding properties, especially the chemical and physical durability, lead to major drawbacks. With a total plastic production of 369 million tons in 2019 (PlasticsEurope, 2020) and typical global rates for incineration and recycling being as low as 24% and 14–18%, respectively (OECD, 2018), a large share ends up in landfills or in the environment. While this process is ongoing ever since the invention of plastics, public awareness has only been rising during the 2010s and it is now seen as one of the major challenges of our times. To solve this problem, it has to be tackled from manifold perspectives including strategies for reducing consumption and efficient ways for disposal and recycling (Prata *et al.*, 2019). While incineration and to some extent also dumping in landfills present an effective way to prevent leakage into the environment, it is also an unnecessary waste of resources. Yet recycling is not widespread as it is largely

intensive in means of cost and energy, depending on the polymer type. Furthermore, the recycled product might not always stand up to the virgin material in terms of material properties (Brouwer *et al.*, 2020; Shen and Worrell, 2014).

The discovery of plastic-degrading enzymes opens up new possibilities for contributing to recycling and biocompatible decomposition for some common plastics, in particular for polyethylene terephthalate (PET) (Wei *et al.*, 2020). Since the first finding of PET-degrading enzymes like TfCut from *Thermobifida fusca* (Müller *et al.*, 2005), many other PETases were reported (Herrero Acero *et al.*, 2011; Hu *et al.*, 2010; Kawai *et al.*, 2014; Sulaiman *et al.*, 2012). These enzymes were affirmed as cutinases and found to share the overall topology of the $\alpha\beta$ hydrolase fold (Ollis *et al.*, 1992). A significant step was the discovery that *Ideonella sakaiensis* features a two-enzyme system where a PETase (IsPETase) degrades PET primarily into mono-(2-hydroxyethyl)terephthalic acid (MHET), whereas an MHETase takes on the final cleavage into terephthalic acid (TPA) and ethylene glycol (Yoshida *et al.*, 2016). This pathway enables the organism to use PET as its main carbon and energy source, by which

this topic gained a whole new dynamic. IsPETase was not only the first enzyme to exhibit reasonable activity at ambient temperatures around 30°C, but it also demonstrated the potential of this enzyme class for PET degradation. Consequently, several studies applied protein engineering on the IsPETase or on other promising cutinases, like leaf and branch compost cutinase (LCC), and yielded the DuraPETase (Cui et al., 2021) or engineered LCC variants (e.g. LCC-WCCG) (Tournier et al., 2020) with impressively improved activity and stability (Austin et al., 2018; Son et al., 2019). Nevertheless, there is a great need for adaptations towards other scenarios and conditions such as stability to solvents, salts or improved activity on PET with a higher degree of crystallinity (Kawai et al., 2019; Wallace et al., 2020). To explore and expand this world of PET-degrading enzymes, including new variants to be found in nature, an effective screening platform is paramount. The first component for such a system is the substrate where either model substrates like 3PET (Herrero Acero et al., 2011; Ribitsch et al., 2011) and other polyesters have been used or PET in the form of films and solids with varying crystallinity (Kawai et al., 2014; Müller et al., 2005; Yoshida et al., 2016) or amorphous nanoparticles (Danso et al., 2018; Pfaff et al., 2021; Wei et al., 2012). Depending on the chosen substrate different readout methods can be employed such as weight loss for solid substrates (Müller et al., 2005; Yoshida et al., 2016), zone of clearance in agar plates containing nanoparticles (Danso et al., 2018), change in turbidity (Belisário-Ferrari et al., 2019; Wei et al., 2014) or absorbance (Zhong-Johnson et al., 2021) and not to forget the gold standard high performance liquid chromatography (HPLC) for direct detection of the degradation products MHET, TPA and bis(2-Hydroxyethyl) terephthalate (BHET) (Ribitsch et al., 2011). While the aforementioned methods have to trade-off between throughput and accurate quantification, the fluorescent determination of TPA after conversion to 2-hydroxy-terephthalate (HOTP) via the Fenton reaction meets both requirements (Wei et al., 2012). In a recently published study, this method combined with PET nanoparticles demonstrated its general functionality also in lysate emphasising the suitability for HT screening (Pfaff et al., 2021). Here we now present a PET degradation platform where a semi-crystalline PET coating on standard lab consumables offers fast and handy substrate provisioning. This is combined with two possible options for activity measurements, namely UHPLC and fluorescent HOTP readout. Additionally, the lysate capabilities of the assay were optimised including the successful integration of a split green fluorescent protein (split GFP) system (Cabantous et al., 2005) for enzyme quantification to level out varying expression levels in lysate-based experiments (Santos-Aberturas et al., 2018). This makes the platform an advanced and versatile tool for investigating PET-degrading enzymes.

Material and methods

Coating

To have a substrate that is realistic and close to environmental conditions, clean post-consumer CleanPET® FK from Veolia Umweltservice GmbH (Germany) was used. The parameters of the starting material were determined as $M_n = 30.155 \text{ g/mol}$ and dispersity $\bar{D} = 1.8$. The PET powder was dissolved in trifluoroacetic acid (TFA, Carl Roth, Germany) at a concentration of 1 or 2% (w/v) and filtrated through a syringe filter (ROTILABO® polyvinylidene fluoride [PVDF], 0.22 µm, 30 mm; Carl Roth Germany). For polymerase chain reaction (PCR) tubes (PCR Kombi 8er Strips, 0.2 ml, polypropylene, Biozym Scientific GmbH, Germany) and 96-well plates (Nunc 96

flat bottom, transparent or black, non-treated, polystyrene, Thermo Fisher Scientific), 25 µl of PET solution was used per well and 20 µl for 384-well plates (Nunc 384 flat bottom, transparent, non-treated, polystyrene, Thermo Fisher Scientific; Microplate pureGrade 384-well, PS, standard, black, Brand GmbH, Germany), respectively. PCR tubes were placed in a bottomless rack during the coating procedure. A polytetrafluoroethylene (PTFE) lid was used to seal the vessels during wetting. In this process the vessels were tilted almost 90° upwards and rotated three times so that the PET solution wetted the walls of the vessel. Then, they were placed on a paper towel to drain excess solution for 90 s. This was immediately followed by a drying step, where the coated vessels were carefully dropped in a water bath heated to 63°C and dried for 20 min. Here the plates or racks shall float on water surface while water must not get in contact with the drying PET coating. Under the given conditions, PVDF (Dyneon - 3M Innovation, 2004) and PTFE (Colder Products Company, 2010) are resistant to TFA, ruling out unwanted contamination of the coating.

Thermal characterisation (polymer)

The degree of crystallinity of the polymer film was investigated by differential scanning calorimetry (DSC) using a Mettler Toledo DSC I (Mettler-Toldeo GmbH, Gießen, Germany). Therefore, a PTFE sheet was coated under identical conditions as the labware vessels. From this flat PTFE surface, the coating could be more easily removed compared with the polystyrene surface of the microtiter plates (MTP) or the PCR tubes. About 5 mg of the scraped-off material was used for analysis. The samples were heated with 10 K/min under N₂-atmosphere from 25 to 300°C (first heating run) and cooled to 25°C again after an isothermal stage of 5 min at 300°C. To calculate the degree of crystallinity χ_c , a fusion enthalpy of $\Delta H_m^\circ = 140.1 \text{ J/g}$ for a hypothetically 100% crystalline PET was used, according to literature (Wunderlich, 2005). For the final value, the degree of crystallinity c_{cryst} caused by amorphous phase crystallisation at a temperature around 125°C was subtracted. For each temperature, coating and subsequent DSC analysis were done in triplicates.

Differential scanning calorimetry

The stability of DuraPETase was investigated by a DSC analysis. For this purpose, the protein was dialysed against assay buffer (50 mM NaCl, 50 mM Borate pH 8.5) and diluted to a final concentration of 1 mg/ml. Before applying the sample, the instrument (Malvern Microcal PEAK DSC) was thermally equilibrated with buffer–buffer runs. The scanning range was set to 40–95°C with a speed of 120 K/h.

Enzymatic incubation and sample preparation

The enzymes were diluted in reaction buffer (50 mM sodium borate, 50 mM NaCl, pH 8.5) to a standard concentration of 200 nM. Depending on the vessel type 50 or 15 µl of enzyme solution or buffer only for blank samples were added per well for PCR tubes/96-well MTP and 384-well MTP, respectively. The plates were sealed with seal mats (Thermo Scientific WebSeal) or strip caps for PCR tubes. Incubation times were 18 h at 30°C or 1.5 h at 60°C for standard experiments. These parameters can easily be adjusted to fit the desired experimental question or to compensate general deviant enzyme performance. After incubation, the sample preparation according to the desired readout method was done directly in the corresponding vessel; for PCR tubes the solution was afterwards transferred to an MTP plate.

For lysate samples, pellets from *Escherichia coli* cultures (T7 Shuffle, New England Biolabs), not carrying a PET hydrolase coding plasmid, were resuspended in assay buffer (50 mM NaCl, 50 mM Borate pH 8.5) with 1 g wet weight pellet per 400 ml buffer 1:400 (w/v). The cells were sonified and subsequently centrifuged for 25 min at 4800 × G to gain the clarified lysate samples from the supernatant. Further handling was analogous to the buffer-based samples.

UHPLC—sample preparation

To prepare the samples for subsequent analysis, four parts UHPLC sample prep mix (acetonitrile + 1% formic acid) were added per part sample into the reaction vessel. The mixture was inverted several times and centrifuged at 4800 × G for 15 min.

Fluorescence—Fenton readout—sample preparation

Five parts of sample (e.g. 50 µl) were mixed with eight parts of fluorescence buffer (100 mM borate, 50 mM NaCl, 1.4 mM ethylenediaminetetraacetic acid (EDTA)) (e.g. 80 µl) containing 325 nM MHEase. The solution was incubated for 10 min at room temperature before two parts Fe(II)sulphate (e.g. 20 µl) with a concentration of 18.8 mM were added followed by another 10-min incubation step at room temperature.

Determination of product formation

UHPLC—analysis

The prepared samples (see above) were analysed on a Thermofisher Ultimate 3000 RS system equipped with a reversed phase C18 column (Kinetex 1.7 µm EVO C18, 100 Å, 50 × 2.1 mm, Phenomenex). The method describes a multi-slope gradient with a flow rate of 1.3 ml/min starting at 100% A (water + 0.1% TFA) increasing solvent B acetonitrile in the following pattern: 0.04 min 15%, 0.4 min 20%, 0.75 min 50%, 0.95 min 80%, 2.1 min 80%. In total, 1 µl of samples were injected to the column; absorption was measured at 240 nm at a rate of 200 Hz.

Fenton—fluorescence readout

The detection of HOTP generated from TPA was done with a Tecan Spark (Tecan Group AG) plate reader. Excitation was set to 315 and 430 nm for emission at a bandwidth of 15 and 30 nm, respectively. Gain was manually fixed at 60, whereas Z-position was chosen for the actual MTP type. Calibration was done individually for every vessel type and experimental setup configuration. The data could only be fitted sufficiently with a polynomial model of degree three. Fitting and subsequent inverse calculation of concentrations were done in R (R Foundation for Statistical Computing, 2020).

Enzyme quantification with GFP complementation

For measuring the enzyme concentration 10 µl of the analyte solution containing the enzyme fused to GFP11 (Cabantous *et al.*, 2005) was added to 90 µl GFP1-10 in TRIS-NaCl-glycerol (TNG) buffer (100 mM NaCl, 50 mM tris(hydroxymethyl)aminomethane (TRIS) 10% glycerol pH 7.5) in a black 96-well MTP, after short mixing the wells were sealed and incubated in the dark at room temperature for 18 h. The fluorescence of the reconstituted GFP was then measured in a plate with excitation at 475 nm and emission at 510 nm with a bandwidth of 20 nm each. The data were fitted with linear model. Fitting and subsequent inverse calculation of concentrations were done in R (R Foundation for Statistical Computing, 2020).

Protein production and purification

The gene sequences for the enzymes and GFP(1–10) were cloned into a pET21 (Merck Millipore Novagen) via Gibson assembly (Gibson *et al.*, 2009); similarly, the MHEase gene (residues 41–603) was cloned into a pMAL-p4x (New England Biolabs) vector in which the MBP sequence was replaced by the mauC signal peptide for periplasmic expression. T7 Shuffle (New England Biolabs) cells were chemically transformed with the enzyme harbouring plasmids, and BL21 (Merck Millipore Novagen) was used for GFP(1–10), respectively. The protein sequences as encoded by the plasmids are shown in Table S1. The main cultures were grown in terrific broth (TB) media at 37°C until an optical density at 600 nm (OD₆₀₀) of 1.5 was reached, then the temperature was lowered to 18°C and protein expression was induced with 300 µM isopropyl β-d-1-thiogalactopyranoside (IPTG). Cells were grown for 18 h and harvested by centrifugation at 5000 × G. The pellet was resuspended in binding buffer (300 mM NaCl, 50 mM phosphate, 50 mM imidazole, pH 7.4) with 10 ml/g wet weight cells followed by sonification. Before loading the lysate onto a Cytivia HisTrap 5 ml column, cell debris was removed by centrifugation for 1 h at 50 000 × G and vacuum filtrated through a 0.22-µm filter. After washing, the protein was eluted from the IMAC column with a linear gradient of elution buffer (300 mM NaCl, 50 mM phosphate, 400 mM imidazole, pH 7.4). The purification of the enzyme variants was finalised with a size exclusion run on a Cytivia Superdex 26/600 75 pg (buffer: 150 mM NaCl, 25 mM 4-(2-hydroxyethyl)-1-piperazineethanesulfonic acid (HEPES), pH 7.4). The proteins were concentrated to 200–300 µM to prepare aliquots of 100 µl, which were flash frozen until further use. After IMAC, GFP(1–10) was dialysed against TNG buffer (100 mM NaCl, 50 mM TRIS 10% glycerol pH 7.5); similarly, aliquots were flash frozen and stored until further use.

Results and discussion

Overview

First, we want to present an overview of our PET assay platform (Fig. 1). The first aspect is the supply of PET as substrate in the platform. With the application of a PET film inside the reaction vessel, this resembles a realistic PET substrate in geometry and size of typical microplastic particles, which are defined as >5 mm in size. The choice for post-consumer PET from recycled bottles as starting material emphasises the life-like scenario in this assay. Additionally, the absence of PET powder or PET nanoparticles prevents potential interference in subsequent measurements.

For the coating process itself, the PET is dissolved in TFA and applied to the reaction vessels where we used either strips of PCR tubes or MTPs in the 96- or 384-well format. In the drying process, the crystallinity of the resulting PET film can be controlled through temperature in the drying step. The enzymatic PET degradation can be conducted in two ways by either using purified enzyme or adding crude lysate. The latter is time-saving and particularly useful when it comes to screening of several variants up to whole libraries in the scope of protein engineering and directed evolution.

For the readout of the enzyme performance two methods can be chosen that show different advantages. While UHPLC/HPLC is very accurate and robust, it is comparably slow and not recommendable for crude lysate application as contaminants may impair the systems lifetime. For this case, the fluorometric readout employing the Fenton reaction offers a complementary option with capability to quantifying TPA as degradation products also in lysate and in

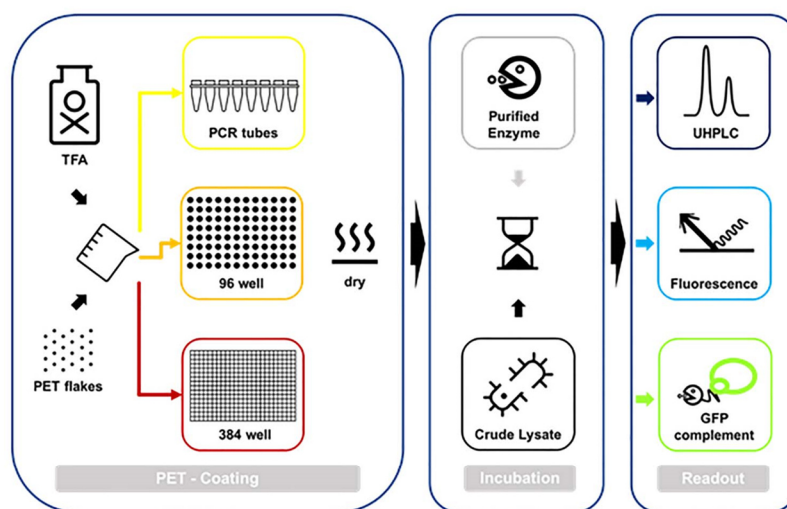


Fig. 1 Schematic overview of the assay platform; selectable options are represented in coloured tiles. For coating, PET powder is dissolved in TFA and then applied on either PCR tubes or MTPs in the 96- or 384-format, whereas crystallinity is determined by the temperature in the drying step. Either purified enzyme or crude cell lysate can be used for the PET degradation screening. In case of purified enzyme, product release can be measured precisely with UHPLC or by fluorescence employing the Fenton reaction to detect TPA. In the option of crude lysate GFP complementation can be used to determine the enzyme concentration.

a high-throughput manner. But this limitation on detecting TPA leads to inaccuracies as most PETases have MHET as their main degradation product, and ratios between TPA and MHET may vary on experimental conditions. Therefore, the supplementation of MHETase in the sample preparations improves the depiction of the whole PET degradation process as MHET is converted into accessible TPA, which leads further to a stronger signal. In the regime of lysate, a normalisation step is useful to rank the performance of the individual variant to its expression level. For this purpose, the option to quantify the enzyme concentration with the split-GFP complementation system was implemented.

Coating

The basis for the assay is the generation of the PET coating on the inside of the reaction vessels. Therefore, PET (in this case post-consumer PET from bottles; Veolia clean PET) was dissolved in TFA before it was applied on the different plastic consumables. Excess liquid was afterwards drained for a certain amount of time (dripping time) before the vessel was placed in a water bath for controlled drying. The material properties and performance, especially to achieve a uniform coating result with low standard deviation, is defined by an interplay of PET concentration and dripping time (Fig. 2).

The performance of the different coating conditions was ranked employing a standard setup with 200 nM DuraPETase at 60°C for 1.5 h; the degradation products (TPA, MHET, BHET) were measured by UHPLC and summed up to a total product release value for each well. At least 60 replicates were used for calculating average and standard deviations; moreover, the results from different batches of the coating were checked for consistency.

Figure 2 demonstrates the influence of the different parameters and depicts the optimisation steps that led to the improved standard coating procedure. For the PET concentration there is a large

difference between 1% and 2% in the product release of 0.9–2.2 mM while higher amounts of PET do not increase the performance but the standard deviation (Fig. 2A). Consequently, we assume that 2% PET and higher leads to a complete surface coverage as the total product release is constant. As liquid handling is more convenient with lower percentage solutions, 2% PET presented the best option. The best corresponding dripping time for the 2% PET solution yielding the lowest standard deviation was found to be 90 s (Fig. 2B), whereas shorter times were ruled out in previous experimental series (data not shown). These optimisations were conducted for each vessel type individually, but 2% PET solution and 90-s dripping time showed the best results in each case. Thus, this parameter combination was chosen as the standard coating procedure, dried at 63°C if not stated differently (Fig. 2C). The most uniform coating can be achieved in 96-well MTPs with an average total product release of 2.0 mM and a standard deviation of 8.0% (Fig. 2C). If the outer rim of wells is not taken into account, the standard deviation can be further lowered to 3.8% for the core segment with an average of 2.2 mM. This is probably due to different thermal interaction in the water bath of the rim wells. The 384-well MTPs behave similar with an average total product release of 1.0 mM and a standard deviation of 13.6%, and 9.0% for the core, respectively. The lowered total product release in this case can be explained by a different ratio of coated surface to volume during the enzymatic incubation while standard deviation is probably higher due to general lower accuracy for handling liquids in lower volumes. The coating of the PCR tubes shows an average total product release of 0.4 mM with a relatively high standard deviation of 14.9%. The latter is likely due to the conical shape of the vessel that makes even wetting and dripping more challenging compared with the other types. Despite their high standard deviation, the PCR tubes are particularly useful for fast characterisation of enzymes at different temperatures employing a PCR thermocycler with temperature gradient option.

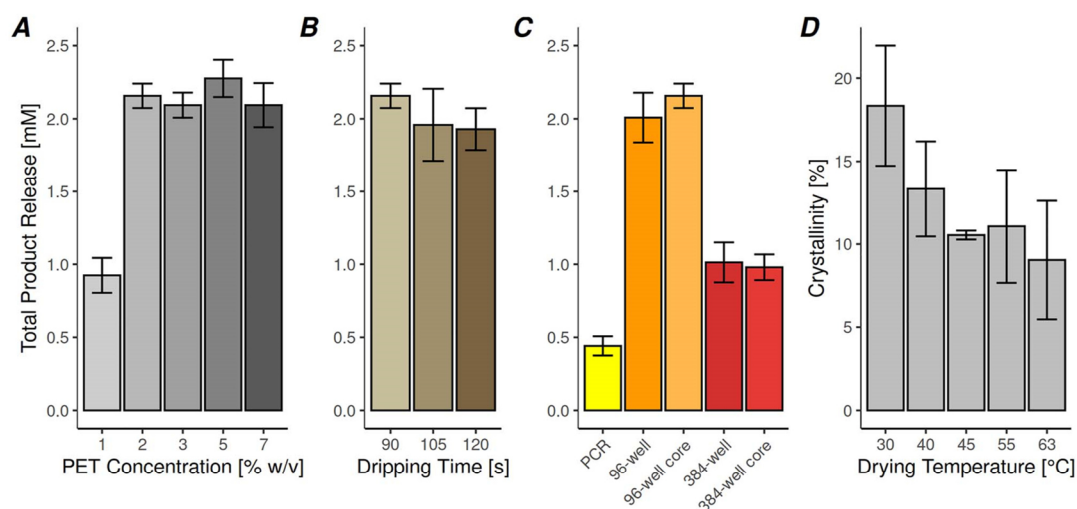


Fig. 2 Parameter screening for an optimised coating procedure. (A) and (B) show how PET concentration and dripping time during the coating influence the average total product release and standard deviation upon enzymatic degradation, when drying temperature was kept at 63°C. (C) displays the final results for all vessels with the new optimised standard parameters: 2% PET, 90-s dripping time and drying at 63°C. Excluding the edge rows of MTPs reduces the standard error (core) as shown in lighter colours. (D) shows the impact of the drying temperature on the resulting crystallinity of the coating calculated from three replicates.

The standard temperature used in the drying step of the coating was 63°C, pragmatically chosen roughly 10°C below the boiling point of TFA. This yielded a sufficiently low crystallinity of the PET, which is accessible for enzymatic degradation. To investigate and eventually influence this process, we propose that higher temperatures lead to faster evaporation of the solvent offering the PET fibres less time to order into crystalline regions. This is similar to quenching during the cooling of polymers (Demirel *et al.*, 2011). For characterisation of the material properties including crystallinity, gaining samples in the way of removing PET coating from a polystyrene surface turned out to be laborious to impossible, especially from the inner walls of the vessels. Therefore, a PTFE sheet was coated with the same procedure, from which PET could easily be removed and analysed with DSC (Fig. 2D).

The results show that lower temperatures result in a higher degree of crystallinity in the coating, with up to 18% at 30°C. With increasing temperatures, the crystallinity decays leading to a low crystallinity PET film with 9% at a temperature of 63°C. Although the coating for this analysis was done on a PTFE surface, we assume that the material properties of the PET coating are similar on the polystyrene labware due to identical thermal treatment controlling crystallinity. The rather high standard deviation in this analysis can probably be attributed to the unprecise coating procedure of the PTFE setup. The flexible and soft surface of the thin PTFE sheet combined with its anti-adhesive character makes the subsequent removal of the very thin PET film possible. But this flexibility leads to a slightly rugged surface where the PET solution cannot be as evenly distributed compared with the labware. This results in fuzzy edges, presumable slight differences in thickness of the film, and eventually to probably higher fluctuations in the measured crystallinity. Therefore, this coating on PTFE can only serve as a workaround to get an adequate estimate of the resulting crystallinity since the removal of actual coating from labware itself was not feasible. In the controlled coating procedure of the lab consumables, a uniform crystallinity can be assumed, reflected by the

low standard deviation during the enzymatic tests (Fig. 2C) which is only possible when all wells present a PET substrate with highly similar crystallinity. This demonstrates the modifiability of the PET substrate to fit the needs for specific experiments, depending on the number of planned samples, vessel type, accuracy and crystallinity.

Fluorometric quantification of TPA and enzyme concentration

The principle of converting TPA into fluorescent HOTP to quantify PET esterase activity has been employed by other studies before. However, they had the general limitation that only TPA was monitored while the main degradation product MHET was not considered. The fact that the ratio between TPA and MHET differs upon experimental conditions adds to this problem. This can easily be addressed by adding the enzyme MHETase in the preparation process where first EDIA and then FeSO₄ are added to promote the conversion from TPA to HOTP. Thus, the EDTA solution was supplemented with 200 nM MHETase and we could confirm a complete enzymatic conversion of even high amounts of MHET after 10 min. The concentration of EDTA and FeSO₄ were optimised for our setup to cover a broad dynamic range for our readout.

The calibration curves show good correlation between measured fluorescence employed TPA amount for both MTP formats and in lysate (Fig. 3A). As the solution column is higher in the 384-well MTP due to the geometry and volume, the signal is slightly higher compared with the 96-well MTP. The signal of the lysate series is in general lower, but the gain was increased to match the values of the other conditions at lower TPA concentrations and to exploit the full dynamic range of the plate reader. All curves show a saturation behaviour with near linear shape only at very low concentrations. In lysate this flattening effect is less pronounced, which is probably due to beneficial effects of the Tween20 component (see section Application examples below). Hence, it might be generally worth looking into

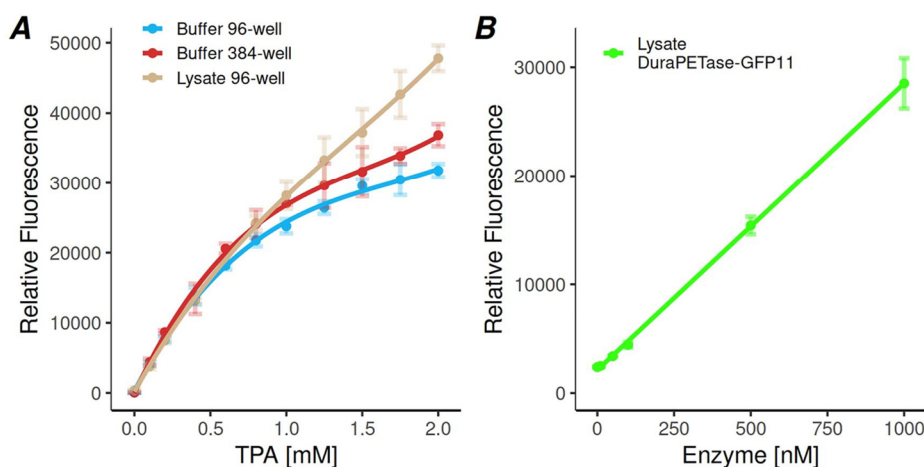


Fig. 3 Calibration curves for fluorometric readouts. **(A)** shows the fluorescence signal for HOTP after the Fenton conversion of TPA at various concentrations. The buffer calibration for the 96- and 384-well MTP are shown in blue and red; the calibration in lysate in beige. **(B)** shows the fluorescence signal of DuraPETase-GFP11 after GFP complementation for different enzyme concentrations in lysate (green).

adding Tween20 before carrying out the Fenton reaction, depending on the individual needs of the user. Taken together this shows that the fluorometric Fenton readout could be robustly integrated in this assay platform for both buffer and lysate, offering a broad dynamic range with a strong and reliable signal.

The split GFP system is a convenient way to monitor expression in general and expression levels directly in our assay, and with this allows better ranking of the enzymes performance independent from the concentration in the lysate. The appendix of the GFP11 fragment at the N-terminus of the enzyme with a (GS)_{17x}-linker in between does not influence the enzymes performance as the average product release for DuraPETase with 1.57 mM (± 0.04 mM) and 1.58 mM (± 0.04 mM) for DuraPETase-GFP11 was unaltered. Thus, we can assume that this type of construct will work also with other PET-degrading enzymes as they all share the same overall topology. Figure 3B shows the calibration curve for a GFP complementation in lysate. Unlike the readout from the Fenton reaction, it shows a linear correlation between employed enzyme and signal. The signal is very stable and true to expectation with increasing standard deviation even at very high enzyme concentrations. Hence, this system is qualified to check for soluble expression as well as for determination of the enzyme concentration.

Application examples

Enzymatic test with different expression levels in lysate

To validate the assay platform under realistic conditions, a test scenario was set up with lysate containing different levels of enzyme ranging from 0 to 1000 nM. For a typical lysate in this assay, we assumed a ratio of 1:400 (w/v) of wet pellet weight to buffer, which would result in a final enzyme concentration of roughly 100–200 nM according to our typical protein expression yields for these enzymes. Therefore, this resembles an experiment with crude lysate where differences in measured activity should be correlated to the measured enzyme concentration. The results can be seen in Figure 4A–C.

The activity that was measured via the fluorescence of HOTP and thereby represents the release of TPA and MHET confirms the expected results. At concentrations of 0 and 10 nM enzyme,

the signal is below the detection limit of ~ 10 μ M HOTP in this setup. While the activity of the LCC variant grows rapidly with increasing enzyme concentrations, the turnover of DuraPETase scales less with the applied enzyme amount with significant release only above 100 nM. This clearly demonstrates the higher performance of LCC-WCCG over DuraPETase. For 500 and 1000 nM enzyme the turnover for both enzymes seems to approach a plateau somewhere above 2 mM HOTP. As this is not the limit for product release upon substrate depletion, which we estimate to be ~ 2.7 mM total product release, this is probably due to substrate accessibility. Especially the shrinking of amorphous regions upon preferred enzymatic attack might play a role for the stagnating PET degradation rate (Wei et al., 2019). The GFP complementation for enzyme quantification of DuraPETase is shown in Figure 4B. The concentrations calculated from the fluorescent readout fit on the ideal line, illustrating that this method determines the present amount of enzyme with high accuracy. The maximum deviation was 7% at 1000 nM, which is considered a minor difference that is to be expected between calibration and an actual measurement.

While testing this assay we encountered an unexpected situation as we observed that IsPETase as well as the engineered DuraPETase did not work in lysate as expected. With the only difference being the presence of the lysed *E. coli* cells in the ratio of 1:400 (w/v), the total product release of DuraPETase (200 nM, 1 h at 60°C) dropped from 1.5 mM to nearly zero (Fig. 4C). The LCC-WCCG in contrast seems to be unaffected in its activity by lysate ruling out a general problem within this setup under lysate regime. For the assay's intended use to identify potentially new PET-degrading enzymes, the unknown compatibility status with lysate of these new variants would comprise a major drawback. To overcome this problem, we identified Tween20 as a compound to partially restore the activity of IsPETase and DuraPETase by presumably disrupting unwanted interactions between lysate and enzyme. The optimum was found to be a final concentration of 0.15% Tween20 where 42% of the activity of DuraPETase is retrieved, whereas LCC-WCCG shows no significant effect on the addition of the detergent in lysate. To investigate how Tween20 influences the performance, we further

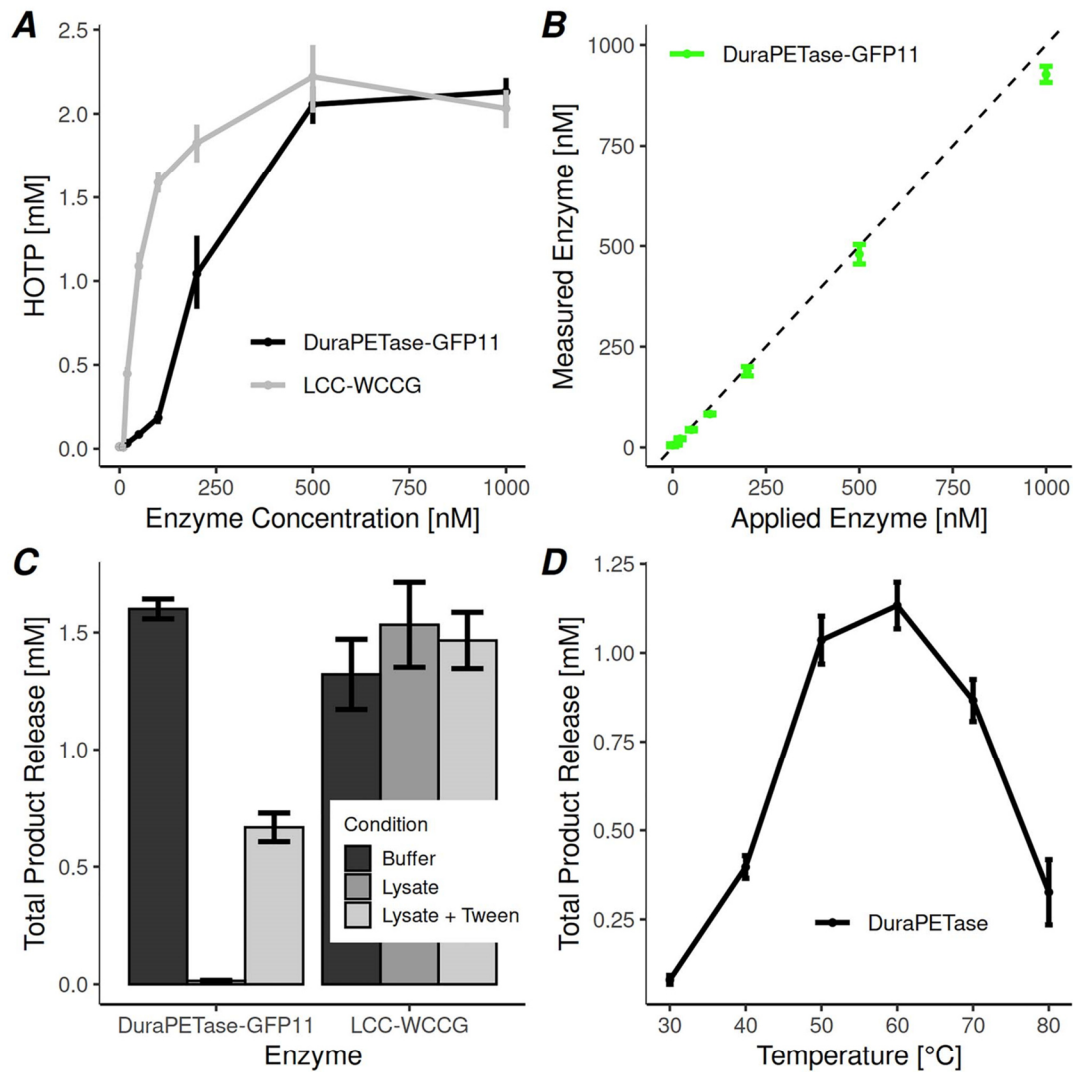


Fig. 4 Practical application of the assay platform: DuraPETase and the LCC-WCCG variant were tested in lysate at different enzyme concentrations for 1.5 h at 60°C (A-C). (A) shows the resulting activity for the respective enzyme concentration, whereas (B) compares the applied enzyme concentration to the concentration measured via GFP complementation (green) for DuraPETase-GFP11, the ideal match is represented as a dashed line. (C) shows the activity of 200 nM of the respective enzyme in buffer and in lysate with and without 0.15% Tween20. The performance of DuraPETase (200 nM) at different temperatures measured in buffer is shown in (D).

tested both enzymes in buffer with different Tween20 concentration ranging from 0.0 to 0.3% (Fig. S1A). For LCC the activity improves in the presence of Tween20 up to ~50% at 0.1%. On the contrary, DuraPETase is losing activity when increasing Tween20 concentration with only 11% relative activity left at 0.3% Tween20 (Fig. S1A). So, we can conclude that the rescue of activity in lysate of DuraPETase by Tween20 is not due to a potential boost of activity by detergent (Furukawa *et al.*, 2018), mediating the enzyme substrate interaction, but is probably a specific interaction between lysate and Tween20. A possible explanation could be the presence of compounds in the

lysate that bind DuraPETase and thereby inhibit the enzyme. Such interactions might be partially disrupted by the addition of Tween20 as detergent.

Eventually 0.15% Tween was used as standard component in the buffers dealing with lysate for this assay platform including the fluorescence readout systems. It is also noteworthy that in lysate DuraPETase shows a sort of sigmoidal activity curve (Fig. 4A). A reference measurement in buffer shows no hints for such a sigmoidal curve for both enzymes, but a steady increase in performance with rising enzyme concentration finally approximating the assay's substrate

capacity (Fig. S1B). Therefore, this behaviour in lysate (Fig. 4A) can also be attributed to an unknown interplay between DuraPETase and lysate compounds.

The DuraPETase engineered by Cui *et al.* (2021) is a remarkable enzyme featuring improved expression yields, thermostability and as such improved activity in general and at higher temperatures. Therefore, it has been conveniently used as a benchmark enzyme in this study for fast optimisation experiments. The overall performance of this improved variant especially profits from the increased T_m of 78°C, which allows the use of the enzyme around the glass transition temperature T_g of PET where polymer chains show significantly higher mobility (Demirel *et al.*, 2011; Wei *et al.*, 2019). To investigate in detail how this thermostability translates into increased PET degradation rates, a 96-well MTP setup was used (200 nM enzyme, 1.5 h) covering incubation temperatures from 30 to 80°C. The activity, represented as average total product release (Fig. 4D), is rapidly increasing with the temperature >40°C. The peak performance was measured at 60°C with 1.1 mM while even higher temperatures decrease the activity again. A DSC analysis of DuraPETase was performed to determine the thermodynamic properties under the given buffer conditions and to link these results, $T_{onset} = 67.2^\circ\text{C}$, $T_g = 76.0^\circ\text{C}$, to the previously measured activity. True to expectations, best activity is observed ~60–65°C, below the T_{onset} s, where the protein starts to unfold, but near to the T_g of PET in humid environments (65–67°C) (Mettler Toledo, n.d.; Chen *et al.*, 1998; Demirel *et al.*, 2011). This suggests that the observed decrease in activity at 70°C and higher can be related to the beginning inactivation of the enzyme through thermal unfolding and thereby deviating from the optimum temperature of DuraPETase. Remarkably, there is even substantial residual activity above the T_m of DuraPETase at 80°C with 0.3 mM and thereby outperforming the PET degradation at 30°C with 0.1 mM of total product release.

Conclusion

With this study we present a new way to supply substrate for experiments with PET-degrading enzymes. Commonly used substrates for this purpose are BHET or other soluble polyesters, but the significance of such results towards real PETase substrates is limited. While it is laborious to distribute PET film pieces to each reaction well, PET nanoparticles are much easier in handling and offer a convenient and obviously good solution. Nevertheless, it is unclear whether there are differences in the enzyme's behaviour due to their shape and size and especially material properties like crystallinity. With the coating approach we can now address several aspects such as easy distribution even for high-throughput applications and for different reaction vessels in general, emulating larger PET surfaces like realistic PET microplastic particles, and modifying the crystallinity of the resulting PET. Subsequently this coating method can also be used to apply different types of PET ranging from virgin material, over recycled PET, as used in this study, to pre-weathered PET from weathering chambers or naturally degraded material. Also, the substitution of PET with PET homologues like polybutylene terephthalate is possible and has been successfully tested. Furthermore, the influence of additives, which are commonly used to alter the polymer material properties, on enzymatic degradation can be easily studied when added to the PET solution before coating.

For all vessel types a coating could be established with a sufficiently low standard deviation regarding the intended individual purpose. The gold standard for analysis of product formation is liquid chromatography, where we customised this method on an UHPLC

system to achieve a run time of only 2.1 min. This was not in focus of this study but still features a decent speed for low to medium throughput experiments. While it is basically compatible with lysate, with the drawback of regularly cleaning and probably increased wear, this is where the fluorescent Fenton readout is the better option. This method offers a wide dynamic range but combined with fast and consistent results up to the 384-well MTP format, enabling high sample quantities. But larger differences in the lysate concentration are influencing the measured fluorescence, which makes it necessary to have similar lysate concentrations in the calibration run and the actual screening experiment. This is not true for the GFP complementation, which is robust regarding different lysate concentrations. Consequently, this way of determining the enzyme concentration with its consistent results is a useful expansion of the assay platform's lysate capabilities. For the screening experiments in lysate, the role of Tween20 must be mentioned. At this point we can only speculate why IsPETase and its engineered descendant DuraPETase are so drastically impaired by even the low lysate concentrations used here. Thus, the same questions are yet to be answered for the effect of Tween20 in this system and how it can recover the activity, and further whether this solution works universally for all potential PETases. Obviously, this might not just be an issue with this type of substrate in the form of coated PET film but a general problem also for other assays working with lysate. We can, however, show that within our platform the use of Tween20 enables tracking of the activity of IsPETase and near homologues.

In conclusion, the accuracy of the lysate-based Fenton readout is lower compared with the ones in buffer as these measurements generally show a higher standard deviation and the higher background fluorescence leads to an impaired lower detection limit of TPA. Furthermore, it must be considered that the influence of lysate on the activity on new uncharacterised enzymes may vary. Therefore, this lysate approach can be seen as a tool to generally check for expression (GFP complementation) and for a rough estimation of PETase activity (Fenton readout), which is fully sufficient for many screening applications. This can then easily be followed by a precise analysis of chosen variants with purified enzyme.

Summarising we present a very versatile and robust assay platform with a novel method for supplying reasonable crystalline substrate in a high-throughput compatible manner. The use of this defined substrate significantly broadens the screening capabilities and in combination adds up to this versatile platform that can easily be adopted from any detailed analysis of single mutants to a broad screening in the scope of enzyme discovery, protein design or directed evolution.

Supplementary data

Supplementary data are available at *PEDS* online.

Funding

This work was funded by the Deutsche Forschungsgemeinschaft (DFG, German Research Foundation) [Project Number 391977956 – SFB 1357 Microplastics, subproject C03].

References

Austin, H.P., Allen, M.D., Donohoe, B.S. *et al.* (2018) *Proc. Natl. Acad. Sci. U. S. A.*, 115, E4350–E4357.

A versatile assay platform for enzymatic poly(ethylene-terephthalate) degradation

9

- Belisário-Ferrari, M.R., Wei, R., Schneider, T., Honak, A. and Zimmermann, W. (2019) *Biotechnol. J.*, **14**, e1800272.
- Brouwer, M.T., Alvarado Chacon, F. and Thoden van Velzen, E.U. (2020) *Packag. Technol. Sci.*, **33**, 373–383.
- Cabantous, S., Terwilliger, T.C. and Waldo, G.S. (2005) *Nat. Biotechnol.*, **23**, 102–107.
- Chen, Y., Lin, Z. and Yang, S. (1998) *J. Therm. Anal. Calorim.*, **52**, 565–568.
- Colder Products Company (2010) *Chemical Compatibility Table. For ChemQuik®, DrumQuik®, DrumQuik PRO & Other Common Colder Series Coupling Materials*. [https://www.tom-parker.co.uk/upload/files/literature/CPC_Chemical_Compatibility_Chart_\(261_KB\).pdf](https://www.tom-parker.co.uk/upload/files/literature/CPC_Chemical_Compatibility_Chart_(261_KB).pdf).
- Cui, Y., Chen, Y., Liu, X. et al. (2021) *ACS Catal.*, **11**, 1340–1350.
- Danso, D., Schmeisser, C., Chow, J., Zimmermann, W., Wei, R., Leggewie, C., Li, X., Hazen, T. and Streit, W.R. (2018) *Appl. Environ. Microbiol.*, **84**. <https://doi.org/10.1128/AEM.02773-17>.
- Demirel, B., Yaraş, A. and Elçiçek, H. (2011) *Balkesir Üniversitesi Fen Bilimleri Enstitüsü Dergisi* [Online], **13**, 26–35.
- Dyneon - 3M Innovation (2004) *Dyneon™ PVDF (Polyvinylidene Fluoride) Chemical Resistance Tables*. <https://multimedia.3m.com/mws/media/2422490/dyneontm-pvdf-chemical-resistance-tables.pdf>.
- Furukawa, M., Kawakami, N., Oda, K. and Miyamoto, K. (2018) *Chem. Sus. Chem.*, **11**, 4018–4025.
- Gibson, D.G., Young, L., Chuang, R.-Y., Venter, J.C., Hutchison, C.A. and Smith, H.O. (2009) *Nat. Methods*, **6**, 343–345.
- Herrero Acero, E., Ribitsch, D., Steinkellner, G. et al. (2011) *Macromolecules*, **44**, 4632–4640.
- Hu, X., Thumarat, U., Zhang, X., Tang, M. and Kawai, F. (2010) *Appl. Microbiol. Biotechnol.*, **87**, 771–779.
- Kawai, F., Kawabata, T. and Oda, M. (2019) *Appl. Microbiol. Biotechnol.*, **103**, 4253–4268.
- Kawai, F., Oda, M., Tamashiro, T., Waku, T., Tanaka, N., Yamamoto, M., Mizushima, H., Miyakawa, T. and Tanokura, M. (2014) *Appl. Microbiol. Biotechnol.*, **98**, 10053–10064.
- Mettler Toledo (n.d.) *Thermal Analysis of Polymers. Selected Applications*. <https://www.mt.com/dam/Analytical/ThermalAnalysis/TA-PDF/Part%20of%20Polymers-Selected%20Applications.pdf>.
- Müller, R.-J., Schrader, H., Profe, J., Dresler, K. and Deckwer, W.-D. (2005) *Macromol. Rapid Commun.*, **26**, 1400–1405.
- OECD. “Improving Plastics Management: Trends, policy responses, and the role of international co-operation and trade”; OECD Environment Policy Papers: Paris, 2018. <https://doi.org/10.1787/c5f7c448-en>.
- Ollis, D.L., Cheah, E., Cygler, M., Dijkstra, B., Frolow, F., Franken, S.M., Harel, M., Remington, S.J., Silman, I. and Schrag, J. (1992) *Protein Eng.*, **5**, 197–211.
- Pfaff, L., Breite, D., Badenhorst, C.P.S., Bornscheuer, U.T. and Wei, R. (2021) *Methods Enzymol.*, **648**, 253–270.
- Plastics Europe (2020) *Plastics – the Facts 2020. An analysis of European plastics production, demand and waste data*. <https://www.plasticseurope.org/en/resources/publications/4312-plastics-facts-2020>.
- Prata, J.C., Silva, A.L.P., Da Costa, J.P., Mouneyrac, C., Walker, T.R., Duarte, A.C. and Rocha-Santos, T. (2019) *Int. J. Environ. Res. Public Health*, **16**. <https://doi.org/10.3390/ijerph16132411>.
- R Foundation for Statistical Computing Placeholder Text(2020) *R: A language and environment for statistical computing*, Vienna, Austria: R Core Team.
- Ribitsch, D., Heumann, S., Trotscha, E. et al. (2011) *Biotechnol. Prog.*, **27**, 951–960.
- Santos-Aberturas, J., Dörr, M. and Bornscheuer, U.T. (2018) *Methods Mol. Biol. (Clifton, N.J.)*, **1685**, 157–170.
- Shen, L., Worrell, E. (2014) *Handbook of Recycling*. Placeholder TextPlaceholder Textpp. 179–190 Elsevier.
- Son, H.F., Cho, I.J., Joo, S., Seo, H., Sagong, H.-Y., Choi, S.Y., Lee, S.Y. and Kim, K.-J. (2019) *ACS Catal.*, **9**, 3519–3526.
- Sulaiman, S., Yamato, S., Kanaya, E., Kim, J.-J., Koga, Y., Takano, K. and Kanaya, S. (2012) *Appl. Environ. Microbiol.*, **78**, 1556–1562.
- Tournier, V., Topham, C.M., Gilles, A. et al. (2020) *Nature*, **580**, 216–219.
- Wallace, N.E., Adams, M.C., Chafin, A.C., Jones, D.D., Tsui, C.L. and Gruber, T.D. (2020) *Environ. Microbiol. Rep.*, **12**, 578–582.
- Wei, R., Breite, D., Song, C., Gräsing, D., Ploss, T., Hille, P., Schwerdtfeger, R., Matysik, J., Schulze, A. and Zimmermann, W. (2019) *Adv. Sci.*, **6**, 1900491.
- Wei, R., Oeser, T., Barth, M., Weigl, N., Lübs, A., Schulz-Siegmund, M., Hacker, M.C. and Zimmermann, W. (2014) *J. Mol. Catal. B: Enzym.*, **103**, 72–78.
- Wei, R., Oeser, T., Billig, S. and Zimmermann, W. (2012) *Biotechnol. J.*, **7**, 1517–1521.
- Wei, R., Tiso, T., Bertling, J., O’Connor, K., Blank, L.M. and Bornscheuer, U.T. (2020) *Nat. Catal.*, **3**, 867–871.
- Wunderlich, B. (2005) *Thermal Analysis of Polymeric Materials*, 1st edn Placeholder Text. Berlin, Heidelberg: Springer Placeholder Text.
- Yoshida, S., Hiraga, K., Takehana, T., Taniguchi, I., Yamaji, H., Maeda, Y., Toyohara, K., Miyamoto, K., Kimura, Y. and Oda, K. (2016) *Science (New York, N.Y.)*, **351**, 1196–1199.
- Zhong-Johnson, E.Z.L., Voigt, C.A. and Sinskey, A.J. (2021) *Sci. Rep.*, **11**, 928.

Supplementary Information for

A versatile assay platform for enzymatic Poly(ethylene-terephthalate) degradation

S. Weigert¹, A. Gagsteiger¹, T. Menzel², B. Höcker¹

Figure S1: Performance of purified DuraPETase and LCC-WCCG in buffer at different conditions in a 96-well setup. **A** shows the total product release of 200 nm enzyme in the presence of Tween20 in concentrations between 0.0 and 0.3 %. The influence of increasing enzyme concentrations (0-1000 nM) on the total product release is displayed in **B**.

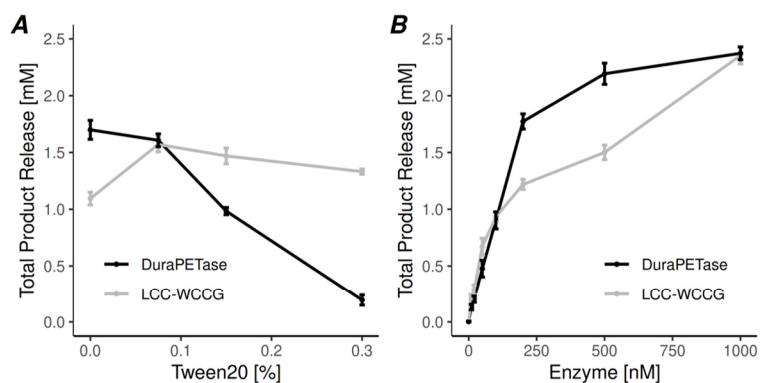


Table S1: Protein sequences of the used constructs displaying the full translated open reading frame beginning with the start codon included in the *NdeI* cleavage site of the pET21 vector. Special features in the sequences are highlighted.

Name	Protein sequence
Features GFP(1-10) GFP(1-10), 6xHisTag	MMSKGEELFTGVVPIVELDGDVNGHKFSVRGEGEGDATIGKLTLLKFI CTTGKLPVPWPTLVTTLYGVQCFSRYPDHMKRHDFFKSAMPEGYVQ ERTISFKDDGKYKTRAVVKFEGDTLVNRIELKGTDFKEDGNILGHKLEY NFNSHNVYITADKQKNGIKANFTVRHNVEDGSVQLADHYQQNTPIGD GPVLLPDNHYLSTQTVLSKDPNEKLLLEHHHHHHH*
MHETase mauC Signal peptide, MHETase(41-603), 6xHisTag	MISATKIRSCLAACVLAAFGATGALASSLASRAACEALKDGNNGDMVWP NAATVVEVAAWRDAAPATASAAAALPEHCEVSGAIAKRTGIDGYPIEIK FRLRMPAEWNGRFFMEGGSGTNGLSAATGSIGGGQIASALSRNFAT IATDGGHDNAVNDNPDALGTVAFGLDPQARLDMGYNSYDQVTQAGK AAVARFYGRAADKSYFIGCSEGGREGMMLSQRFP SHYDGIVAGAPGY QLPKAGISGAWTTQSLAPA AAVGLDAQGVPLINKSFSDADLHLLSQAILG TCDALDGLADGIVDNYRACQAAFDPATANPANGQALQC VGAKTADC LSPVQVTAIKRAMAGPVNSAGTPLYNRWAWDAGMSGLSGTTYNQGW RSWWLGSFNSSANNAQRVSGFSARSWLVDFATPPEPMPMTQVAAR MMKFDIDPLKIWATSGQFTQSSMDWHGATSTDLA AAFRDRGGKMIL YHGMSDAAFSALDTADY YERLGAAMPGAAGFARLFLVPGMNHCSGG PGTDRFDMLTPLVAWVERGEAPDQISAWSGTPGYFGVAARTRPLCPY PQIARYKSGDINTEANFACAAPPSRSSGHHHHHHH*
LCC-WCCG LCC-WCCG, 6xHisTag	MSNPYQRGNPRTSALTADGPFVATYTVSRLSVSGFGGGVIYYPTG TSLTFGGIAMSPGYTADASSLAWLGRRLASHGFVVLVINTNSRFDGPD SRASQLSAALNYLRTSSPSAVRARLDANRLAVAGHSMGGGGTLRIAE QNP SLKAAVPLTPWHTDKTFNTSVPVLIVGAEADTVAPVSQHAIPFYQ NLPSTTPKYVELCNASHWAPNSNNAAISVYTISWMKLVVDNDTRYR QFLCNVNDPALCDFRTNNRHCQVDKLA AALEHHHHHHH*
DuraPETase- GFP11 GFP11, GS-Linker, DuraPETase, 6xHisTag	MSSRDHMLHEYVNAAGITGSGSGSGSGSGSGSGSQTNPYARGP NPTAASLEASAGPFTVRSFTVSRPSGYGAGTVYYPTNAGGTVGAIIV PGYTARQSSIKWWGPRLASHGFVITIDTNSTFDY PSSRSSQQMAALR QVASLNGDSSSPIYGKVD TARMGVMGHSMGGGASLRS AANNPSLKA AIPQAPWDSQTNFSSVTVPTLIFACENDSIAPVNSHALPIYDMSRNAK QFLEINGGSHSCANSNGNSNQALIGKKGVAWMKRFMDNDTRYSTFACE NPNSTAVSDFRTANCSLES GHHHHHHH*

Article

Impact of Enzymatic Degradation on the Material Properties of Poly(Ethylene Terephthalate)

Teresa Menzel ^{1,†}, Sebastian Weigert ^{2,*}, Andreas Gagsteiger ², Yannik Eich ¹, Sebastian Sittl ³, Georg Papastavrou ³, Holger Ruckdäschel ¹, Volker Altstädt ¹ and Birte Höcker ^{2,*}

- ¹ Department of Polymer Engineering, University of Bayreuth, Universitätsstraße 30, 95447 Bayreuth, Germany; Teresa.Menzel@uni-bayreuth.de (T.M.); bt716629@uni-bayreuth.de (Y.E.); holger.ruckdaeschel@uni-bayreuth.de (H.R.); volker.altstaedt@uni-bayreuth.de (V.A.)
² Department of Biochemistry, University of Bayreuth, Universitätsstraße 30, 95447 Bayreuth, Germany; Sebastian.Weigert@uni-bayreuth.de (S.W.); Andreas.Gagsteiger@uni-bayreuth.de (A.G.)
³ Department of Physical Chemistry II, University of Bayreuth, Universitätsstraße 30, 95447 Bayreuth, Germany; sebastian.sittl@uni-bayreuth.de (S.S.); Georg.Papastavrou@uni-bayreuth.de (G.P.)
 * Correspondence: birte.hoecker@uni-bayreuth.de
 † These authors contributed equally to this work.



Citation: Menzel, T.; Weigert, S.; Gagsteiger, A.; Eich, Y.; Sittl, S.; Papastavrou, G.; Ruckdäschel, H.; Altstädt, V.; Höcker, B. Impact of Enzymatic Degradation on the Material Properties of Poly(Ethylene Terephthalate). *Polymers* **2021**, *13*, 3885. <https://doi.org/10.3390/polym13223885>

Academic Editor: Andrea Sorrentino

Received: 23 September 2021
 Accepted: 8 November 2021
 Published: 10 November 2021

Publisher's Note: MDPI stays neutral with regard to jurisdictional claims in published maps and institutional affiliations.



Copyright: © 2021 by the authors. Licensee MDPI, Basel, Switzerland. This article is an open access article distributed under the terms and conditions of the Creative Commons Attribution (CC BY) license (<https://creativecommons.org/licenses/by/4.0/>).

Abstract: With macroscopic litter and its degradation into secondary microplastic as a major source of environmental pollution, one key challenge is understanding the pathways from macro- to microplastic by abiotic and biotic environmental impact. So far, little is known about the impact of biota on material properties. This study focuses on recycled, bottle-grade poly(ethylene terephthalate) (r-PET) and the degrading enzyme PETase from *Ideonella sakaiensis*. Compact tension (CT) specimens were incubated in an enzymatic solution and thermally and mechanically characterized. A time-dependent study up to 96 h revealed the formation of steadily growing colloidal structures. After 96 h incubation, high amounts of BHET dimer were found in a near-surface layer, affecting crack propagation and leading to faster material failure. The results of this pilot study show that enzymatic activity accelerates embrittlement and favors fragmentation. We conclude that PET-degrading enzymes must be viewed as a potentially relevant acceleration factor in macroplastic degradation.

Keywords: polymer degradation; microplastic; nanoplastic; PETase; crack formation; fatigue crack propagation resistance; BHET; enzymatic degradation; enzyme; *Ideonella sakaiensis*; bis(hydroxyethyl)terephthalate

1. Introduction

Since the discovery of microplastics (MPs) in 2004 [1], particles have been detected in almost every natural environment. Primary MP is already produced on a micrometer scale, whereas secondary MP arises by degradation and fragmentation of macroplastic. As the amount of secondary MP to be found in nature is drastically larger than that of primary MP, the degradation of macroplastic has recently gained new attention [2–4]. Once in the environment, polymers are exposed to a range of external environmental impacts. These can be categorized as abiotic factors such as UV-radiation, temperature, humidity, and mechanical stress, and biotic factors such as living or dead organisms, e.g., biofilm formation by bacteria, fungi, algae, or ingestion [5,6]. A complex interplay of natural stress factors is supposed to lead to molecular degradation, fragmentation, and therefore MP formation [7–9]. However, knowledge of the underlying processes is still lacking. It is evident that material properties decisively influence the fragmentation towards MP and dramatically change during this process, creating a feedback loop on the degradation itself.

Regarding biotic degradation, polyesters, especially polyethylene terephthalate (PET), are the subject of many studies due to their molecular structure [10]. Ester bonds are omnipresent in key positions within metabolic networks and biological molecules. Although other common polymer bond types like C-C are more challenging in a biological

perspective, a whole variety of hydrolases is known to deal with ester bonds in nature. Particularly in recent years, PET-degrading enzymes have come into focus as a new perspective for biological MP decomposition and recycling applications [11]. In this regard, cutinase enzymes are of particular interest, as their aliphatic ester substrate, cutin, has a chemical resemblance to PET. Consequently, all PET-degrading enzymes with relevant activity known to date can be assigned to this group of cutinases [10], including the best-studied variants TtCut-1/2 (*Thermobifida fusca*) [11], LCC (uncultured organism) [12], and PETase (*Ideonella sakaiensis*) [13]. The latter piqued researchers' interest, as it appeared as the first evolved PET-degrading enzyme with substantial activity at ambient temperatures. This activity profile, combined with the presence of potential PET-degrading enzymes in different ecosystems [14], suggests the altering of PET's material properties upon biological activity under real conditions.

On a chemical level, abiotic factors are relatively well characterized: Photooxidation by UV radiation and oxygen leads to radical-induced chain scission and the formation of new polar functional end groups, e.g., carboxylic acids, aldehydes, hydroxides, or peroxides [15–18]. Hydrolytic degradation strongly depends on an interplay of humidity, temperature, pH, and the crystallinity of the material [17,19–21]. Both processes lead to a decrease in the molecular weight. Regarding material properties, it is well known that the transition of the molecular weight below the critical molar mass (M_c , 17 kg/mol for PET [22]) causes a change in material behavior from ductile to brittle [23]. In general, abiotic degradation and stepwise embrittlement accelerate the fragmentation upon external mechanical forces like wind and waves [24,25]. However, except for one study [22], there is a lack of detailed information about changes in mechanical properties on PET depending on environmental impact in the literature. When it comes to biotic degradation of PET and its impact on the material, even less is known besides the investigation of changes in PET crystallinity during enzymatic degradation [26].

A sensitive method for the determination of micromechanical material changes can be supplied by mechanical testing under dynamic load [27,28]. This technique gives precise information on the fatigue crack propagation (FCP) behavior at various crack propagation speeds and is claimed to be the most sensitive regarding the relationships between the polymer structure and deformation mechanism. The stress state at the crack tip is well defined compared to conventional tensile or impact testing. This allows possible correlations between the interaction of the crack tip, propagation of the fatigue crack, and the sensitivity of a specific polymer to environmental stress. It is well known that the FCP rate is strongly affected by the degree of crystallinity and the tie molecule density of polymers [29,30], as well as by their molecular weight [31]. Eventually, the linear dependency of the FCP rate on the applied stress intensity, indicating stable crack growth, provides qualitative information about improved or deteriorated material behavior [32].

To the best of our knowledge, there have been no studies focusing on the impact of biotic stresses on macroscopic PET properties. For detailed information on the formation of MP on their pathway from macro to micro, biotic factors on material properties must be considered. Within this feasibility study, we combine the methods and techniques of biochemistry and engineering sciences. This interdisciplinary combination allows first insights into the change of material properties in a laboratory-controlled biotic degradation process. Overall, the aim of our study is to understand the impact of biotic degradation by PETase on a macro- and microscopic level by focusing on PET material properties. Insights into the underlying processes enable us to comprehend how biotic degradation impacts PET fragmentation.

2. Materials and Methods

A commercially available, recycled, low-molecular-weight PET (CleanPET® FK) (Veolia Deutschland GmbH, Berlin, Germany) was used with a number-averaged molecular weight of $M_n = 30.155$ g/mol and dispersity $\mathcal{D} = 1.8$ determined by GPC measurements (Agilent 1200 Series, Agilent Technologies, Waldbronn, Germany) with HFIP with potas-

sium trifluoroacetate (4.8 g in 600 mL HFIP) as solvent. The PET flakes were acquired from disposable, post-consumer bottles and therefore contained an undeterminable amount of several additives. Thus, the material composition reflected a realistic condition regarding real-life environmental conditions.

2.1. Protein Production and Purification

The gene of *isPETase* was cloned via Gibson assembly [33] in a pMAL-p4x vector, in which the MPB sequence was replaced with the *mauC* signal peptide for periplasmic expression. *E. coli* BL21 cells containing the plasmid were grown in TB media at 37 °C; after an OD₆₀₀ of 1.5 was reached the temperature was lowered to 18 °C and protein expression was induced with a final concentration of 300 µM IPTG. After 18 h, cells were harvested and resuspended for sonication in lysis buffer (300 mM NaCl, 40 mM imidazole, 50 mM phosphate pH 7.4). The lysate was clarified through centrifugation (50,000× *g*) and vacuum filtration (0.2 µm filter), and subsequently loaded onto a NiIMAC column (HisTrap FF 5 mL, Cytiva Europe, Freiburg, Germany). After loading and washing, the protein was recovered from the column with elution buffer (300 mM NaCl, 400 mM imidazole, 50 mM phosphate pH 7.4). For final polishing, the protein was applied to a SEC column (Superdex 75pg 26/60, Cytiva) equilibrated with SEC buffer (150 mM NaCl, 25 mM HEPES, pH 7.4). A total of 100 µL aliquots of the enzyme with a concentration of 25 µM were flash frozen and kept at −80 °C until further use.

2.2. PET Sample Preparation

Compact tension (CT) specimens with a width and thickness of 40 and 4 mm, respectively, were prepared by injection molding (Arburg Allrounder 470H 1000-170, Arburg GmbH, Loßburg, Germany). Each sample was tapped with a new razor blade into the V-notch to create a sharp crack. For a time-dependent degradation study of the surfaces, squares with 2 cm edge length were sawn out of the injection-molded CT specimen for easier handling.

2.3. Sample Incubation with *PETase*

For the time-dependent degradation study, the squares with 2 cm edge length were fully covered with an enzyme-buffer solution in a 50 mL centrifuge tube. The enzyme concentration was constantly set to 200 nM in a reaction buffer of 50 mM NaCl and 50 mM borate at pH 8.5. A control sample was covered under the absence of enzyme with a buffer solution only. All samples were incubated at 30 °C for 24 h, 48 h, and 96 h, respectively. The sample without enzyme is further referred to as control. The PET samples, additionally incubated with enzyme, are further referred to as PET*24 h, PET*48 h, and PET*96 h.

For mechanical testing, the CT specimens were placed in purpose-built holders made of stainless steel (Figure 1). This setup ensured the sufficient coverage of solution at the notch and along the expected crack propagation. The sample holder was assembled with a specimen and filled with 2 mL of the abovementioned enzyme-buffer solution. Again, a specimen incubated with buffer solution only serves as control sample. The sample holders were placed in a gastight container comprising additional reaction buffer on the bottom to minimize evaporation of the solution within the sample holder. The specimens for mechanical testing were incubated at 30 °C for 96 h. After exposure, the CT specimen was rinsed with water and a standard PET drying procedure (6 h at 140 °C) was applied to eliminate the influence of moisture in further characterization steps.

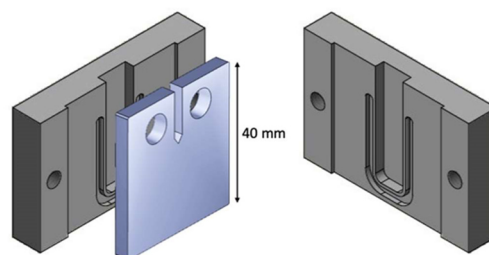


Figure 1. CT specimen and sample holders for the incubation with enzyme-buffer solution. The CT specimen is placed between two perfectly fitting parts, and tightly secured with screws. The indentations are filled either with buffer or enzyme-buffer solution. To avoid leakage of the solutions, U-shaped seals are fixed between specimen and sample holder. The setup ensures the total coverage of the specimen with solution within the expected crack propagation direction.

For this study, incubation parameters such as buffer composition, temperature, and enzyme concentration were chosen primarily to optimize enzymatic activity. Although they did not necessarily reflect conditions in natural settings, they allowed for the best results to establish the methodology.

2.4. Ultra-High Performance Liquid Chromatography (UHPLC)

The water-soluble degradation products of PET were quantified with a Thermofisher RS3000 UHPLC system equipped with a Phenomenx Kinetex 1.7 μm EVO C18 (100 \AA , 50 mm \times 2.1 mm) reversed-phase column. For sample preparation, one part of the sample buffer solution of the PET control, PET*24 h, PET*48 h, and PET*96 h after incubation was mixed with four parts acidic acetonitrile (1% formic acid) and centrifuged at $21,000 \times g$ for 10 min. A quantity of 1 μL of the supernatant was applied to the column running a gradient from 100% solvent A (water + 0.1% trifluoroacetic acid) to 20% solvent A and 80% solvent B (acetonitrile) at a flow rate of 1.3 mL/min and the column was heated to 55 $^{\circ}\text{C}$. The product amounts for TPA, MHET, and BHET were quantified based on calibration runs. For the time-dependent monitoring of the enzymatic activity, the three degradation products were summed up to the total product concentration for better comparison.

2.5. Optical and Topographical Characterization

To visualize the enzymatic degradation on a microscopic scale, field-emission scanning electron microscopy (FESEM) was performed on the surfaces with a Zeiss Ultra plus (Carl Zeiss Microscopy Deutschland GmbH, Oberkochen, Germany) at an acceleration voltage of 3 kV for the control and the enzyme-degraded samples. All samples were sputtered with 1.3 nm platinum at a Cressington Platin-Sputter Coater 208HR (TESCAN GmbH, Dortmund, Germany) and additionally steamed with 20 nm carbon at a Leica EM ACE 600 (Leica Microsystems GmbH, Wetzlar, Germany).

The surface topography of the enzymatically degraded PET*96 h and control PET sample was acquired by atomic force microscopy (AFM) imaging in PeakForce tapping mode in air. All images were acquired using a Dimension Icon AFM (Bruker Corporation Billerica, Massachusetts, USA) equipped with a NanoScope V controller. For imaging, ScanAsyst Air cantilevers (Bruker Nano Inc., nominal spring constant 0.4 N/m, nominal resonance frequency 70 kHz) were used. The PeakForce frequency was set to 2 kHz with an amplitude of 150 nm. The AFM images were processed with NanoScope Analysis software (version 1.80, Bruker Nano Inc.). In an additional set of experiments, the samples, i.e., enzyme-degraded and control sample surfaces, were treated for about 30 s by a CO_2 gun (SnowJet, Tectra GmbH, Frankfurt, Germany) in order to remove potential organic contaminants.

2.6. Thermal Characterization

Differential scanning calorimetry (DSC) was examined with a Mettler Toledo DSC I (Mettler-Toledo GmbH, Gießen, Germany) with 8–10 mg sample material. Material was collected between 0 and 1 mm depth from the surface. The samples were heated under an N₂ atmosphere from −10 °C to 300 °C (1st heating run), and cooled to −10 °C again after an isothermal stage of 5 min at 300 °C. For determination of the degree of crystallinity x_c a fusion enthalpy of $\Delta H_m^\circ = 140.1$ J/g for a hypothetically 100% crystalline PET was used, based on the literature [34].

2.7. Mechanical Characterization

The FCP behavior was determined according to test method ISO 15850/ASTM E647 at 23 °C and a relative humidity of 50% on a servo-hydraulic testing machine (IST IPLH10I, Schenck, Germany) applying a dynamical load with a frequency of 10 Hz to the samples. The stress intensity factor's $\Delta K = K_{\max} - K_{\min}$ amplitude was increased in proportion to the crack length with a constant $R = K_{\min}/K_{\max}$ of 0.1. The crack was supposed to grow perpendicular to the load within the solution covered area until the end of the sample. For measurement of the crack opening displacement during crack growth, a clip-on extensometer (632.29-30, MTS Sensor Technology GmbH & Co. KG, Rottenburg am Neckar, Germany) was used. Each experiment loaded under tension mode was repeated at least three times. Analysis was done with the software R [35]; Zone II was defined manually between $\Delta K = 2.2$ and $\Delta K = 3.05$.

3. Results and Discussion

3.1. Analysis of Soluble Products

To monitor enzymatic degradation on the molecular level, the control buffer solution and enzyme buffer solution were analyzed by ultra-high-performance liquid chromatography (UHPLC) after the given incubation time of 24 h, 48 h, and 96 h. Regarding product composition, the exemplarily plotted buffer solution of PET*96 h contained the typical degradation products terephthalic acid (TPA), mono-(2-hydroxyethyl)terephthalic acid (MHET), and bis(hydroxyethyl)terephthalate (BHET) (Figure 2a). In the case of the control buffer, none of the typical degradation products could be detected (Figure 2a). The quantification of the degradation products for PET*96 h (Figure 2b) gave high amounts of MHET and TPA with 2.3 mM and 1.3 mM, respectively. Further, small amounts of 0.1 mM BHET were identified. For the time-dependent study, the total product concentration for PET*24 h, PET*48 h, and PET*96 h was determined. The total product concentration increased in relation to the incubation time, with a slight slowdown after 48 h (Figure 2c). The results of the solution analysis represent a typical activity profile for PETase on PET with MHET as the dominant product [13].

The UHPLC measurements verify that the observed PET degradation could only be attributed to enzymatic activity and no side reaction or autohydrolysis occurred during incubation. Furthermore, the results reflect the consistency in our setup, including sample generation and incubation. True to expectations [36], the total product release, consisting of TPA, MHET, and BHET, steadily rose with increasing exposure time (Figure 2c). This indicates a constantly ongoing degradation of PET by PETase over incubation time. In summary, the setup ensured a reliable procedure for monitoring enzymatic activity of a macroscopic substrate on the molecular level.

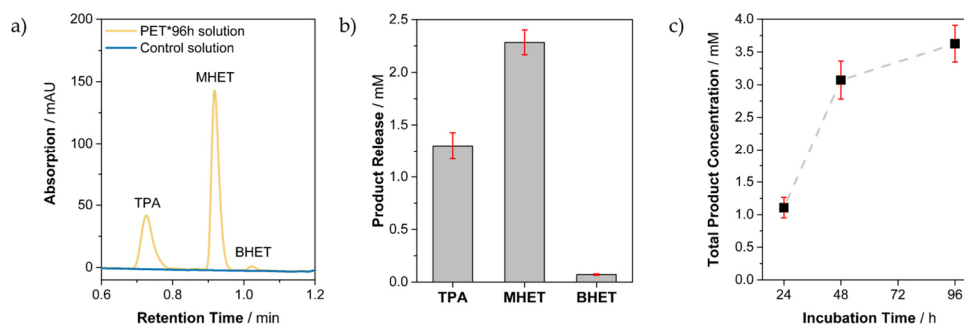


Figure 2. Analysis of soluble products. (a) UHPLC results of the control buffer solution (blue) and enzyme buffer solution (orange) of PET*96 h. For the control buffer solution, no release products could be detected. (b) Product concentrations of PET*96 h to display the product composition in mM and (c) total product concentration of PET*24 h, PET*48 h, and PET*96 h solution versus incubation time.

3.2. Characterization of PET Material Properties

To investigate the result of degradation on a visible level, scanning electron microscopy (SEM) micrographs of the surfaces of the control and incubated PET samples were recorded (Figure 3).

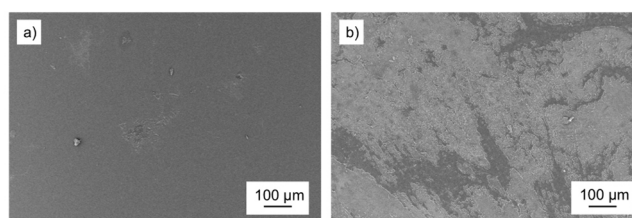


Figure 3. SEM micrographs for comparison of the (a) control PET surface and (b) PET surface of PET*96 h after incubation.

In the case of the control PET, the micrographs displayed a smooth and unaffected surface (Figure 3a). The exposure of the samples to PETase enzyme led to visible degradation by surface erosion (Figure 3b), indicating successful trials and degradation. The overview at low magnification depicted the spatial heterogeneity of the enzymatic treatment, reflected by the presence of unaffected and degraded areas. Furthermore, the investigation of the control sample surface verified that it was not affected by autohydrolysis of the buffer solution and degradation only arose due to the impact of enzymes. For a deeper investigation of the topographical surfaces' changes, a time-dependent surface SEM study was performed.

The SEM micrographs of the time-dependent degradation study are shown in Figure 4. The affected areas at higher magnitudes showed the presence of colloidal structures upon enzymatic treatment. They constantly grew with increasing incubation time to a diameter of approx. 2 μm. However, at that point we could not distinguish between surface erosion and the congregation of side products on the PET surface during the enzymatic degradation.

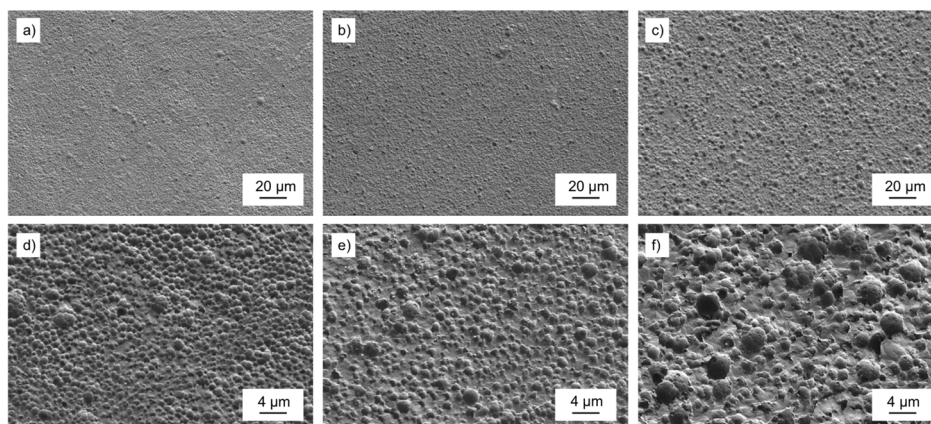


Figure 4. Time-dependent SEM micrographs at different degradation stages of (a) PET*24 h, (b) PET*48 h, and (c) PET*96 h and with higher magnification at (d) PET*24 h, (e) PET*48 h, and (f) PET*96 h.

To corroborate the topography changes upon enzymatic treatment as determined by SEM, we studied the PET surface of the control and enzyme-treated PET*96 h sample additionally by AFM. For those measurements we used PeakForce Tapping mode (Figure 5) as the imaging mode to correlate the colloidal growth with surface roughness.

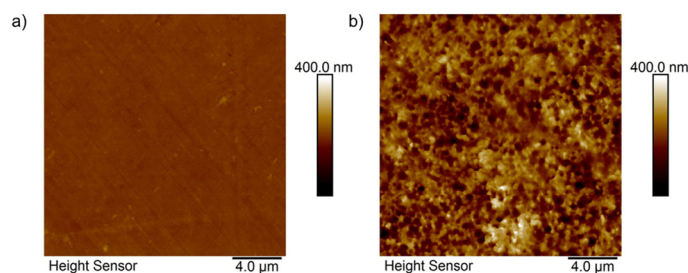


Figure 5. PeakForce Tapping mode AFM images of the control PET surface (a) and PET*96 h surface (b).

The blank PET surface was smooth (Figure 5a). The sample showed a homogeneous surface without any distinct topographical features. On the other hand, the PET*96 h surface, which was incubated and treated with the PETase, showed a significant increase in roughness. Figure 5b bears distinct differences in surface topography with features that are absent for the bare control PET substrate (cf. Figure 5a). The observed increase in surface roughness is in line with the findings from the SEM investigations (cf. Figure 4) and indicates that the enzymatic treatment was accompanied by changes in the surface topography. In order to further quantify this finding, the arithmetic surface roughness was evaluated for at least three AFM images for each type of PET sample. The untreated surface bore a roughness of $7.3 \text{ nm} \pm 3.7 \text{ nm}$ and the PETase-treated samples bore a roughness of $37.0 \text{ nm} \pm 7.8 \text{ nm}$, respectively.

Differential scanning calorimetry (DSC) measurements allow inferences to be drawn from thermal transition temperatures about molecular arrangements. Until now, the focus in literature dealing with enzymatic degradation has been the identification of degradation products in solution [13,26,37], but no concrete measurements have been carried out on

PET sample surfaces. DSC thermograms of the heating curves and cooling curves for the PET control and PET*96 h sample are shown in Figure 6. The DSC samples were taken along the crack of a CT specimen at a 0–1 mm sample depth.

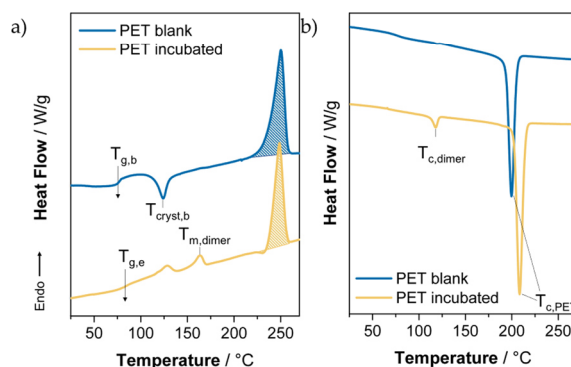


Figure 6. DSC thermograms of the first heating run (a) and first cooling run (b) for PET blank (blue) and PET incubated with PETase (orange). For the enzyme-treated samples, the rise of a second melting peak was identified as BHET dimer.

In the first heating curve (Figure 6a), both samples showed the PET typical melting point $T_m = 250$ °C [38]. Beside the glass transition $T_{g,b} = 76$ °C, the control sample additionally showed an exothermic peak at $T_{cryst,b} = 120$ °C related to amorphous phase crystallization. In the case of the incubated PET*96 h sample, the glass transition showed a weak signal at $T_{g,e} = 84$ °C. The increase in the glass transition temperature of incubated PET can be explained by the emergence of crystalline units of two different molecular species in a range from 109 to 172 °C (Figure 6a). They were supposed to immobilize the amorphous chains [39], which led to the slight increase of 8 K.

The appearance of these new melting peaks can be attributed in detail to PET oligomers with a varying length of one and two monomer repeating units, respectively [40]. Whereas the weaker signal from 109 °C to 135 °C could be attributed to monomeric BHET, the melting point at $T_{m,dimer} = 164$ °C clearly indicates the presence of BHET dimer [41–43]. The observed BHET dimer was water-insoluble and therefore not detectable in UHPLC measurements of the solutions. We conclude that the observed colloidal structures (Figure 4) on the surface were composed of BHET oligomer species. However, the accumulation of BHET and its dimer indicates that they were not preferably degraded by the PETase.

A possible explanation for this behavior lies in the topology of the enzyme itself. Although there is no experimental proof for the exact binding mode of PET substrate to PETase, it is known that the PET binding site includes an L-shaped shallow groove neighboring the active site. Several studies using computational calculations to dock a PET oligomer in the active and binding site yielded a binding pose that provides space for the equivalent of either a BHET trimer or tetramer [26,44,45]. Shorter substrates such as the BHET dimer are not able to cover the full binding site, leading to a potentially decreased number of atomic contacts that contribute to the binding of the substrate. This would result in a higher affinity for higher oligomers in enzymatic catalysis followed by an accumulation of BHET dimer. Consequently, enzymatic activity might be underestimated when only soluble products are tracked.

The degree of crystallinity decreased with enzymatic treatment from $x_{c,b} = 22\%$ for the PET control to $x_{c,e} = 18\%$ for the PET*96 h sample. It is known that high crystallinity impairs enzymatic activity, which led to the conclusion that PETase was mainly active in the amorphous regions. If this was the case, crystallinity should have increased. However, our results show that the degree of PET crystallinity decreased after enzymatic incubation,

as reported in previous studies [22]. We assume that this lower degree in crystallinity of PET was not directly caused by enzymatic attack on crystalline regions, but rather by BHET species disrupting the crystalline order on the surface, explaining how crystallinity can decrease despite preferred enzymatic degradation of amorphous regions. The presence of BHET was also observed in the cooling curves (Figure 6b). Whereas the control sample only showed one sharp recrystallization peak at $T_{c,PET} = 200$ °C typical for PET, the PET*96 h cooling curve showed an additional peak at $T_{c,dimer} = 117$ °C, corresponding to BHET dimer recrystallization. The earlier onset of PET incubated with PETase recrystallization could be a nucleation effect induced by the additional oligomeric fraction.

To further investigate the impact of enzymatic degradation on the surface and therefore on the material's properties, dynamic mechanical measurement over a whole range of stress intensities was performed. In Figure 7, the fatigue growth rate, da/dN , for six averaged curves of PET*96 h and PET control sample versus the applied stress intensity factor ΔK at the crack tip was plotted to investigate the FCP behavior.

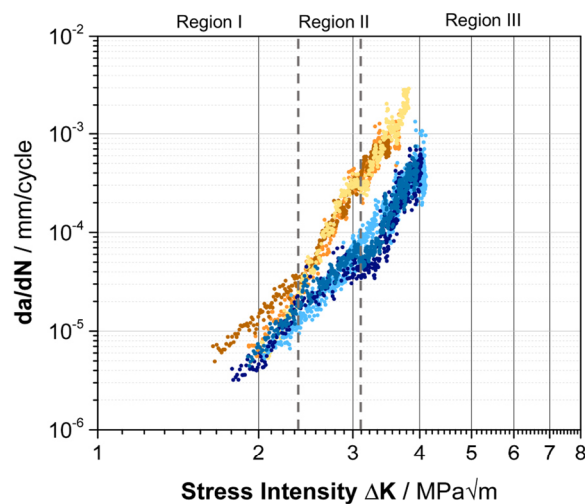


Figure 7. FCP behavior of the PET control (light blue, blue, dark blue) and PET*96 h (yellow, orange, brown) samples in a double logarithmic scale with the division into three relevant regions, marked by the dashed lines and grey color.

In general, da/dN curves can be subdivided into three different crack propagation regions, as shown in Figure 7. Region I describes the crack propagation after reaching the threshold value ΔK_{th} . Below this value, crack propagation is negligibly low. Region II represents stable crack growth according to the Paris–Erdogan Equation $da/dN = C (\Delta K)^m$, where C and m are material constants. Region III is determined by instable crack propagation until the final fracture of the sample.

In the case of PET, the behavior of the material did not significantly differ from the control sample in region I, except for one enzyme-incubated sample with a lower threshold value. This can be explained by the inhomogeneities of biotic treatment, as observed in SEM (Figure 3). However, with increasing mechanical load upon region II, the empowered crack propagation rates of the PET*96 h samples indicate the reduction in crack growth resistance. These results are consistent with the formation of BHET species on the surface, which is associated with the breakdown of individual polymer chains and material deterioration. The degradation of individual polymer chains results in a decreasing number of links between the crystalline PET units, so-called tie-molecules. With decreasing tie-molecule density, the craze network is destabilized, and the induced dynamic load causes

molecular fracture, resulting in macroscopically brittle behavior [46,47]. Additionally, the development of a craze network could be interrupted by those additional crystalline units of BHET oligomers. Consequently, complete failure of the enzyme-treated material can be investigated at lower stress intensities compared to the control samples in region III accompanied by a faster crack growth velocity.

To quantify the influence of enzymatic degradation, a fit was applied to each measurement in the linear-dependent stable crack propagation in region II (Figure 8). The linear fit in a logarithmic scale shows the impact of enzymes in combination with mechanical stress. Without enzymatic treatment, an average slope of $m_b = 5.5 \pm 1.1$ can be calculated according to $y = a \times x^m$ for the PET control. In comparison to the PET*96 h sample, the value of the slope increased to $m_e = 10.2 \pm 1.4$. This clearly identifies an impact of PETase on the degradation behavior on the path from macro- to microplastic by fragmentation due to mechanical stress.

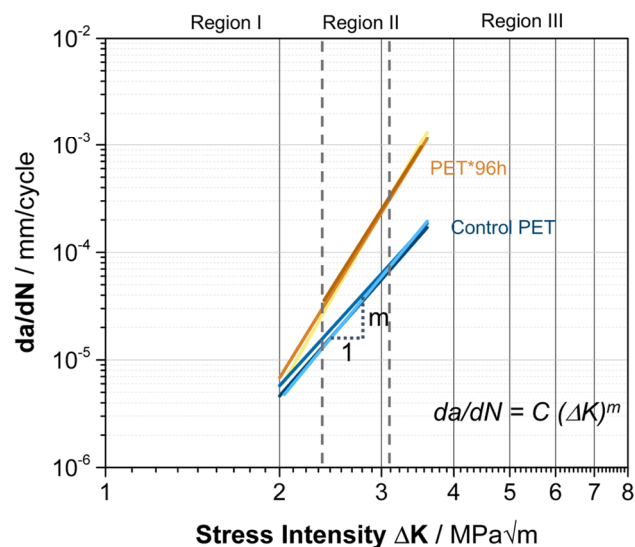


Figure 8. Power function fit of the FCP data on the linear range in region II in a double logarithmic scale with curves for the PET control (light blue, blue, dark blue) and PET*96 h (yellow, orange, dark orange). The averaged parameters for the fit are $m_b = 5.5 \pm 1.1$, $C_b = 10^{-7.9} \pm 0.5$ for the PET control samples, and $m_e = 10.2 \pm 1.4$, $C_e = 10^{-8.4} \pm 0.6$ for PET*96 h.

4. Conclusions

The time-dependent investigation of PET samples exposed to PETase showed the formation of colloidal structures growing with incubation time and thereby increasing the surface roughness. These structures could be attributed to BHET dimer affecting the crystalline structure on the PET surface. The interruption of the crystalline order accompanied by the degradation of single polymer chains facilitated the crack propagation under mechanical stress, resulting in earlier failure of the incubated sample compared to the control. Within this study, we showed that biotic factors have a relevant impact on the pathway from macro- to microplastic, as material properties play a decisive role in the progress of plastic fragmentation. The investigations further hinted at certain preferences in substrate binding to PETase. Our results provide a first step towards understanding the impact of enzymatic treatment through the establishment of a reliable method for the quantification and development of a new experimental setup. The applied methods provide reliable data for the quantitative analysis of biotic impact by enzymatic degradation.

The results gained from this pilot study provide the basis for future interdisciplinary research combining biochemistry and material science. Here, we established a method for the determination of enzymatic activity on material properties in a quantifiable fashion. This protocol can act as a foundation towards a full understanding of the interplay between enzyme and material. Future experiments must consider time-resolved analysis as well as a detailed characterization of the surface erosion and chemistry. Moreover, to fully cover the degradation process in nature with its implications on material properties, there is a need to include abiotic factors such as temperature, pH, stage of weathering of PET material, and material composition with the parameters of biotic degradation like enzyme type or concentrations, incubation time, and buffer composition. The described method now provides a reliable platform to perform these studies in the future.

Author Contributions: Conceptualization, T.M., S.W. and B.H.; writing—original draft preparation, T.M. and S.W.; writing—review and editing, B.H., H.R. and V.A.; investigation, T.M., S.W., A.G., Y.E. and S.S.; supervision, B.H., H.R., V.A. and G.P. All authors have read and agreed to the published version of the manuscript.

Funding: This work was funded by the Deutsche Forschungsgemeinschaft (DFG, German Research Foundation)—project number 391977956—SFB 1357 Microplastics, subproject B01, C01, and C03.

Data Availability Statement: The data set used in this study is published on Zenodo, <https://doi.org/10.5281/zenodo.5657200>, accessed on 10 November 2021.

Acknowledgments: The authors would like to thank Sebastian Gröschel for sample preparation, Rika Schneider for GPC measurements, Alexander Brückner for dynamic-mechanical measurements, and Annika Pfaffenberger for SEM micrographs. We further acknowledge financial support by the University of Bayreuth Open Access Publishing Fund.

Conflicts of Interest: The authors declare no conflict of interest.

References

1. Thompson, R.C.; Olsen, Y.; Mitchell, R.P.; Davis, A.; Rowland, S.J.; John, A.W.G.; McGonigle, D.; Russell, A.E. Lost at Sea: Where Is All the Plastic? *Science* **2004**, *304*, 838. [\[CrossRef\]](#)
2. Weinstein, J.E.; Crocker, B.K.; Gray, A.D. From macroplastic to microplastic: Degradation of high-density polyethylene, polypropylene, and polystyrene in a salt marsh habitat. *Environ. Toxicol. Chem.* **2016**, *35*, 1632–1640. [\[CrossRef\]](#)
3. Waldman, W.R.; Rillig, M.C. Microplastic Research Should Embrace the Complexity of Secondary Particles. *Environ. Sci. Technol.* **2020**, *54*, 7751–7753. [\[CrossRef\]](#) [\[PubMed\]](#)
4. Khoironi, A.; Hadiyanto, H.; Anggoro, S.; Sudarno, S. Evaluation of polypropylene plastic degradation and microplastic identification in sediments at Tambak Lorok coastal area, Semarang, Indonesia. *Mar. Pollut. Bull.* **2020**, *151*, 110868. [\[CrossRef\]](#) [\[PubMed\]](#)
5. Zhang, K.; Hamidian, A.H.; Tubić, A.; Zhang, Y.; Fang, J.K.; Wu, C.; Lam, P.K. Understanding plastic degradation and microplastic formation in the environment: A review. *Environ. Pollut.* **2021**, *274*, 116554. [\[CrossRef\]](#) [\[PubMed\]](#)
6. Chamas, A.; Moon, H.; Zheng, J.; Qiu, Y.; Tabassum, T.; Jang, J.H.; Abu-Omar, M.M.; Scott, S.L.; Suh, S. Degradation Rates of Plastics in the Environment. *ACS Sustain. Chem. Eng.* **2020**, *8*, 3494–3511. [\[CrossRef\]](#)
7. Julienne, F.; Delorme, N.; Lagarde, F. From macroplastics to microplastics: Role of water in the fragmentation of polyethylene. *Chemosphere* **2019**, *236*, 124409. [\[CrossRef\]](#)
8. Kalogerakis, N.; Karkanorachaki, K.; Kalogerakis, G.C.; Triantafyllidi, E.I.; Gotsis, A.D.; Partsinevelos, P.; Fava, F. Microplastics Generation: Onset of Fragmentation of Polyethylene Films in Marine Environment Mesocosms. *Front. Mar. Sci.* **2017**, *4*, 84. [\[CrossRef\]](#)
9. Gewert, B.; Plassmann, M.M.; MacLeod, M. Pathways for degradation of plastic polymers floating in the marine environment. *Environ. Sci. Process. Impacts* **2015**, *17*, 1513–1521. [\[CrossRef\]](#) [\[PubMed\]](#)
10. Kawai, F.; Kawabata, T.; Oda, M. Current knowledge on enzymatic PET degradation and its possible application to waste stream management and other fields. *Appl. Microbiol. Biotechnol.* **2019**, *103*, 4253–4268. [\[CrossRef\]](#) [\[PubMed\]](#)
11. Müller, R.-J.; Schrader, H.; Profe, J.; Dresler, K.; Deckwer, W.-D. Enzymatic Degradation of Poly(ethylene terephthalate): Rapid Hydrolyse using a Hydrolase from *T. fusca*. *Macromol. Rapid Commun.* **2005**, *26*, 1400–1405. [\[CrossRef\]](#)
12. Sulaiman, S.; Yamato, S.; Kanaya, E.; Kim, J.-J.; Koga, Y.; Takano, K.; Kanaya, S. Isolation of a Novel Cutinase Homolog with Polyethylene Terephthalate-Degrading Activity from Leaf-Branch Compost by Using a Metagenomic Approach. *Appl. Environ. Microbiol.* **2012**, *78*, 1556–1562. [\[CrossRef\]](#)
13. Yoshida, S.; Hiraga, K.; Takehana, T.; Taniguchi, I.; Yamaji, H.; Maeda, Y.; Toyohara, K.; Miyamoto, K.; Kimura, Y.; Oda, K. A bacterium that degrades and assimilates poly(ethylene terephthalate). *Science* **2016**, *351*, 1196–1199. [\[CrossRef\]](#) [\[PubMed\]](#)

14. Danso, D.; Schmeisser, C.; Chow, J.; Zimmermann, W.; Wei, R.; Leggewie, C.; Li, X.; Hazen, T.; Streit, W.R. New Insights into the Function and Global Distribution of Polyethylene Terephthalate (PET)-Degrading Bacteria and Enzymes in Marine and Terrestrial Metagenomes. *Appl. Environ. Microbiol.* **2018**, *84*, e02773-17. [[CrossRef](#)]
15. Fechine, G.; Souto-Maior, R.M.; Rabello, M.S. Structural changes during photodegradation of poly(ethylene terephthalate). *J. Mater. Sci.* **2002**, *37*, 4979–4984. [[CrossRef](#)]
16. Fechine, G.; Rabello, M.; Maior, R.S.; Catalani, L. Surface characterization of photodegraded poly(ethylene terephthalate). The effect of ultraviolet absorbers. *Polymer* **2004**, *45*, 2303–2308. [[CrossRef](#)]
17. Ioakeimidis, C.; Fotopoulou, K.N.; Karapanagioti, H.K.; Geraga, M.; Zeri, C.; Papatheodorou, E.; Galgani, F.; Papatheodorou, G. The degradation potential of PET bottles in the marine environment: An ATR-FTIR based approach. *Sci. Rep.* **2016**, *6*, 23501. [[CrossRef](#)] [[PubMed](#)]
18. Meides, N.; Menzel, T.; Poetzschner, B.; Löder, M.G.J.; Mansfeld, U.; Strohriegel, P.; Altstaedt, V.; Senker, J. Reconstructing the Environmental Degradation of Polystyrene by Accelerated Weathering. *Environ. Sci. Technol.* **2021**, *55*, 7930–7938. [[CrossRef](#)] [[PubMed](#)]
19. Allen, N.S.; Edge, M.; Mohammadian, M.; Jones, K. Hydrolytic degradation of poly(ethylene terephthalate): Importance of chain scission versus crystallinity. *Eur. Polym. J.* **1991**, *27*, 1373–1378. [[CrossRef](#)]
20. Edge, M.; Hayes, M.; Mohammadian, M.; Allen, N.; Jewitt, T.; Brems, K.; Jones, K. Aspects of poly(ethylene terephthalate) degradation for archival life and environmental degradation. *Polym. Degrad. Stab.* **1991**, *32*, 131–153. [[CrossRef](#)]
21. Sammon, C.; Yarwood, J.; Everall, N. An FT-IR study of the effect of hydrolytic degradation on the structure of thin PET films. *Polym. Degrad. Stab.* **2000**, *67*, 149–158. [[CrossRef](#)]
22. Arhant, M.; Le Gall, M.; Le Gac, P.-Y.; Davies, P. Impact of hydrolytic degradation on mechanical properties of PET—Towards an understanding of microplastics formation. *Polym. Degrad. Stab.* **2019**, *161*, 175–182. [[CrossRef](#)]
23. Fayolle, B.; Audouin, L.; Verdu, J. A critical molar mass separating the ductile and brittle regimes as revealed by thermal oxidation in polypropylene. *Polymer* **2004**, *45*, 4323–4330. [[CrossRef](#)]
24. Awaja, F.; Pavel, D. Recycling of PET. *Eur. Polym. J.* **2005**, *41*, 1453–1477. [[CrossRef](#)]
25. OECD. Improving Plastics Management: Trends, policy responses, and the role of international co-operation and trade. *OECD Environ. Policy Pap.* **2018**, *12*, 20. [[CrossRef](#)]
26. Austin, H.P.; Allen, M.D.; Donohoe, B.S.; Rorrer, N.; Kearns, F.; Silveira, R.L.; Pollard, B.C.; Dominick, G.; Duman, R.; El Omari, K.; et al. Characterization and engineering of a plastic-degrading aromatic polyestherase. *Proc. Natl. Acad. Sci. USA* **2018**, *115*, E4350–E4357. [[CrossRef](#)] [[PubMed](#)]
27. Altstädt, V. The Influence of Molecular Variables on Fatigue Resistance in Stress Cracking Environments. In *Intrinsic Molecular Mobility and Toughness of Polymers II*; Springer: Berlin/Heidelberg, Germany, 2005; pp. 105–152.
28. Liu, H.-Y.; Wang, G.; Mai, Y.-W. Cyclic fatigue crack propagation of nanoparticle modified epoxy. *Compos. Sci. Technol.* **2012**, *72*, 1530–1538. [[CrossRef](#)]
29. Runt, J.; Gallagher, K.P. The influence of microstructure on fatigue crack propagation in polyoxymethylene. *J. Mater. Sci.* **1991**, *26*, 792–798. [[CrossRef](#)]
30. Ramirez, A.; Manson, J.A.; Hertzberg, R.W. Fatigue crack propagation in amorphous poly(ethylene terephthalate). *Polym. Eng. Sci.* **1982**, *22*, 975–981. [[CrossRef](#)]
31. Altstaedt, V.; Keiter, S.; Renner, M.; Schlarb, A. Environmental Stress Cracking of Polymers Monitored by Fatigue Crack Growth Experiments. *Macromol. Symp.* **2004**, *214*, 31–46. [[CrossRef](#)]
32. Kothmann, M.; Zeiler, R.; de Anda, A.R.; Brückner, A.; Altstädt, V. Fatigue crack propagation behaviour of epoxy resins modified with silica-nanoparticles. *Polymer* **2015**, *60*, 157–163. [[CrossRef](#)]
33. Gibson, D.G.; Young, L.; Chuang, R.Y.; Venter, J.C.; Hutchison, C.A.; Smith, H.O. Enzymatic assembly of DNA molecules up to several hundred kilobases. *Nat. Methods* **2009**, *6*, 343–345. [[CrossRef](#)]
34. Wunderlich, B. *Thermal Analysis of Polymeric Materials*; Springer Science & Business Media: Berlin/Heidelberg, Germany, 2005.
35. R Core Team. *R: A Language and Environment for Statistical Computing*; R Foundation for Statistical Computing: Vienna, Austria, 2021.
36. Kawai, F. The Current State of Research on PET Hydrolyzing Enzymes Available for Biorecycling. *Catalysts* **2021**, *11*, 206. [[CrossRef](#)]
37. Son, H.F.; Cho, I.J.; Joo, S.; Seo, H.; Sagong, H.-Y.; Choi, S.Y.; Lee, S.Y.; Kim, K.-J. Rational Protein Engineering of Thermo-Stable PETase from *Ideonella sakaiensis* for Highly Efficient PET Degradation. *ACS Catalysis* **2019**, *9*, 3519–3526. [[CrossRef](#)]
38. Groeninckx, G.; Reynaers, H. Morphology and melting behavior of semicrystalline poly(ethylene terephthalate). II. Annealed PET. *J. Polym. Sci. Polym. Phys. Ed.* **1980**, *18*, 1325–1341. [[CrossRef](#)]
39. Mancini, S.D.; Zanin, M. Recyclability of PET from virgin resin. *Mater. Res.* **1999**, *2*, 33–38. [[CrossRef](#)]
40. Güçlü, G.; Kasgöz, A.; Özbudak, S.; Özgümüş, S.; Orbay, M. Glycolysis of poly(ethylene terephthalate) wastes in xylene. *J. Appl. Polym. Sci.* **1998**, *69*, 2311–2319. [[CrossRef](#)]
41. Baliga, S.; Wong, W.T. Depolymerization of poly(ethylene terephthalate) recycled from post-consumer soft-drink bottles. *J. Polym. Sci. Part A Polym. Chem.* **1989**, *27*, 2071–2082. [[CrossRef](#)]
42. Krehula, L.K.; Hrnjak-Murđić, Z.; Jelenčić, J.; Andričić, B. Evaluation of Poly(ethylene-terephthalate) Products of Chemical Recycling by Differential Scanning Calorimetry. *J. Polym. Environ.* **2009**, *17*, 20–27. [[CrossRef](#)]

43. Imran, M.; Kim, B.-K.; Han, M.; Cho, B.G.; Kim, D.H. Sub- and supercritical glycolysis of polyethylene terephthalate (PET) into the monomer bis(2-hydroxyethyl) terephthalate (BHET). *Polym. Degrad. Stab.* **2010**, *95*, 1686–1693. [[CrossRef](#)]
44. Fecker, T.; Galaz-Davison, P.; Engelberger, F.; Narui, Y.; Sotomayor, M.; Parra, L.P.; Ramírez-Sarmiento, C.A. Active Site Flexibility as a Hallmark for Efficient PET Degradation by *I. sakaiensis* PETase. *Biophys. J.* **2018**, *114*, 1302–1312. [[CrossRef](#)] [[PubMed](#)]
45. Tournier, V.; Topham, C.M.; Gilles, A.; David, B.; Folgoas, C.; Moya-Leclair, E.; Kamionka, E.; Desrousseaux, M.-L.; Texier, H.; Gavalda, S.; et al. An engineered PET depolymerase to break down and recycle plastic bottles. *Nat. Cell Biol.* **2020**, *580*, 216–219. [[CrossRef](#)]
46. Pecorini, T.; Hertzberg, R. The fracture toughness and fatigue crack propagation behaviour of annealed PET. *Polymer* **1993**, *34*, 5053–5062. [[CrossRef](#)]
47. Yeh, J.T.; Runt, J. Fatigue crack-propagation in annealed poly(butylene terephthalate). *J. Mater. Sci.* **1989**, *24*, 2637–2642. [[CrossRef](#)]

Investigation of the halophilic PET hydrolase PET6 from *Vibrio gazogenes*

Investigation of the halophilic PET hydrolase PET6 from *Vibrio gazogenes*

Weigert, Sebastian¹; Perez-Garcia, Pablo^{2,3}; Gisdon, Florian J¹; Gagsteiger, Andreas¹; Chibani, Cynthia M³; Schmitz, Ruth A³; Schweinshaut, Kristine¹; Ullmann, Matthias⁴; Chow, Jennifer²; Streit, Wolfgang²; Höcker, Birte^{1,*}

¹Department of Biochemistry, University of Bayreuth, 95447 Bayreuth, Germany

²Department of Microbiology and Biotechnology, University of Hamburg, 22609 Hamburg, Germany

³Institute for General Microbiology, Christian-Albrechts-Universität zu Kiel, 24118 Kiel, Germany

⁴Computational Biochemistry, University of Bayreuth, 95447 Bayreuth, Germany

Keywords: HMM, hydrolases, PETase, metagenome, metagenomic screening, PET degradation, Polyethylene terephthalate (PET), BHET, TPA

The authors declare no conflict of interest.

***Correspondence**

Investigation of the halophilic PET hydrolase PET6 from *Vibrio gazogenes*

The handling of plastic waste and the associated ubiquitous occurrence of microplastic poses one of the biggest challenges of our time. Recent investigations of plastic degrading enzymes have opened new prospects for biological microplastic decomposition as well as recycling applications. Especially for the degradation of polyethylene terephthalate (PET) enzymes with promising performance, such as LC-cutinases or PETase from *Ideonella sakaiensis*, were found. We employed homology searches to discover other PET degrading enzymes with novel characteristics and identified an interesting candidate, PET6, from the halophile *Vibrio gazogenes*. While investigations of PET6 showed only a moderate turnover of PET substrate compared to other enzymes, we detected a remarkable salt tolerance with considerable enzymatic activity even above 1M sodium chloride. The enzyme's crystal structure, which confirms it as a member of the α/β -hydrolase fold, provides insights into structural adaptation to its saline environment. By grafting beneficial mutations from other PET degrading enzymes onto PET6, we could increase the activity up to threefold, demonstrating the evolutionary potential of the enzyme. With tremendous amounts of plastic waste ending up in the ocean and *Vibrio gazogenes* being widely present in marine biofilms, the reversed salt activity profile could signify that PET6 is a worthy candidate for natural PET decomposition. Therefore, we mapped the occurrence of *Vibrios* containing PET6 homologs and demonstrated their ubiquitous prevalence in the pangenome of several *Vibrio* strains. Considering the global occurrence of *Vibrio* in saltwater ecosystems and the halo-tolerance of PET6, our findings suggest *Vibrio* and the PET6 enzyme itself as interesting subjects to study ongoing PET degradation in marine environments.

INTRODUCTION

Plastic pollution, which is considered an urgent current threat, is a consequence of the massive popularity of plastic materials starting in the 1950s and paired with enduring inadequate waste management worldwide. While the world plastic production has grown to enormous 415 million tons in 2016¹, rates for recycling and incineration are still low, with over 50% of the plastic waste being discarded despite large improvements over the last decades². As a result, plastic is constantly leaking into the environment via different paths, where a large share eventually enters the oceans^{3,4}. The downside of plastics' inherent beneficial material properties, such as high mechanical strength and resistance to various chemical and environmental factors, is that it facilitates persistence in the environment for decades⁵. Nevertheless, plastics also suffer from weathering where factors such as UV radiation, temperature, humidity, and physical forces from wind or waves treat material leading to embrittlement and finally fragmentation⁶⁻⁹. This continuous disintegration yields high amounts of microplastic (< 5mm in size) and even more nanoplastic particles (<1 μ m), which have both raised major health-related and ecological concerns¹⁰⁻¹². The size of those particles determines adverse interactions with organisms where macroscopic litter might harm through entanglement. In contrast, microplastic particles are ingested and impair energy uptake and subsequent viability^{13,14}, while smaller particles can cause irritation and might get incorporated in tissues and cells, causing detrimental effects^{15,16}. Plastics are not inert upon biological contact but can be affected by microbial degradation through enzymes, especially those polymers featuring a heteroatom backbone¹⁷. These polymer types include polyamides (PA), polyurethanes (PU), and polyesters, which in theory can be cleaved by members of the extensive class of hydrolases. Insights into PA and PU degrading enzymes are comparably sparse, but many enzymes are known to be active on polyesters. In the scope of plastic pollution, hydrolases with activity on the commodity plastic polyethylene terephthalate (PET) came to the fore. The first PET degrading enzyme TfH was reported in 2015 by Müller *et al.*, which was isolated from *Thermobifida fusca* belonging to the order of *Actinomycetales*¹⁸. As members of this order are common in the context of plant material degradation, including cutin¹⁹, many PET degrading enzymes identified were found from bacteria of this order, including prominent TfCut2, Thc_Cut1, Est119, and LCC¹⁹⁻²³. Over the last years, protein engineering was applied to increase activity and thermostability of these enzymes, enabling future recycling applications. Recently this culminated in the publication of Tournier *et al.* presenting a proof of concept for enzymatic PET recycling employing engineered variants of LCC²⁴. In 2016, the discovery of *Ideonella sakaiensis*, a bacteria that can exploit PET as sole energy and carbon source, attracted

Investigation of the halophilic PET hydrolase PET6 from *Vibrio gazogenes*

attention²⁵. This ability is facilitated by a two-enzyme system that consists of a cutinase-like enzyme called PETase (IsPETase) undertaking the coarse degradation whose main product mono-(2-hydroxyethyl)-terephthalate (MHET) is further hydrolyzed by the second enzyme MHETase. The latter is related to feruloyl esterase and shows a comparably high specificity towards its substrate MHET²⁶, and increases PET hydrolysis rates of IsPETase when used together²⁷.

In contrast to most previously characterized enzymes, IsPETase shows decent activity at temperatures of 30°-40°C, implying the possibility for substantial PET degradation in the environment. To evaluate this scenario, the prevalence of those enzymes must be analyzed, and their actual degradation activity on PET subsequently investigated. Therefore Danso et al. conducted a bioinformatic search employing a hidden Markov model (HMM) approach trained with the structure-function relationships from known PET hydrolase to identify new potential enzymes in genomic samples from various environments²⁸. They identified several new potential enzymes, and PET hydrolase activity was measured among other for PET6²⁸. This enzyme is found in the proteobacteria *Vibrio gazogenes* from the genus *Vibrio*, whose members are ubiquitously present in saline and marine environments²⁹. Of particular interest in the scope of plastic pollution is their prevalence in estuaries, salt marshes, and in the plastisphere, which describes the microbial environment around plastic particles³⁰⁻³³. As there are million tons of plastic particles in the oceans and rivers as a main entrance path for plastic in the environments³⁴ mounding in estuaries and neighboring salt marshes, PET6 is a reasonable candidate to investigate its PET degradation potential. In particular, those ecosystems like estuaries and salt marshes combine the reported prevalence of *Vibrio* species and high concentrations of plastics and microplastics^{35,36}.

In this study we characterize PET6 in detail and evaluate its potential for PET degradation in near-realistic saline conditions. This enables insights into the adaptation of this enzyme towards its environment and allows for rough estimation of whether *Vibrios* might facilitate PET degradation in the environment.

Investigation of the halophilic PET hydrolase PET6 from *Vibrio gazogenes*

RESULTS and DISCUSSION

Characterization of PET6 activity

PET6 was expressed heterologously in *E.coli* and purified to homogeneity using an encoded histidine tag. After purification, we first wanted to validate and characterize the enzyme's capabilities to degrade PET. Here, we employed our previously developed assay platform for PET degradation, which works with a PET coating inside standard lab consumables as substrate³⁷. The coating was prepared from post-consumer PET bottles to achieve a near-realistic substrate with a crystallinity of around 10%. Besides the general capacity for PET degradation, the enzyme's individual optima regarding temperature and ionic strength were investigated. The experimental setup for examining the enzyme's activity in the presence of salt covered sodium chloride concentrations between 25 and 2500 mM based on the saline origin of *V. gazogenes*, and was conducted in PET coated 96-well microtiter plates. Similarly, PCR tubes were used to screen the optimal temperature, utilizing the temperature gradient function of a thermo-cycler to cover the range from 30 to 55 °C (Figure 1). It should be noted that the application of PET coating on PCR tubes causes higher standard deviations in the experiments, which can also be seen in the presented measurements. As a reference, the well-studied IsPETase was included for both quantitative benchmark and qualitative comparison of the determined optima. The activity was determined by UHPLC summing up TPA, BHET, and MHET to the total product release. As IsPETase showed substantially higher activity at the given conditions, the concentration was adjusted to fit the substrate limits of the assay. Therefore, IsPETase was used at 20 nM while PET6 was employed at 2 μM.

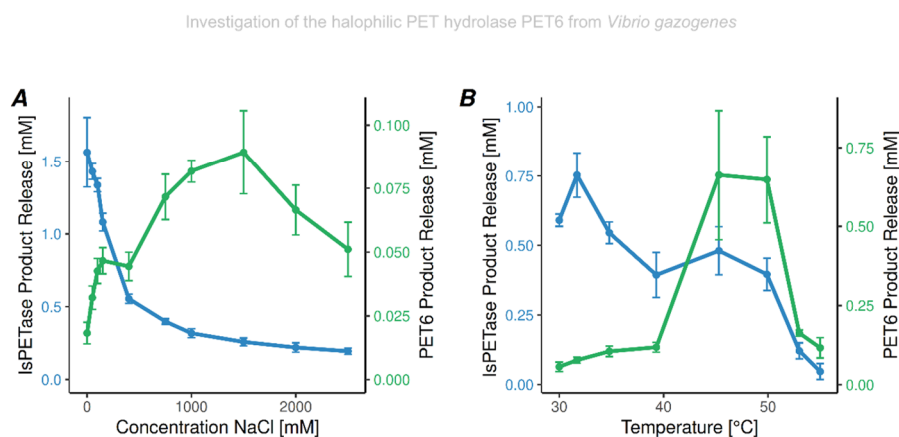


FIGURE 1- Activity of PET6 and IsPETase at varying temperatures and salt concentrations on PET. PET6 and IsPETase were incubated for 18h at a concentration of 2 μ M and 20 nM, respectively. **A** The effect of salt concentrations on the two enzymes varied between 0 and 2500 mM (measured in a 96-well MTP setup at 30 °C). **B** Different incubations temperatures in the range of 30 and 55 °C were tested (measured in coated PCR tubes) with the sodium chloride concentration fixed at 50 mM.

The results indicate that IsPETase has a relatively broad temperature range for activity with an optimum at around 30°C, whereas PET6 shows a distinct optimum between 45 and 50 °C. The different behavior of the two enzymes is even more noticeable when looking at the impact of ionic strength on the PET degradation activity. While PET6 shows little activity at low salt concentrations, the product release increases rapidly with an optimum between 1 and 1.5 M NaCl. On the contrary, IsPETase displays the opposite behavior towards salt with an optimum at low salt and rapidly decreasing activity with rising ionic strength. Still, when compared quantitatively, IsPETase outperforms PET6 in every scenario, in particular considering the differently used concentrations of the enzymes.

Structural Analysis

Next we aimed to investigate if the differences between IsPETase and PET6 activity are reflected on a molecular level. Thus, crystal trials were set up as a first step to obtain an X-ray structure of PET6. The protein crystallized in a condition containing Sodium Potassium Phosphate and 2-Methyl-2,4-pentanediol (MPD), yielding crystals suitable for x-ray diffraction experiments without further optimization. The

Investigation of the halophilic PET hydrolase PET6 from *Vibrio gazogenes*

crystallographic data quality indicators show good results throughout with the resolution cut-off at 1.4 Å resulting in a R-meas of 5.4% (30.0%), $I/\sigma(I)$ of 19.45 (4.70), and CC1/2 of 99.9 (92.3), with the expression in brackets as the respective value in the highest resolution (Table S1). However, the moderate data completeness of 95.6% (91% in the highest resolution shell) is typical for the P1 space group. The solved structure shows three protein entities in the asymmetric unit, together with three phosphates, two sodium and one chloride ion symmetrically arranged around each chain (Figure 2 A).

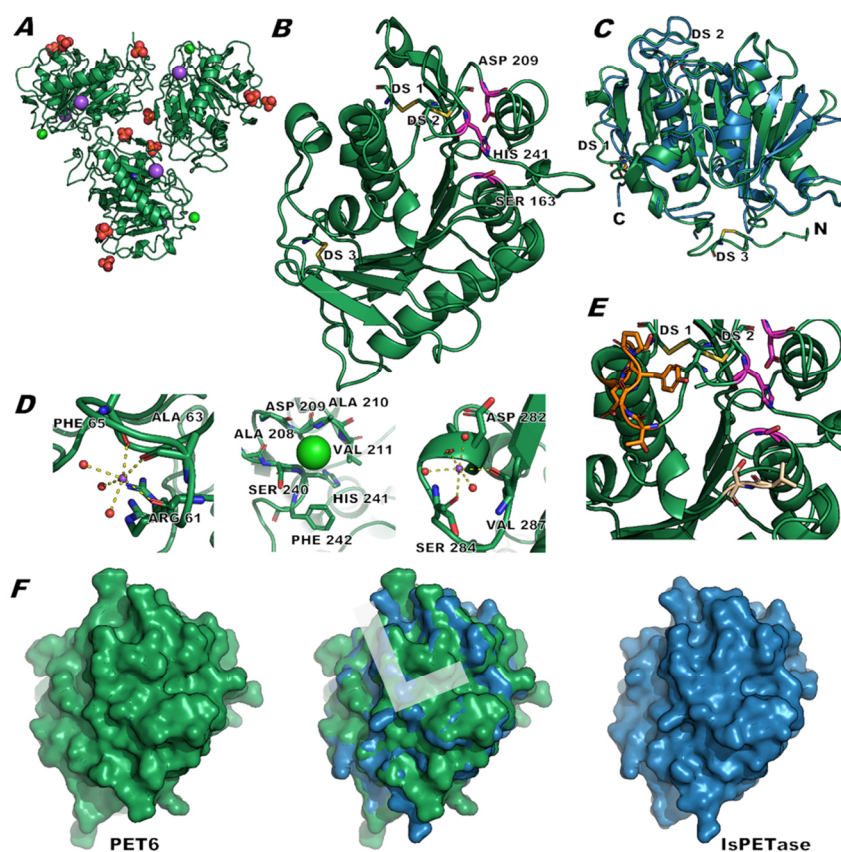


FIGURE 2 Crystal structure of PET6 (green) and comparison to IsPETase (blue). Figure A shows the asymmetric unit of the PET6 crystal structure (green) containing three protein molecules, ions are depicted as colored spheres, including phosphate (orange-red), sodium (purple), and chloride (neon green). B displays a single chain, with the catalytic triad (Ser-His-Asp) highlighted in pink; the three disulfide bonds are labeled DS1-3. C illustrates how the superimposed structures of PET6

Investigation of the halophilic PET hydrolase PET6 from *Vibrio gazogenes*

and IsPETase have only a few deviations at loops and termini. **D** highlights ion binding with the two sodium ions (violet) being coordinated by three carbonyl oxygens and three waters, while chloride (neon green) is located in a hydrophobic pocket. The positions of subsequent mutations are shown in **E** with the loop region (Ex-Loop) in dark orange and two residues for the double mutant VSTA in beige in proximity to the active site colored in pink. **F** compares the surface of the two proteins with a focus on the putative substrate-binding site approximated as L shape in the superimposed structure.

As indicated by the sequence similarity to other PET degrading enzymes, PET6 can be identified as an enzyme of the alpha/beta hydrolase fold. The characteristic topology of this class features eight beta-strands connected with alpha-helices and a conserved arrangement of the catalytic triad (Ser163, Asp209, and His241), with all of them present in PET6 (Figure 2 B-C). As observed in other solved PETase crystal structures, all these enzymes are highly alike, with only minor differences in loop regions. The pseudo symmetry indicated by the crystallographic parameters is also reflected in the asymmetric unit of the solved structure. The arrangement of the three protein chains, including surrounding and bound ions, is highly symmetrical (Figure 2 C). Consequently, the chains show an all-atom RMSD of only 0.61 to 0.68 Å among each other. PET6 features three disulfide bonds labeled with DS 1-3 (Figure 2 B, C, E). DS 1 is located close to the C-terminus and is formed between residue 277 and 294 and is conserved in all cutinases. Therefore it was included in the HMM search model from Danso *et al.*²⁸. The second disulfide bond DS 2 connects the residues 206 and 243 and is located close to the active site. This disulfide bond position has been mainly described for fungal cutinases but is also found in the IsPETase. DS 3 is located at the N-terminus between residues 27 and 30 and is not commonly described for PET hydrolases or cutinases.

The presence of three coordinated ions per chain in the asymmetric unit is of particular interest. Binding sites for divalent cations such as Ca²⁺, Zn²⁺, and Mg²⁺ have been described for several cutinases and PET hydrolases, showing stabilizing effects and increasing activity when bound³⁸. PET6, on the contrary, shows binding of monovalent ions with one sodium ion coordinated by the carbonyl oxygens of the residues Arg 61, Ala 63, and Phe 65; the typical octahedral coordination is completed by three water molecules (Figure 2 D). The same scheme is repeated for a second sodium ion, interacting with the residues Asp 282, Ser 284, and Val 287. The chloride ion is positioned in a shallow pocket created by the residues Ala 208, Asp 209, Ala 210, Val 211, Ser 240, His241, Phe 242, forming a relative hydrophobic environment. Thereby the chloride ion forms no direct polar contacts with the surrounding residues. Comparing these ion binding sites with other cutinase structures revealed the same chloride binding site in Thc_Cut1 (PDB-ID: 5LUI, 2x Mg²⁺ 3x Cl⁻) and Cut190 (PDB-ID: 4WFK). The latter further shares the

Investigation of the halophilic PET hydrolase PET6 from *Vibrio gazogenes*

ion binding site around the residues 61, 63, and 65 of PET6 (Figure 2 D) but coordinates a Ca^{2+} instead. This behavior towards monovalent ions might be a result of adapting to saline environments with high sodium chloride concentrations. Further, it hints at how salt concentrations impact the enzyme's activity.

Due to the high similarity of IsPETase and PET6 (Figure 2 C), the resulting shape and surface are also highly alike (Figure 2F), with slight differences in the loop regions and positioning of side chains. The predicted binding site of the PET strand for IsPETase is a very distinct shallow binding groove on both sides of the active site. Docking studies conducted by Joo *et al.* proposed an L-shaped binding pose³⁹. A part of this binding site described by the authors is formed by a series of six residues, which are referred to as the extended loop. The surface of PET6 shows a similarly shaped binding groove but with one knob blocking the upper leg of the hypothetical L-binding site, as visible in the figure of the superimposed surfaces (Figure 2F). This knob originates from Tyr248, while IsPETase's corresponding residue, within the extended loop region, is the smaller asparagine³⁹ (Figure 2 E). The B-factors of Tyr248, including the sidechain, show no abnormalities compared to the neighboring residues. Thus, there is no sign of particular flexibility that might indicate a flopping out movement. Consequently, this tyrosine might comprise an obstacle for the proposed binding mode analogous to IsPETase and, therefore, reduce activity. Yet this mode of this L-shaped binding was also questioned, mainly asking whether the PET substrate would take on the necessary conformation for that binding mode⁴⁰.

PET 6 variants

To explore the evolutionary potential of PET6, we tested some mutants of the enzyme. The first variant targets the tyrosine in the extended loop of PET6 that was revealed in the crystal structure. To check if this tyrosine is hindering substrate-binding based on the mode described by Joo *et al.*³⁹, we mutated this residue to the less bulky alanine (PET6-YLA, mutation Y248A). For another variant, the entire extended loop (residues 246-251, sequence TGYPS) was exchanged with the SGNSNQ-sequence from IsPETase (PET-ExLoop). Joo *et al.*³⁹ had also reported the conservation of Thr88 and Ala89 (IsPETase numbering), which we transferred to PET6, changing the corresponding valin to threonine and serine to alanine, creating PET6-VSTA (mutations V91T, S92A). The three variants were benchmarked against each other and IsPETase at high and low salt concentrations with 50 and 1000 mM NaCl and at temperatures between 30, 40, and 50 °C. Due to the significantly higher activity of IsPETase compared to

Investigation of the halophilic PET hydrolase PET6 from *Vibrio gazogenes*

PET6, IsPETase was employed in a lower concentration to fit within the experimental substrate limits; eventually, the results were extrapolated accordingly by a factor of 10 to compare them to the PET6 variants (Figure 3 C-D).

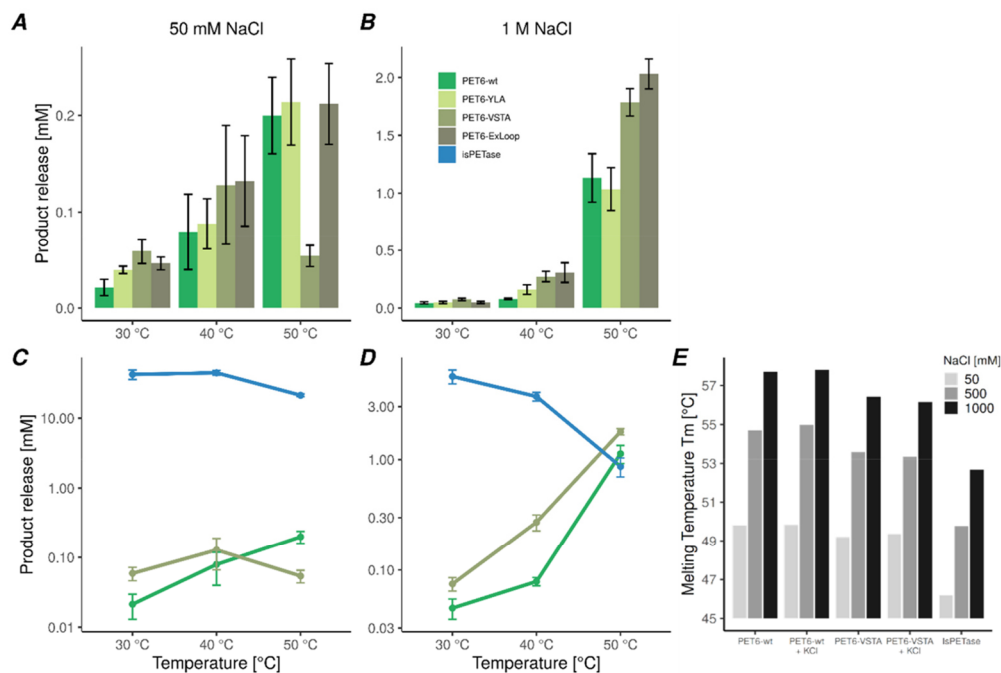


FIGURE 3 Performance of PET6 variants compared to IsPETase at different temperatures and salt concentrations. PET6 variants were used at a concentration of 2 μ M and IsPETase at 200 nM. Therefore, the total product release of IsPETase was extrapolated by a factor of 10 to obtain for comparable results within the activity experiments (A-D). The performance of the PET6 variants at different temperatures is compared in A at 50 mM and B at 1 M salt. The same data is shown in C and D for PET6-wt and PET6-VSTA with IsPETase for comparison; therefore, the y axis is log10 scaled to account for strongly varying performance levels. E shows the analysis of T_m for PET6-wt, PET6-VSTA and IsPETase at varying salt concentrations with differential scanning calorimetry (DSC). The T_m of the enzymes was determined at 50, 500 and 1000 mM NaCl; the two PET6 variants were further characterized in the same conditions with additional 10mM KCl.

At the lower salt concentration of 50mM, all PET6 variants show considerably low activity. Yet, the introduced mutations led to improvements in activity, especially at 30 °C. At higher temperatures the increase in activity is less significant or entirely within the error margin as for 50 °C. The variant VSTA stands out, showing the best improvements but for 50 °C, where the performance breaks down dramatically to a total product release of 0.05 mM

Investigation of the halophilic PET hydrolase PET6 from *Vibrio gazogenes*

compared to 0.2 mM of the other variants, including PET6-wt. At 1 M salt the PET degradation is, as expected, much higher for all PET6 variants, but especially at 40 and 50 °C, the introduced mutations led to a significant increase in performance. In particular, this is true for PET6-ExLoop and VSTA at 40 °C where the total product release reaches 0.31 ± 0.06 and 0.27 ± 0.05 μM , respectively, compared to 0.08 ± 0.01 μM for the wild type. Comparably somewhat less improvement can be seen at 50 °C, where PET6-ExLoop and PET6-VSTA outperform PET6-wt by 79% and 58%, respectively. On the contrary, the single mutant PET6-YLA, reconstructing the aforementioned L-shaped binding site by removing the tyrosine as an obstacle in the binding groove, shows only a slight improvement in all conditions. However, the exchange of the whole extended loop improved the PET degradation performance, especially at 40-50 °C and 1 M salt, suggesting a more complex contribution of these residues. Eventually, these results cannot tell whether this L-shaped binding mode might be accurate or if the increase in activity upon exchange of the residues along the extended loop has different reasons. Given these results, PET6-VSTA is an appealing candidate for further experiments, for one because of its massive boosts in activity with only two mutations compared to the wild type, for the other due to its surprising performance drop at 50 °C at low salt.

When these results of PET6-wt and PET6-VSTA are compared with IsPETase, it is obvious that in the presence of 50 mM NaCl, IsPETase is magnitudes more active at all temperatures with an extrapolated total product release between 21 and 45 μM in contrast to 0.02-0.2 μM for PET6-variants (Figure 3 C). As seen in previous experiments (Figure 1 B), the performance of IsPETase decreases at temperatures around 50 °C (Figure 3 C). At 1 M sodium chloride, IsPETase's performance is decreased to a total product release of 5.6 μM total product release at 30 °C, which further decreases with rising temperatures. This opposite temperature preference of PET6 and IsPETase culminates at 50 °C, where PET6-VSTA and PET6-wt take the lead with 1.8 and 1.1 μM product release over IsPETase with 0.9 μM after extrapolation. This proves a decent PET degradation potential of PET6 under appropriate conditions and categorizes it as PET hydrolase according to Kawai *et al.*⁴¹.

In general, these results suggest that temperature and thereby protein stability in combination with salt might be crucial for PET6-wt activity, as well as for its variants and IsPETase. Therefore, DSC measurements were carried out for PET6-wt and PET-VSTA at 50, 500, and 1000 mM NaCl to determine the melting temperature and investigate this interplay.

Investigation of the halophilic PET hydrolase PET6 from *Vibrio gazogenes*

The analysis shows that higher salt levels generally stabilize the proteins, e.g., PET6-wt gains around 7°C in T_m from 49.8°C to 57.7 °C (Figure 2 E). The same applies in principle for the PET6-VSTA variant, but the two introduced mutations show a destabilizing effect accounting for a 0.5 to 1 °C decrease in T_m compared to the PET-wt at corresponding salt levels. Nevertheless, there is an evident trend in how PET6 benefits from improved stability at higher salt concentrations. Furthermore, the data offers a possible explanation as to why the performance of PET6-VSTA breaks down at 50 °C and low salt in contrast to the wildtype. Both enzymes are employed near or even above their T_m in this condition. However, the small additional destabilization by about 0.6 °C upon the mutations in PET6-VSTA might be sufficient to cause this dramatic activity loss.

Interestingly, the stability of IsPETase is also increased with higher salt concentrations from 46.2 °C at 50 mM to 52.7 °C at 1 M salt. However, this enhanced stability does not translate to higher activity (Figure 3). Once more, this demonstrates the close relation between PET6 performance and ionic strength, which raises the question, whether the type of monovalent ions plays a role. A natural candidate, besides sodium and chloride, is potassium. It is not only a typical component of seawater with high similarity to sodium but also present in the successful crystallization condition containing sodium-potassium phosphate. Compounds in successful crystallization conditions often have stabilizing effects on the protein, eventually promoting crystallization. Another series of DSC measurements were conducted to test whether 10 mM potassium chloride show a stabilizing effect. However, there is no clear difference in the measurements between corresponding conditions (Figure 3 E). The effect of potassium ions on the activity itself was tested in an experimental setup with 1 M salt as a base to minimize the relative increase in total ionic strength upon adding 10 mM potassium chloride. After incubation at 50°C for 18h the total product release of PET6-wt increased about 10% from $476 \pm 22 \mu\text{M}$ to $524 \pm 33 \mu\text{M}$, while rising by 8% for PET6-VSTA from $745 \pm 47 \mu\text{M}$ to $810 \pm 86 \mu\text{M}$. Despite the high standard deviation, these results strongly suggest a positive impact of the potassium ions. Under the given conditions, 10mM KCl means only a rise of about 1 % of the total ionic strength, making it unlikely that this performance increase can only be attributed to the increased ion concentration in general. Additionally, divalent ions including Ca^{2+} , Co^{2+} , Cu^{2+} , Mg^{2+} , Mn^{2+} , Ni^{2+} and Zn^{2+} have been tested in a concentration of 10 mM, but no increase in activity could be detected. This emphasizes the preference of PET6 towards monovalent ions and their specific impact on its activity in contrast to other cutinases and their interaction with divalent metal ions.

Investigation of the halophilic PET hydrolase PET6 from *Vibrio gazogenes*

Binding mode analysis of a PET tetramer to PET6 and PET6-VSTA

The interaction of PET6-wt and PET6-VSTA with a PET tetramer as model substrate was investigated with molecular dynamics (MD) simulations. The simulation parameters were set to 323°K and a total ionic strength of 1050 mM representing the high salt condition where PET6-wt showed the best performance. For the analysis, protein-ligand interaction fingerprints were calculated to obtain interaction types and binding modes.

The trajectories of both enzymes indicate hydrophobic interactions with a particular emphasis on π -stacking as the prevalent substrate-enzyme interaction. The PET tetramer substrate remains largely in the predicted binding region around the active site. For PET6-wt two repeating units of the substrate are frequently in solution or not bound in a defined way, while for PET6-VSTA, three of the four units of the PET tetramer are frequently bound in a defined way. This can be quantified by a higher number of π -stacking interactions for PET6-wt compared to PET6-VSTA, respectively 76% and 94%. Independent of some positional shift of the PET-tetramer units on the protein surface, the following residues primarily involved in the protein-ligand interactions are found in the vicinity of the active site and are identical for both enzymes: Tyr90, TRP162, Met164, Trp187, Leu189, Val211, His241, and Phe242 (see Figure S1). These residues define a region, which is approximately binding two units of the PET tetramer. Another protein residue frequently interacts with substrate, Ser95, and is located in the region where the third unit of PET is binding. Consistently with our findings that the substrate is bound in a more defined way in PET6-VSTA, we find this interaction with Ser95 more frequently in PET6-VSTA (44%) compared to PET6-wt (26%). Additionally to the more defined binding of the substrate, we observed a significantly higher interaction frequency between the ligand and the catalytic histidine (His241) for PET6-VSTA (69%) compared to PET6-wt (24%), which could indicate a positive influence on catalysis. These observed differences are a consequence of the introduced mutations Val91 to threonine and Ser92 to alanine. We observed interactions of Val91 in PET6-wt with the third unit of the PET tetramer in 44% of the simulated trajectory, while interactions with the other PET units are around 15%-20%. A similar result can be found for Ser92 in PET6-wt, where 38% of the trajectory shows an interaction with the third unit of PET, while interactions with the other PET units are again around 15%-20%. The interactions in the mutant, however, mainly focus on the second and third unit of the PET tetramer (Thr91 – 69% with the second PET unit and 29% with the third PET unit, and Ala92 – 54% with the second PET unit and 46% with the third PET unit). Thus, the interactions of the protein with the substrate in PET6-VSTA are more consistent throughout the trajectories and might lead to a better substrate orientation with a positive effect on the catalysis.

Investigation of the halophilic PET hydrolase PET6 from *Vibrio gazogenes*

In order to analyze binding modes of the ligand in our simulations, we calculated the Tanimoto similarity coefficient between each protein-ligand interaction fingerprint of the MD trajectories, where a coefficient of 1 means an identical interaction pattern and a coefficient of 0 means no identical interactions. Similar interaction patterns of all the structures in the trajectories can then be clustered. These clusters correlate to protein-ligand complexes that represent frequently appearing binding modes, while the structure closest to the cluster center is used to represent the respective binding mode.

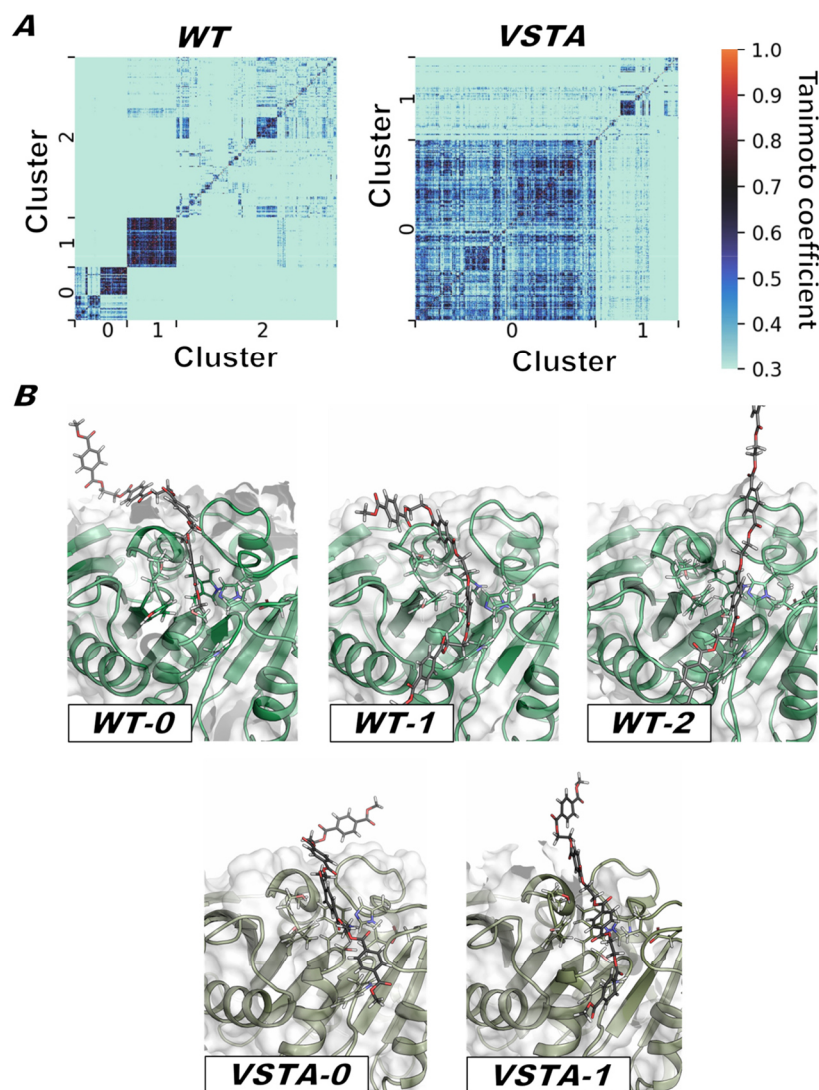
Investigation of the halophilic PET hydrolase PET6 from *Vibrio gazogenes*


Figure 4. Binding mode analysis of PET6-wt and PET6-VSTA with PET tetramer. (A) The Tanimoto similarity matrices for each enzyme clustered according to similar interaction patterns show three clusters for PET6-wt and two for PET6-VSTA. The color range indicates the Tanimoto coefficient, which is a measure for the similarity of the interaction fingerprint, where a coefficient of 1 denotes an identical interaction pattern and a coefficient of 0 signifies no identical interactions. (B) WT-0 to WT-2 and VSTA-0 to VSTA-1 are representative structures from these simulations for each corresponding cluster for PET6-wt and PET6-VSTA, respectively. These representative structures represent the different binding modes.

Investigation of the halophilic PET hydrolase PET6 from *Vibrio gazogenes*

The analysis of the MD trajectories for PET6-wt identified three clusters of different binding modes numbered from 0 to 2 (Figure 4 A), each visualized with a representative structure (Figure 4 B, WT-0 to WT-2). Particularly striking is the shift of the substrate within the binding region in the comparison of WT-0 and WT-1, indicating a more extended binding groove and a possible sliding motion of the substrate. WT-2 shows the representative structure of the largest cluster, i. e. the prevalent binding mode in our calculations (Figure 4 A). This binding mode of the PET tetramer shows that only two repetition units of the ligand are bound close to the active site of the protein, whereas the remaining units are in solution. In contrast, PET6-VSTA shows a more refined interaction with the substrate, as described above. The binding mode analysis for PET6-VSTA identifies only two clusters. These two clusters additionally show similarities among themselves, which are apparent through similar interaction fingerprints between structures of the two clusters (Figure 4A, higher Tanimoto coefficients on the off-diagonal between the clusters). The similarities between the clusters can also be observed by comparing the substrate position in the binding sites of the representative structures, where the substrate binds only with a slight shift compared with one another (Figure 4 B, VSTA-1 and VSTA-2). These results indicate that the interactions between the PET tetramer and the protein are more consistent than in the wildtype, as already concluded from the interaction analysis above. This enhanced interaction of PET6-VSTA with the PET tetramer could be one reason for the observed increase in activity. Structurally, the exchange of Ser92 to alanine seems to introduce the ability for improved hydrophobic interactions at this position, especially since polar contacts of this serine are hardly pronounced in our calculations. We assume that this enhanced substrate coordination in the immediate vicinity to the active site eventually causes improved PET degradation. This underpins the evolutionary potential of PET6 and raises the question of how common PET6 and related variants are in nature.

Global PET-degrading potential of the *Vibrio* genus

It is well known that *Vibrio* species are found nearly everywhere, especially in marine environments, where they play a critical role in carbon and nitrogen cycling⁴². Furthermore, atmospheric warming is enhancing the global occurrence of this genus⁴³. In several studies describing the microbial community on plastic debris ("plasticsphere"), the genus *Vibrio* was found to be the most abundant taxon able to colonize PET (40 %), polyethylene (PE, 30 %) or polypropylene (PP, 33 %)⁴⁴⁻⁴⁶. Moreover, several pathogenic *Vibrios* have been identified on the aforementioned

Investigation of the halophilic PET hydrolase PET6 from *Vibrio gazogenes*

plastics recovered from the oceans, but also on polystyrene (PS) and polyvinyl chloride (PVC; see Table 1 in Bowley et al. 2020⁴⁷). To which extent these *Vibrio* could be involved in degradation of these plastics remains yet unknown. With the aim of identifying other putative PET-degrading *Vibrios*, a BLASTp search against NCBI's non-redundant database filtered for *Vibrio* species (taxid 662) was performed. This resulted in eight hits with full coverage and more than 79 % sequence identity compared to the PET-hydrolyzing PET6 in *V. gazogenes*, *V. spartinae*, *V. ruber*, *V. zhugei* and *V. palustris* (Supplementary Table S2). All of these species were isolated from marine or saline environments⁴⁸⁻⁵¹, suggesting comparable conditions as for PET6. A similar search recovered 95 homologs of the MHETase of *I. sakaiensis* 201-F6 (WP_054022745.1; query coverage > 80 %, sequence identity 28-40 %). Most hits were linked to *V. vulnificus* (85x), but also other species were found (Supplementary Table S2). These sequences were annotated as "tannase/feruloyl esterase family alpha/beta hydrolase". In contrast to *I. sakaiensis*²⁵, no *Vibrio* was found to harbor both enzymes, but a second tannase was found in the genomes of *V. mangrovi*, *V. nitrifigilis* and *V. ziniensis*.

A pangenomic analysis of one representative genome of each PETase- or MHETase-containing *Vibrio* species revealed a core genome of 1,038 gene clusters (GCs; FIGURE 5). All putative PETases and MHETases were assigned to the accessory genome, which ranged from 2,105 to 3,622 GCs for the analyzed isolates. Due to their high sequence similarity, all 4 PETases were allocated in the same GC. By contrast, MHETases/tannases were assigned to six different GCs due to their sequence diversity (Figure 5 and Supplementary Figure S2 A). Surprisingly, PETase- and MHETase-containing *Vibrios*, respectively, did not cluster together according to Average Nucleotide Identity (ANI), strongly suggesting the horizontal transfer of these genes (Figure 5). The "plastisphere" of both aquatic and soil environments has been identified as a "hotspot" for gene transfer^{52,53}. This is further supported by the extended analysis in Supplementary Figure S2 B, including 18 additional genomes from representative pathogenic and non-pathogenic *Vibrios* that do not contain genes coding for PETases nor MHETases. ANI analysis revealed the presence of two main *Vibrio* clades (I and II), where most *Vibrios* with predicted PET-degrading ability were allocated in Clade II. The PETase-coding *V. gazogenes*, *V. spartinae* and *V. ruber* clustered closely together, but *V. palustris* and *V. zhugei* were closer related to the MHETase-containing *V. tritonus* and *V. nitrifigilis*. Only *V. ziniensis*, *V. aestivus* and *V. vulnificus* were assigned to Clade I.

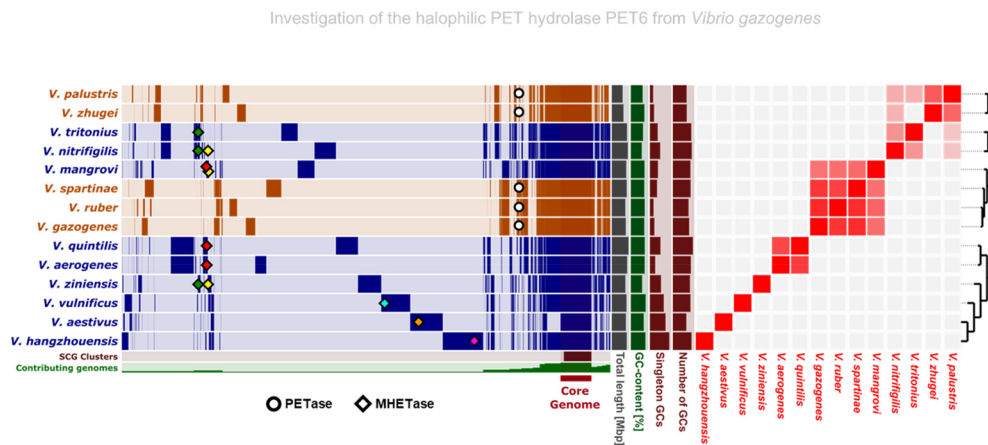


Figure 5. Pangenomic analysis of 5 PETase- (orange) and 9 MHETase-containing (purple) *Vibrio* genomes.

The analysis includes 16,384 gene clusters (GCs) involving 58,208 individual gene calls. The 14 first tracks represent protein-coding gene clusters of individual genomes organized by average nucleotide identity (ANI, red squares and cladogram) of the aligned fraction. Presence of a GC in a genome is indicated in dark colors, absence in light. The core genome of the analyzed *Vibrio* genomes is indicated in dark red. The green track indicates the number of genomes harboring a defined GC. The dark red layer represents the Single Copy Gene (SCG) clusters, in which dark red indicates the presence and light red the absence of these. Other genome statistics (from left to right: total length [0-6 Mbp], GC content [30-50 %], number of singleton gene clusters [0-1,500] and number of gene clusters [0-5,000]) are indicated as additional bar charts on the right. The GC containing PETase-coding genes is highlighted with a white circle for each species, the presence of MHETase homologs (tannase/feruloyl esterase) is marked with squares, in which different colors indicate different GCs (Supplementary Figure S2 A).

The genes related to the metabolism of the PET monomers TPA and EG have been described in several species of the genus *Comamonas*, *Pseudomonas*, *Rhodococcus* or *Raemlibacter*⁵⁴. A BLASTp search with the sequence of the terephthalate 1,2-dioxygenase from *Comamonas* sp. (UniProtKB Q3C1D5), the first enzyme involved in TPA degradation, revealed potential homologs in all PETase-containing *Vibrios*, the MHETase-containing *V. vulnificus*, *V. nitrifigilis* and *V. mangrovi* and others (Supplementary Table S2).

Taken together, these results might indicate that some *Vibrios* are theoretically equipped to act on PET, making *Vibrio*-mediated PET hydrolysis in marine ecosystems conceivable.

Investigation of the halophilic PET hydrolase PET6 from *Vibrio gazogenes*

CONCLUSION

The enzyme PET6 discussed in this study shows a fascinating adaptation towards its saline environment. Sodium and chloride ions stabilize the protein and decisively promote its activity, similar to other PET hydrolases and their interaction with divalent cations. We determined the optimal working conditions of the enzyme to be around 50°C and about 1 to 1.5 M salt. The X-ray structure confirmed the expected fold and stabilizing interactions but also highlighted some differences that led to testable mutants. MD simulations further revealed a stable interaction between enzyme and substrate with specific molecular contacts positioning the substrate appropriately towards the active site. The comparison of the double mutant additionally provided insights into how the structural changes translate to the increased activity. An ongoing discussion about PET degrading enzymes is their actual contribution to PET waste decomposition in the environment, which has not been assessed by any study on an experimental level yet. Based on our findings, we propose that PET6 is a worthy candidate to study this topic. The genus *Vibrio* is ubiquitous in saline environments, and we demonstrated the prevalence of PET6 homologs in several *Vibrio* species. There is also a coincidence of high plastic concentrations in salt marshes, estuaries, and oceans with the confirmed occurrence of *Vibrio* in these environments and even of the plastisphere itself. Hence, a PET degradation activity of PET6 in nature seems feasible. And as recently shown by Menzel *et al.*⁵⁵; even comparatively low levels of enzyme activity can significantly impact the integrity and thus the fate of PET material.

Investigation of the halophilic PET hydrolase PET6 from *Vibrio gazogenes*

MATERIAL AND METHODS

Cloning

The *pet6* gene (residues 25-297, NCBI Ref. Seq. WP_077316261.1) was cloned into a pET28a vector (Merck Millipore Novagen) via the restriction sites *NdeI* and *SalI*, creating a construct with a N-terminal 6x-HisTag upon expression, while the IsPETase gene (residues 28-290) was inserted into a pET21b vector (Merck Millipore Novagen) using *NdeI* and *XhoI* as to feature a C-terminal 6x-HisTag upon expression. Primers for the introduction of mutations were designed with the tool NEBaseChanger (New England Biolabs), the PCR was conducted according to the parameters suggested by the design tool. After PCR cleanup, 6 µl DNA (≈50 ng/µl) was combined with 1 µl each of T4 Ligase Buffer (10x), T4 Ligase (400 U/µl), *DpnI* (20 U/µl), and T4 PNK (10 U/µl) (New England Biolabs) and incubated for 1 h at RT. After transformation of TOP10 cells with ligation mix, positive clones were identified by DNA sequencing (Eurofins Genomics GmbH).

Protein production and purification

T7 Shuffle cells (New England Biolabs) were chemically transformed with the vectors containing the genes of the enzymes; afterward, the corresponding antibiotics were constantly present in the media. Main cultures were grown in TB media at 37 °C to an OD of 1.5 before the temperature was lowered to 18 °C, and protein expression was induced by adding IPTG to a final concentration of 300 µM. After 18 h, the cells were harvested by centrifugation at 5000 xG and resuspended in IMAC binding buffer (300 mM NaCl, 50 mM phosphate, 50 mM Imidazole, pH 7.4) with 10 ml per g wet weight. After sonication, cell debris was removed by centrifugation for 1 h at 50 000 xG and vacuum filtrated through a 0.22 µm filter. The clarified lysate was loaded onto a Cytivia HisTrap 5 ml column. After washing with 20 column volumes (CV) binding buffer, the protein was eluted with a linear gradient (25 CV) of elution buffer (300 mM NaCl, 50 mM phosphate, 400 mM Imidazole, pH 7.4). The purification of the enzymes IsPETase and PET6 wildtype were polished with a size exclusion (SEC) run on a Cytivia Superdex 26/600 75pg (SEC buffer: 150 mM NaCl, 25 mM HEPES, pH 7.4), while the PET6 variants were dialyzed in SEC buffer after the IMAC step. Eventually, the proteins were concentrated to 50-300µM to prepare aliquots of 100 µl, which were flash-frozen until further use.

Crystallization of PET6 and structure determination

Sitting drop vapor diffusion experiments were conducted with various premixed crystal screens, including the JCSG Core Suite from Qiagen. The crystal screening was done in Intelli 3well plates which were set up with a Crystal Phoenix (Art Robbins Instruments) setting drops in a 1:1 ratio with 0.4 μ l each, where PET6 was used in a concentration of 12.3 mg/ml. The obtained crystals were frozen without the addition of a cryoprotectant and diffraction data was collected at the BESSY synchrotron. Two datasets from the same crystal were recorded at the beamline MX14.2 with 13.5 keV with an exposure time of 0.15 s per 0.1° and 2000 images each. The datasets were processed with XDSAPP 2 and merged with Xdsconv; the phase was solved using Phenix Phaser employing a homology model of PET6 generated by MODELLER⁵⁶. Refinement and model building was done with Phenix Refine⁵⁷ and Coot⁵⁸. During processing and solving of the structure, it could not be overlooked that this crystal with the triclinic space group P1 is strongly tending towards a higher symmetry, the cell parameters ($a = 44.8$, $b = 72.6$, $c = 72.8$, $\alpha = 119.8^\circ$, $\beta = 91.6^\circ$; $\gamma = 91.8^\circ$) are very close to a hexagonal crystal system with theoretical cell dimensions $a = b \neq c$ and $\alpha = \beta = 90^\circ$; $\gamma = 120^\circ$. But processing the data sets merged or unmerged at higher symmetry did not successfully solve the structure, suggesting that higher symmetry was distorted. This could be related to the omission of cryoprotectant during the flash freezing step, only relying on the present MPD in the condition itself.

Activity Assay on PET

The PETase activity of the enzymes was measured by incubating the enzymes in PET-coated 96-well microtiter plates. The coating is part of an assay platform described in detail in our previous paper³⁷. In short, commercially available post-consumer PET (CleanPET, Veolia GmbH) is dissolved in trifluoroacetic acid and applied on 96-well microtiter plates (Nunc 96-well clear, Fisher Scientific), excess PET solution drained, and eventually, the plate is dried at 63 °C to obtain the PET coating. For the actual experiments, each well was filled with 50 μ l enzyme solution where 50 mM borate pH 8.5 was the basis while enzyme and sodium chloride concentration as well as incubation temperature and time were varied according to the individual experiment. After incubation, the solution was mixed with 4 parts acetonitrile containing 1 % formic acid followed by centrifugation. The degradation products were analyzed using the UHPLC (ThermoFisher Ultimate 3000 RS) system on a reversed phase C18 column (Kinetex

Investigation of the halophilic PET hydrolase PET6 from *Vibrio gazogenes*

1.7 μm EVO C18, 100 \AA , 50 x 2.1 mm Phenomenex). For fast separation at a flow rate of 1.3 ml/min the following multi-slope gradient was employed starting at 100% solvent A (water + 0.1% TFA) increasing acetonitrile as solvent B in the following pattern: 0.04 min – 15%, 0.4 min 20%, 0.75 min – 50%, 0.95 min – 80%, 2.1 min – 80%. 1 μl samples were injected onto the column; absorption was measured at 240 nm at a rate of 50 Hz. 6-30 replicates were used for every condition to calculate a mean total product release where TPA, MHET, and BHET are combined.

Differential scanning calorimetry (DSC)

DSC runs were done with the proteins under different buffer conditions to determine the stability and melting point of the enzymes. While the buffer basis was kept constant with 50 mM borate pH 8.5, sodium chloride concentrations were varied (50, 500, 1000 mM), with the optional addition of 10 mM KCl. The proteins were dialyzed extensively and prepared in a final concentration between 0.5 and 1.2 mg/ml. Before applying the sample, the instrument (Malvern Microcal PEAK DSC) was thermally equilibrated with corresponding buffer-buffer runs; scanning range was set between 25-70 $^{\circ}\text{C}$ with a speed of 120 K/h.

Bioinformatic analysis

A BLASTp search with the sequence of PET6 (WP_021018894.1) as a query was performed against all *Vibrio* proteomes (taxid 662) in the non-redundant database from NCBI to identify closely related homologs of the PETase (query coverage > 99 %, sequence identity > 80 %). A similar search was performed against the same subset of the database with the sequence of the MHETase from *I. sakaiensis* 201-F6 (WP_054022745.1) to detect *Vibrio* species that code for this enzyme in their genomes (query coverage > 80 %). Multiple sequence alignments were carried out with T-Coffee in Espresso mode⁵⁹. Maximum likelihood trees were calculated with RAxML 8.2.10⁶⁰ with 500 bootstraps and visualized on MEGA X⁶¹.

The genomes of the PETase-coding *V. gazogenes* (GCF_002196515.1), *V. palustris* (GCF_900162645.1), *V. ruber* (GCF_900163965.1), *V. spartinae* (GCF_900149295.1), *V. zhugei* (GCF_003716875.1), and the MHETase-containing *V. aerogenes* (GCF_900130105.1), *V. aestivus* (GCF_003263845.1), *V. hangzhouensis* (GCF_900107935.1), *V. mangrovi* (GCF_900184095.1), *V. nitrifigilis* (GCF_015686695.1), *V. quintilis* (GCF_900143745.1), *V. tritonius* (GCF_001547935.1), *V. vulnificus* (GCF_004319645.1), *V. ziniensis*

Investigation of the halophilic PET hydrolase PET6 from *Vibrio gazogenes*

(GCF_011064285.1) in GenBank format were fetched from NCBI. After file pre-processing with the script “anvi-script-process-genbank”, a pangenome analysis was conducted with Anvi'o 7.1⁶²⁻⁶⁴. Gene clusters (GCs) were built with a minbit of 0.5. Average nucleotide identity (ANI) was calculated using FastANI⁶⁵. For the more extensive pangenomic analysis in Supplementary FIGURE S2, the genomes of *V. fischeri* (*Aliivibrio fischeri*; GCF_000011805.1), *V. casei* (GCF_003335255.1), *V. alginovor* (GCF_007623795.1), *V. mediterranei* (GCF_002214345.1), *V. maritimus* (GCF_003263775.1), *V. splendidus* (GCF_003050125.1), *V. coralliilyticus* (GCF_013266665.1), *V. diabolicus* (GCF_011801455.1), *V. parahaemolyticus* (GCF_000196095.1), *V. hepatarius* (GCF_013114105.1), *V. harveyi* (GCF_000770115.1), *V. alginolyticus* (GCF_001471275.2), *V. natriegens* (GCF_001456255.1), *V. fluvialis* (GCF_001558415.2), *V. cholera* (GCF_000006745.1), *V. proteolyticus* (GCF_000467125.1), *V. metschnikovii* (GCF_009763765.1), *V. anguillarum* (GCF_002287545.1) were included and processed as described above.

Molecular dynamics simulations and binding mode analysis

The PET6 crystal structure was prepared with the program CHARMM⁶⁶, using the CHARMM36^{67,68} force field. For the simulations we used chain A of the crystal structure and the corresponding water molecules. The mutations for the PET6-VSTA structure were introduced with PyMOL⁶⁹. Disulfide bonds were set, and hydrogens were added with the HBUILD routine in CHARMM. Protonation probabilities were calculated using MEAD^{70,71} and GMCT⁷². 200 equilibration scans and 100000 production scans were performed at 323 K with 1.05 M ionic strength and permittivity 4 for the protein and 80 for the solvent in the pH range 0 to 14 with steps of 0.25. The protonation states of titratable groups were set according to this calculation. For the MD simulations we used a PET tetramer as ligand applying published parameters⁷³. The initial position of the ligand was modeled according to the inhibitor p-nitrophenol bound in the crystal structure with the PDB-ID 5XH2. Both protein structures were superimposed and the second repeat unit of the PET tetramer was superimposed with the phenyl ring of p-nitrophenol. The prepared protein with ligand was solved in a cubic box of water molecules extending at least 25 Å from the protein ligand complex with an ion concentration of 1.05 M NaCl. All MD simulations were run with ACEMD⁷⁴ at 323.15 K. For each protein, we performed 5 independent production runs each 50 ns long. The processing of the MD trajectories was performed with MDanalysis^{75,76}. The analysis of interactions and the Tanimoto interaction fingerprint analysis were performed with ProLIF⁷⁷. Clustering for the binding mode analysis was performed with the kMeans algorithm

Investigation of the halophilic PET hydrolase PET6 from *Vibrio gazogenes*

of scikit-learn⁷⁸. The optimal number of clusters was obtained by the Calinski-Harabasz score. As representative structure for each cluster the closest structure to the cluster center was taken.

ACKNOWLEDGEMENTS

This work was funded by the Deutsche Forschungsgemeinschaft (DFG, German Research Foundation) – Project Number 391977956 – SFB 1357 Microplastics, subproject C03 at Bayreuth University.

This work was in part supported by the BMBF within the programs FKZ-XXXX, XXXX and XXXX at the University of Hamburg.

Investigation of the halophilic PET hydrolase PET6 from *Vibrio gazogenes*

REFERENCES

- (1) Boucher, J.; Billard, G.; Simeone, E.; Sousa, J. *The Marine Plastic Footprint*; IUCN, International Union for Conservation of Nature, 2020. <https://doi.org/10.2305/IUCN.CH.2020.01.en>.
- (2) Geyer, R.; Jambeck, J. R.; Law, K. L. Production, Use, and Fate of All Plastics Ever Made. *Science Advances* **3** (7), e1700782. <https://doi.org/10.1126/sciadv.1700782>.
- (3) Lechthaler, S.; Waldschläger, K.; Stauch, G.; Schüttrumpf, H. The Way of Macroplastic through the Environment. *Environments* **2020**, *7* (10), 73. <https://doi.org/10.3390/environments7100073>.
- (4) Meijer, L. J. J.; van Emmerik, T.; van der Ent, R.; Schmidt, C.; Lebreton, L. More than 1000 Rivers Account for 80% of Global Riverine Plastic Emissions into the Ocean. *Science Advances* **7** (18), eaaz5803. <https://doi.org/10.1126/sciadv.aaz5803>.
- (5) Chamas, A.; Moon, H.; Zheng, J.; Qiu, Y.; Tabassum, T.; Jang, J. H.; Abu-Omar, M.; Scott, S. L.; Suh, S. Degradation Rates of Plastics in the Environment. *ACS Sustainable Chemistry & Engineering* **2020**. <https://doi.org/10.1021/acssuschemeng.9b06635>.
- (6) Zhang, K.; Hamidian, A. H.; Tubić, A.; Zhang, Y.; Fang, J. K. H.; Wu, C.; Lam, P. K. S. Understanding Plastic Degradation and Microplastic Formation in the Environment: A Review. *Environmental Pollution* **2021**, *274*, 116554. <https://doi.org/10.1016/j.envpol.2021.116554>.
- (7) Meides, N.; Menzel, T.; Poetzschner, B.; Löder, M. G. J.; Mansfeld, U.; Strohriegel, P.; Altstaedt, V.; Senker, J. Reconstructing the Environmental Degradation of Polystyrene by Accelerated Weathering. *Environ. Sci. Technol.* **2021**, *55* (12), 7930–7938. <https://doi.org/10.1021/acs.est.0c07718>.
- (8) Gewert, B.; M. Plassmann, M.; MacLeod, M. Pathways for Degradation of Plastic Polymers Floating in the Marine Environment. *Environmental Science: Processes & Impacts* **2015**, *17* (9), 1513–1521. <https://doi.org/10.1039/C5EM00207A>.
- (9) Day, M.; Wiles, D. M. Photochemical Degradation of Poly(Ethylene Terephthalate). III. Determination of Decomposition Products and Reaction Mechanism. *Journal of Applied Polymer Science* **1972**, *16* (1), 203–215. <https://doi.org/10.1002/app.1972.070160118>.
- (10) Thompson, R. C.; Olsen, Y.; Mitchell, R. P.; Davis, A.; Rowland, S. J.; John, A. W. G.; McGonigle, D.; Russell, A. E. Lost at Sea: Where Is All the Plastic? *Science* **2004**, *304* (5672), 838–838. <https://doi.org/10.1126/science.1094559>.
- (11) Yee, M. S.-L.; Hii, L.-W.; Looi, C. K.; Lim, W.-M.; Wong, S.-F.; Kok, Y.-Y.; Tan, B.-K.; Wong, C.-Y.; Leong, C.-O. Impact of Microplastics and Nanoplastics on Human Health. *Nanomaterials (Basel)* **2021**, *11* (2), 496. <https://doi.org/10.3390/nano11020496>.
- (12) Lehner, R.; Weder, C.; Petri-Fink, A. Emergence of Nanoplastic in the Environment and Possible Impact on Human Health.
- (13) Thiel, M.; Luna-Jorquera, G.; Álvarez-Varas, R.; Gallardo, C.; Hinojosa, I. A.; Luna, N.; Miranda-Urbina, D.; Morales, N.; Ory, N.; Pacheco, A. S.; Portflitt-Toro, M.; Zavalaga, C. Impacts of Marine Plastic Pollution From Continental Coasts to Subtropical Gyres—Fish, Seabirds, and Other Vertebrates in the SE Pacific. *Frontiers in Marine Science* **2018**, *5*, 238. <https://doi.org/10.3389/fmars.2018.00238>.
- (14) Gall, S. C.; Thompson, R. C. The Impact of Debris on Marine Life. *Marine Pollution Bulletin* **2015**, *92* (1), 170–179. <https://doi.org/10.1016/j.marpolbul.2014.12.041>.
- (15) Sendra, M.; Saco, A.; Yeste, M. P.; Romero, A.; Novoa, B.; Figueras, A. Nanoplastics: From Tissue Accumulation to Cell Translocation into *Mytilus Galloprovincialis* Hemocytes. Resilience of Immune Cells Exposed to Nanoplastics and Nanoplastics plus *Vibrio Splendidus* Combination. *Journal of Hazardous Materials* **2020**, *388*, 121788. <https://doi.org/10.1016/j.jhazmat.2019.121788>.

Investigation of the halophilic PET hydrolase PET6 from *Vibrio gazogenes*

- (16) Xu, M.; Halimu, G.; Zhang, Q.; Song, Y.; Fu, X.; Li, Y.; Li, Y.; Zhang, H. Internalization and Toxicity: A Preliminary Study of Effects of Nanoplastic Particles on Human Lung Epithelial Cell. *Science of The Total Environment* **2019**, *694*, 133794. <https://doi.org/10.1016/j.scitotenv.2019.133794>.
- (17) Mohanan, N.; Montazer, Z.; Sharma, P. K.; Levin, D. B. Microbial and Enzymatic Degradation of Synthetic Plastics. *Frontiers in Microbiology* **2020**, *11*, 2837. <https://doi.org/10.3389/fmicb.2020.580709>.
- (18) Müller, R.-J.; Schrader, H.; Profe, J.; Dresler, K.; Deckwer, W.-D. Enzymatic Degradation of Poly(Ethylene Terephthalate): Rapid Hydrolyse Using a Hydrolase from *T. Fusca*. *Macromolecular Rapid Communications* **2005**, *26* (17), 1400–1405. <https://doi.org/10.1002/marc.200500410>.
- (19) Maurya, A.; Bhattacharya, A.; Khare, S. K. Enzymatic Remediation of Polyethylene Terephthalate (PET)-Based Polymers for Effective Management of Plastic Wastes: An Overview. *Frontiers in Bioengineering and Biotechnology* **2020**, *8*, 1332. <https://doi.org/10.3389/fbioe.2020.602325>.
- (20) Chen, S.; Tong, X.; Woodard, R. W.; Du, G.; Wu, J.; Chen, J. Identification and Characterization of Bacterial Cutinase*. *Journal of Biological Chemistry* **2008**, *283* (38), 25854–25862. <https://doi.org/10.1074/jbc.M800848200>.
- (21) Herrero Acero, E.; Ribitsch, D.; Steinkellner, G.; Gruber, K.; Greimel, K.; Eiteljoerg, I.; Trotscha, E.; Wei, R.; Zimmermann, W.; Zinn, M.; Cavaco-Paulo, A.; Freddi, G.; Schwab, H.; Guebitz, G. Enzymatic Surface Hydrolysis of PET: Effect of Structural Diversity on Kinetic Properties of Cutinases from *Thermobifida*. *Macromolecules* **2011**, *44* (12), 4632–4640. <https://doi.org/10.1021/ma200949p>.
- (22) Kitadokoro, K.; Thumarat, U.; Nakamura, R.; Nishimura, K.; Karatani, H.; Suzuki, H.; Kawai, F. Crystal Structure of Cutinase Est119 from *Thermobifida Alba* AHK119 That Can Degrade Modified Polyethylene Terephthalate at 1.76Å Resolution. *Polymer Degradation and Stability* **2012**, *97* (5), 771–775. <https://doi.org/10.1016/j.polymdegradstab.2012.02.003>.
- (23) Sulaiman, S.; Yamato, S.; Kanaya, E.; Kim, J.-J.; Koga, Y.; Takano, K.; Kanaya, S. Isolation of a Novel Cutinase Homolog with Polyethylene Terephthalate-Degrading Activity from Leaf-Branch Compost by Using a Metagenomic Approach. *Appl Environ Microbiol* **2012**, *78* (5), 1556–1562. <https://doi.org/10.1128/AEM.06725-11>.
- (24) Tournier, V.; Topham, C. M.; Gilles, A.; David, B.; Folgoas, C.; Moya-Leclair, E.; Kamionka, E.; Desrousseaux, M.-L.; Texier, H.; Gavalda, S.; Cot, M.; Guémard, E.; Dalibey, M.; Nomme, J.; Cioci, G.; Barbe, S.; Chateau, M.; André, I.; Duquesne, S.; Marty, A. An Engineered PET Depolymerase to Break down and Recycle Plastic Bottles. *Nature* **2020**, *580* (7802), 216–219. <https://doi.org/10.1038/s41586-020-2149-4>.
- (25) Yoshida, S.; Hiraga, K.; Takehana, T.; Taniguchi, I.; Yamaji, H.; Maeda, Y.; Toyohara, K.; Miyamoto, K.; Kimura, Y.; Oda, K. A Bacterium That Degrades and Assimilates Poly(Ethylene Terephthalate). *Science* **2016**, *351* (6278), 1196–1199. <https://doi.org/10.1126/science.aad6359>.
- (26) Palm, G. J.; Reisky, L.; Böttcher, D.; Müller, H.; Michels, E. A. P.; Walczak, M. C.; Berndt, L.; Weiss, M. S.; Bornscheuer, U. T.; Weber, G. Structure of the Plastic-Degrading *Ideonella Sakaiensis* MHETase Bound to a Substrate. *Nat Commun* **2019**, *10* (1), 1717. <https://doi.org/10.1038/s41467-019-09326-3>.
- (27) Knott, B. C.; Erickson, E.; Allen, M. D.; Gado, J. E.; Graham, R.; Kearns, F. L.; Pardo, I.; Topuzlu, E.; Anderson, J. J.; Austin, H. P.; Dominick, G.; Johnson, C. W.; Rorrer, N. A.; Szostkiewicz, C. J.; Copié, V.; Payne, C. M.; Woodcock, H. L.; Donohoe, B. S.; Beckham, G. T.; McGeehan, J. E. Characterization and Engineering of a Two-Enzyme System for Plastics Depolymerization. *PNAS* **2020**, *117* (41), 25476–25485. <https://doi.org/10.1073/pnas.2006753117>.
- (28) Danso, D.; Schmeisser, C.; Chow, J.; Zimmermann, W.; Wei, R.; Leggewie, C.; Li, X.; Hazen, T.; Streit, W. R. New Insights into the Function and Global Distribution of Polyethylene Terephthalate (PET)-Degrading Bacteria and Enzymes in Marine and Terrestrial Metagenomes. *Appl Environ Microbiol* **2018**, *84* (8), e02773-17. <https://doi.org/10.1128/AEM.02773-17>.
- (29) Thompson, F. L.; Iida, T.; Swings, J. Biodiversity of *Vibrios*. *Microbiol Mol Biol Rev* **2004**, *68* (3), 403–431. <https://doi.org/10.1128/MMBR.68.3.403-431.2004>.

Investigation of the halophilic PET hydrolase PET6 from *Vibrio gazogenes*

- (30) Mullenger, L.; R. Gill, N. *Vibrio Natriegens*: A Rapidly Growing Micro-Organism Ideally Suited for Class Experiments. *Journal of Biological Education* **1973**, *7* (5), 33–39. <https://doi.org/10.1080/00219266.1973.9653881>.
- (31) Lovell, C. R. Ecological Fitness and Virulence Features of *Vibrio Parahaemolyticus* in Estuarine Environments. *Appl Microbiol Biotechnol* **2017**, *101* (5), 1781–1794. <https://doi.org/10.1007/s00253-017-8096-9>.
- (32) Kirstein, I. V.; Kirmizi, S.; Wichels, A.; Garin-Fernandez, A.; Erler, R.; Löder, M.; Gerdts, G. Dangerous Hitchhikers? Evidence for Potentially Pathogenic *Vibrio* Spp. on Microplastic Particles. *Marine Environmental Research* **2016**, *120*, 1–8. <https://doi.org/10.1016/j.marenvres.2016.07.004>.
- (33) Kesy, K.; Labrenz, M.; Scales, B. S.; Kreikemeyer, B.; Oberbeckmann, S. *Vibrio* Colonization Is Highly Dynamic in Early Microplastic-Associated Biofilms as Well as on Field-Collected Microplastics. *Microorganisms* **2021**, *9* (1), 76. <https://doi.org/10.3390/microorganisms9010076>.
- (34) Lebreton, L. C. M.; van der Zwet, J.; Damsteeg, J.-W.; Slat, B.; Andrady, A.; Reisser, J. River Plastic Emissions to the World's Oceans. *Nat Commun* **2017**, *8* (1), 15611. <https://doi.org/10.1038/ncomms15611>.
- (35) López, A. G.; Najjar, R. G.; Friedrichs, M. A. M.; Hickner, M. A.; Wardrop, D. H. Estuaries as Filters for Riverine Microplastics: Simulations in a Large, Coastal-Plain Estuary. *Frontiers in Marine Science* **2021**, *8*, 1200. <https://doi.org/10.3389/fmars.2021.715924>.
- (36) Lloret, J.; Pedrosa-Pamies, R.; Vandal, N.; Rorty, R.; Ritchie, M.; McGuire, C.; Chenoweth, K.; Valiela, I. Salt Marsh Sediments Act as Sinks for Microplastics and Reveal Effects of Current and Historical Land Use Changes. *Environmental Advances* **2021**, *4*, 100060. <https://doi.org/10.1016/j.envadv.2021.100060>.
- (37) Weigert, S.; Gagsteiger, A.; Menzel, T.; Höcker, B. A Versatile Assay Platform for Enzymatic Poly(Ethylene-Terephthalate) Degradation. *Protein Engineering, Design and Selection* **2021**, *34*, gzab022. <https://doi.org/10.1093/protein/gzab022>.
- (38) Nikolaivits, E.; Kanelli, M.; Dimarogona, M.; Topakas, E. A Middle-Aged Enzyme Still in Its Prime: Recent Advances in the Field of Cutinases. *Catalysts* **2018**, *8* (12), 612. <https://doi.org/10.3390/catal8120612>.
- (39) Joo, S.; Cho, I. J.; Seo, H.; Son, H. F.; Sagong, H.-Y.; Shin, T. J.; Choi, S. Y.; Lee, S. Y.; Kim, K.-J. Structural Insight into Molecular Mechanism of Poly(Ethylene Terephthalate) Degradation. *Nat Commun* **2018**, *9* (1), 382. <https://doi.org/10.1038/s41467-018-02881-1>.
- (40) Wei, R.; Song, C.; Gräsing, D.; Schneider, T.; Bielytskyi, P.; Böttcher, D.; Matysik, J.; Bornscheuer, U. T.; Zimmermann, W. Conformational Fitting of a Flexible Oligomeric Substrate Does Not Explain the Enzymatic PET Degradation. *Nat Commun* **2019**, *10* (1), 5581. <https://doi.org/10.1038/s41467-019-13492-9>.
- (41) Kawai, F.; Kawabata, T.; Oda, M. Current Knowledge on Enzymatic PET Degradation and Its Possible Application to Waste Stream Management and Other Fields. *Appl Microbiol Biotechnol* **2019**, *103* (11), 4253–4268. <https://doi.org/10.1007/s00253-019-09717-y>.
- (42) Brumfield, K. D.; Usmani, M.; Chen, K. M.; Gangwar, M.; Jutla, A. S.; Huq, A.; Colwell, R. R. Environmental Parameters Associated with Incidence and Transmission of Pathogenic *Vibrio* Spp. *Environ Microbiol* **2021**, 1462-2920.15716. <https://doi.org/10.1111/1462-2920.15716>.
- (43) Vezzulli, L.; Baker-Austin, C.; Kirschner, A.; Pruzzo, C.; Martinez-Urtaza, J. Global Emergence of Environmental NON-O1 / O139 *Vibrio Cholerae* Infections Linked with Climate Change: A Neglected Research Field? *Environ Microbiol* **2020**, *22* (10), 4342–4355. <https://doi.org/10.1111/1462-2920.15040>.
- (44) Zettler, E. R.; Mincer, T. J.; Amaral-Zettler, L. A. Life in the “Plastisphere”: Microbial Communities on Plastic Marine Debris. *Environ. Sci. Technol.* **2013**, *47* (13), 7137–7146. <https://doi.org/10.1021/es401288x>.
- (45) Delacuvellerie, A.; Cyriaque, V.; Gobert, S.; Benali, S.; Wattiez, R. The Plastisphere in Marine Ecosystem Hosts Potential Specific Microbial Degraders Including *Alcanivorax Borkumensis* as a

Investigation of the halophilic PET hydrolase PET6 from *Vibrio gazogenes*

- Key Player for the Low-Density Polyethylene Degradation. *Journal of Hazardous Materials* **2019**, *380*, 120899. <https://doi.org/10.1016/j.jhazmat.2019.120899>.
- (46) Amaral-Zettler, L. A.; Zettler, E. R.; Mincer, T. J. Ecology of the Plastisphere. *Nat Rev Microbiol* **2020**, *18* (3), 139–151. <https://doi.org/10.1038/s41579-019-0308-0>.
- (47) Bowley, J.; Baker-Austin, C.; Porter, A.; Hartnell, R.; Lewis, C. Oceanic Hitchhikers – Assessing Pathogen Risks from Marine Microplastic. *Trends in Microbiology* **2021**, *29* (2), 107–116. <https://doi.org/10.1016/j.tim.2020.06.011>.
- (48) Harwood, C. S. *Beneckeia Gazogenes* Sp. Nov., a Red, Facultatively Anaerobic, Marine Bacterium. *Current Microbiology* **1978**, *1* (4), 233–238. <https://doi.org/10.1007/BF02602849>.
- (49) Lucena, T.; Arahal, D. R.; Ruvira, M. A.; Navarro-Torre, S.; Mesa, J.; Pajuelo, E.; Rodriguez-Llorente, I. D.; Rodrigo-Torres, L.; Piñar, M. J.; Pujalte, M. J. *Vibrio Palustris* Sp. Nov. and *Vibrio Spartinae* Sp. Nov., Two Novel Members of the *Gazogenes* Clade, Isolated from Salt-Marsh Plants (*Arthrocnemum Macrostachyum* and *Spartina Maritima*). *International Journal of Systematic and Evolutionary Microbiology* **2017**, *67* (9), 3506–3512. <https://doi.org/10.1099/ijsem.0.002155>.
- (50) Guo, Z.; Li, W.; Wang, Y.; Hou, Q.; Zhao, H.; Sun, Z.; Zhang, Z. *Vibrio Zhugei* Sp. Nov., a Moderately Halophilic Bacterium Isolated from Pickling Sauce. *International Journal of Systematic and Evolutionary Microbiology* **2019**, *69* (5), 1313–1319. <https://doi.org/10.1099/ijsem.0.003308>.
- (51) Shieh, W. Y. *Vibrio Ruber* Sp. Nov., a Red, Facultatively Anaerobic, Marine Bacterium Isolated from Sea Water. *INTERNATIONAL JOURNAL OF SYSTEMATIC AND EVOLUTIONARY MICROBIOLOGY* **2003**, *53* (2), 479–484. <https://doi.org/10.1099/ijms.0.02307-0>.
- (52) Arias-Andres, M.; Klümper, U.; Rojas-Jimenez, K.; Grossart, H.-P. Microplastic Pollution Increases Gene Exchange in Aquatic Ecosystems. *Environmental Pollution* **2018**, *237*, 253–261. <https://doi.org/10.1016/j.envpol.2018.02.058>.
- (53) Zhu, D.; Ma, J.; Li, G.; Rillig, M. C.; Zhu, Y.-G. Soil Plastispheres as Hotspots of Antibiotic Resistance Genes and Potential Pathogens. *ISME J* **2021**. <https://doi.org/10.1038/s41396-021-01103-9>.
- (54) Salvador, M.; Abdulmutalib, U.; Gonzalez, J.; Kim, J.; Smith, A. A.; Faulon, J.-L.; Wei, R.; Zimmermann, W.; Jimenez, J. I. Microbial Genes for a Circular and Sustainable Bio-PET Economy. *Genes* **2019**, *10* (5), 373. <https://doi.org/10.3390/genes10050373>.
- (55) Menzel, T.; Weigert, S.; Gagsteiger, A.; Eich, Y.; Sittl, S.; Papastavrou, G.; Ruckdäschel, H.; Altstädt, V.; Höcker, B. Impact of Enzymatic Degradation on the Material Properties of Poly(Ethylene Terephthalate). *Polymers* **2021**, *13* (22), 3885. <https://doi.org/10.3390/polym13223885>.
- (56) Zimmermann, L.; Stephens, A.; Nam, S.-Z.; Rau, D.; Kübler, J.; Lozajic, M.; Gabler, F.; Söding, J.; Lupas, A. N.; Alva, V. A Completely Reimplemented MPI Bioinformatics Toolkit with a New HHpred Server at Its Core. *Journal of Molecular Biology* **2018**, *430* (15), 2237–2243. <https://doi.org/10.1016/j.jmb.2017.12.007>.
- (57) Liebschner, D.; Afonine, P. V.; Baker, M. L.; Bunkóczi, G.; Chen, V. B.; Croll, T. I.; Hintze, B.; Hung, L.-W.; Jain, S.; McCoy, A. J.; Moriarty, N. W.; Oeffner, R. D.; Poon, B. K.; Prisant, M. G.; Read, R. J.; Richardson, J. S.; Richardson, D. C.; Sammito, M. D.; Sobolev, O. V.; Stockwell, D. H.; Terwilliger, T. C.; Urzhumtsev, A. G.; Videau, L. L.; Williams, C. J.; Adams, P. D. Macromolecular Structure Determination Using X-Rays, Neutrons and Electrons: Recent Developments in Phenix. *Acta Cryst D* **2019**, *75* (10), 861–877. <https://doi.org/10.1107/S2059798319011471>.
- (58) Emsley, P.; Cowtan, K. Coot: Model-Building Tools for Molecular Graphics. *Acta Crystallogr D Biol Crystallogr* **2004**, *60* (Pt 12 Pt 1), 2126–2132. <https://doi.org/10.1107/S0907444904019158>.
- (59) Armougom, F.; Moretti, S.; Poirot, O.; Audic, S.; Dumas, P.; Schaeli, B.; Keduas, V.; Notredame, C. Espresso: Automatic Incorporation of Structural Information in Multiple Sequence Alignments Using 3D-Coffee. *Nucleic Acids Research* **2006**, *34* (suppl_2), W604–W608. <https://doi.org/10.1093/nar/gkl092>.

Investigation of the halophilic PET hydrolase PET6 from *Vibrio gazogenes*

- (60) Stamatakis, A. RAxML Version 8: A Tool for Phylogenetic Analysis and Post-Analysis of Large Phylogenies. *Bioinformatics* **2014**, *30* (9), 1312–1313. <https://doi.org/10.1093/bioinformatics/btu033>.
- (61) Kumar, S.; Stecher, G.; Li, M.; Knyaz, C.; Tamura, K. MEGA X: Molecular Evolutionary Genetics Analysis across Computing Platforms. *Molecular Biology and Evolution* **2018**, *35* (6), 1547–1549. <https://doi.org/10.1093/molbev/msy096>.
- (62) Eren, A. M.; Esen, Ö. C.; Quince, C.; Vineis, J. H.; Morrison, H. G.; Sogin, M. L.; Delmont, T. O. Anvi'o: An Advanced Analysis and Visualization Platform for 'omics Data. *PeerJ* **2015**, *3*, e1319. <https://doi.org/10.7717/peerj.1319>.
- (63) Buchfink, B.; Xie, C.; Huson, D. H. Fast and Sensitive Protein Alignment Using DIAMOND. *Nat Methods* **2015**, *12* (1), 59–60. <https://doi.org/10.1038/nmeth.3176>.
- (64) Edgar, R. C. MUSCLE: Multiple Sequence Alignment with High Accuracy and High Throughput. *Nucleic Acids Research* **2004**, *32* (5), 1792–1797. <https://doi.org/10.1093/nar/gkh340>.
- (65) Jain, C.; Rodriguez-R, L. M.; Phillippy, A. M.; Konstantinidis, K. T.; Aluru, S. High Throughput ANI Analysis of 90K Prokaryotic Genomes Reveals Clear Species Boundaries. *Nat Commun* **2018**, *9* (1), 5114. <https://doi.org/10.1038/s41467-018-07641-9>.
- (66) Brooks, B. R.; Bruccoleri, R. E.; Olafson, B. D.; States, D. J.; Swaminathan, S.; Karplus, M. CHARMM: A Program for Macromolecular Energy, Minimization, and Dynamics Calculations. *J. Comput. Chem.* **1983**, *4* (2), 187–217. <https://doi.org/10.1002/jcc.540040211>.
- (67) MacKerell, A. D.; Bashford, D.; Bellott, M.; Dunbrack, R. L.; Evanseck, J. D.; Field, M. J.; Fischer, S.; Gao, J.; Guo, H.; Ha, S.; Joseph-McCarthy, D.; Kuchnir, L.; Kuczera, K.; Lau, F. T. K.; Mattos, C.; Michnick, S.; Ngo, T.; Nguyen, D. T.; Prodhom, B.; Reiher, W. E.; Roux, B.; Schlenkrich, M.; Smith, J. C.; Stote, R.; Straub, J.; Watanabe, M.; Wiórkiewicz-Kuczera, J.; Yin, D.; Karplus, M. All-Atom Empirical Potential for Molecular Modeling and Dynamics Studies of Proteins. *J. Phys. Chem. B* **1998**, *102* (18), 3586–3616. <https://doi.org/10.1021/jp973084f>.
- (68) Best, R. B.; Zhu, X.; Shim, J.; Lopes, P. E. M.; Mittal, J.; Feig, M.; MacKerell, A. D. Optimization of the Additive CHARMM All-Atom Protein Force Field Targeting Improved Sampling of the Backbone ϕ , ψ and Side-Chain χ_1 and χ_2 Dihedral Angles. *J. Chem. Theory Comput.* **2012**, *8* (9), 3257–3273. <https://doi.org/10.1021/ct300400x>.
- (69) Schrödinger LLC. *PyMol - The PyMOL Molecular Graphics System*.
- (70) Bashford, D.; Gerwert, K. Electrostatic Calculations of the PKa Values of Ionizable Groups in Bacteriorhodopsin. *Journal of Molecular Biology* **1992**, *224* (2), 473–486. [https://doi.org/10.1016/0022-2836\(92\)91009-E](https://doi.org/10.1016/0022-2836(92)91009-E).
- (71) Bashford, D. An Object-Oriented Programming Suite for Electrostatic Effects in Biological Molecules An Experience Report on the MEAD Project. In *Scientific Computing in Object-Oriented Parallel Environments*; Ishikawa, Y., Oldehoeft, R. R., Reynders, J. V. W., Tholburn, M., Eds.; Goos, G., Hartmanis, J., van Leeuwen, J., Series Eds.; Lecture Notes in Computer Science; Springer Berlin Heidelberg: Berlin, Heidelberg, 1997; Vol. 1343, pp 233–240. https://doi.org/10.1007/3-540-63827-X_66.
- (72) Ullmann, R. T.; Ullmann, G. M. GMCT: A Monte Carlo Simulation Package for Macromolecular Receptors. *J. Comput. Chem.* **2012**, *33* (8), 887–900. <https://doi.org/10.1002/jcc.22919>.
- (73) Cruz-Chu, E. R.; Ritz, T.; Siwy, Z. S.; Schulten, K. Molecular Control of Ionic Conduction in Polymer Nanopores. *Faraday Discuss.* **2009**, *143*, 47. <https://doi.org/10.1039/b906279n>.
- (74) Harvey, M. J.; Giupponi, G.; Fabritiis, G. D. ACEMD: Accelerating Biomolecular Dynamics in the Microsecond Time Scale. *J. Chem. Theory Comput.* **2009**, *5* (6), 1632–1639. <https://doi.org/10.1021/ct9000685>.
- (75) Michaud-Agrawal, N.; Denning, E. J.; Woolf, T. B.; Beckstein, O. MDAAnalysis: A Toolkit for the Analysis of Molecular Dynamics Simulations. *J. Comput. Chem.* **2011**, *32* (10), 2319–2327. <https://doi.org/10.1002/jcc.21787>.
- (76) Gowers, R.; Linke, M.; Barnoud, J.; Reddy, T.; Melo, M.; Seyler, S.; Domański, J.; Dotson, D.; Buchoux, S.; Kenney, I.; Beckstein, O. MDAAnalysis: A Python Package for the Rapid Analysis of

Investigation of the halophilic PET hydrolase PET6 from *Vibrio gazogenes*

- Molecular Dynamics Simulations; Austin, Texas, 2016; pp 98–105. <https://doi.org/10.25080/Majora-629e541a-00e>.
- (77) Bouysset, C.; Fiorucci, S. ProLIF: A Library to Encode Molecular Interactions as Fingerprints. *J Cheminform* **2021**, *13* (1), 72. <https://doi.org/10.1186/s13321-021-00548-6>.
- (78) Pedregosa, F.; Varoquaux, G.; Gramfort, A.; Michel, V.; Thirion, B.; Grisel, O.; Blondel, M.; Prettenhofer, P.; Weiss, R.; Dubourg, V.; Vanderplas, J.; Passos, A.; Cournapeau, D.; Brucher, M.; Perrot, M.; Duchesnay, É. Scikit-Learn: Machine Learning in Python. *Journal of Machine Learning Research* **2011**, *12* (85), 2825–2830.
- (79) Urbanczyk, H.; Ast, J. C.; Higgins, M. J.; Carson, J.; Dunlap, P. V. Reclassification of *Vibrio Fischeri*, *Vibrio Logei*, *Vibrio Salmonicida* and *Vibrio Wodanis* as *Aliivibrio Fischeri* Gen. Nov., Comb. Nov., *Aliivibrio Logei* Comb. Nov., *Aliivibrio Salmonicida* Comb. Nov. and *Aliivibrio Wodanis* Comb. Nov. *International Journal of Systematic and Evolutionary Microbiology* **2007**, *57* (12), 2823–2829. <https://doi.org/10.1099/ijs.0.65081-0>.

Supporting information for Investigation of the halophilic PET hydrolase PET6 *Vibrio gazogenes*

Supporting Information

for

Investigation of the halophilic PET hydrolase PET6 from *Vibrio gazogenes*

Weigert, Sebastian¹; Perez-Garcia, Pablo^{2,3}; Gisdon, Florian¹; Gagsteiger, Andreas¹; Chibani, Cynthia M³;
Schmitz, Ruth A³; Schweinshaut, Kristine¹; Ullmann, Matthias⁴; Chow, Jennifer²; Streit, Wolfgang²; Höcker, Birte^{1,*}

The file includes:

- **Table S1** Quality indicators for crystallographic data and model building for the crystal structure of PET6
- **Figure S1** Detailed representation of residues frequently engaged in enzyme-ligand interaction for PET6-wt
- **Table S2** BLASTp searches against NCBI taxid662 *Vibrio*
- **Figure S2** Molecular relations between all putative *Vibrio* PETases and MHETases

Supporting information for Investigation of the halophilic PET hydrolase PET6 *Vibrio gazogenes*

Table S1 Quality indicators for crystallographic data and model building for the crystal structure of PET6.

Statistics for the highest resolution shell are shown in parentheses.

Structure (PDB ID)	PET6 XXXX (to be assigned)
Wavelength (Å)	0.9184
Resolution range (Å)	25.7 - 1.4 (1.45 - 1.4)
Space group	P 1
Unit cell	
a, b, c (Å)	44.82, 72.61, 72.76,
α , β , γ (°)	119.78, 91.64, 91.82
Total reflections	566942 (37590)
Unique reflections	150015 (14386)
Multiplicity	3.8 (2.6)
Completeness (%)	95.77 (91.87)
Mean I/ σ (I)	19.45 (4.70)
Wilson B-factor	9.53
R-merge	0.04679 (0.2477)
R-meas	0.05424 (0.3)
R-pim	0.0271 (0.1654)
CC _{1/2}	0.999 (0.928)
CC*	1 (0.981)
Reflections used in refinement	149922 (14378)
Reflections used for R-free	7493 (718)
R _{work}	0.0996 (0.1431)
R _{free}	0.1264 (0.1727)
CC _{work}	0.982 (0.956)
CC _{free}	0.975 (0.931)
Number of non-hydrogen atoms	8045
macromolecules	6815
ligands	648
solvent	960
Protein residues	831
RMS(bonds)	0.014
RMS(angles)	1.52
Ramachandran favored (%)	98.18
Ramachandran allowed (%)	1.82
Ramachandran outliers (%)	0.00
Rotamer outliers (%)	0.66
Clashscore	6.67
Average B-factor	15.68
macromolecules	13.05
ligands	36.27
solvent	28.56

Supporting information for Investigation of the halophilic PET hydrolase PET6 *Vibrio gazogenes*

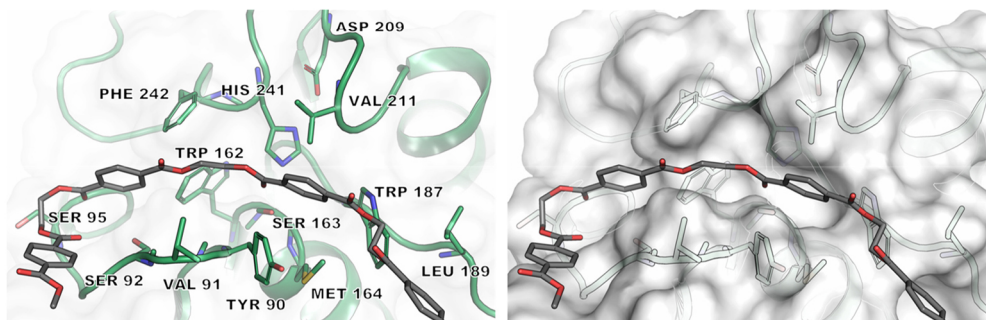


Figure S1 Detailed representation of residues frequently involved in enzyme-ligand interaction for PET6-wt based on the representative structure of cluster WT-1 from the fingerprint analysis (compare Figure 4). The left side shows the enzyme in cartoon representation with the interacting residues as well as the catalytic triad (Ser163, Asp209, His241) depicted in sticks. The same perspective is shown on the right but with a less transparent surface to better visualize the positioning of the ligand within the binding region.

Supporting information for Investigation of the halophilic PET hydrolase PET6 *Vibrio gazogenes*

Table S2 BLASTp searches against NCBI taxid662 *Vibrio*

Description	Scientific Name	Max Score	Total Score	Query Cover	E value	Per. Ident	Acc. Len	Accession
Rieske 2Fe-2S domain-containing protein [Vibrio parahaemolyticus]	Vibrio parahaemolyticus	274	274	98%	3.00E-86	36.33%	407	MB440824.1
aromatic ring-hydroxylating dioxygenase subunit alpha [Vibrio sp. dhg]	Vibrio sp. dhg	124	124	96%	3.00E-29	27.44%	452	WP_118118405.1
aromatic ring-hydroxylating dioxygenase subunit alpha [Vibrio parahaemolyticus]	Vibrio parahaemolyticus	124	124	96%	5.00E-29	27.21%	452	WP_17268206.1
aromatic ring-hydroxylating dioxygenase subunit alpha [Vibrio natriegens]	Vibrio natriegens	124	124	96%	5.00E-29	27.21%	452	WP_020333184.1
aromatic ring-hydroxylating dioxygenase subunit alpha [Vibrio natriegens]	Vibrio natriegens	122	122	96%	2.00E-28	26.98%	452	WP_062929598.1
aromatic ring-hydroxylating dioxygenase subunit alpha [Vibrio sp. EY3]	Vibrio sp. EY3	122	122	96%	2.00E-28	26.98%	452	WP_014231692.1
aromatic ring-hydroxylating dioxygenase subunit alpha [Vibrio nitrifigilis]	Vibrio nitrifigilis	160	160	96%	2.00E-42	29.86%	434	WP_196112236.1
aromatic ring-hydroxylating dioxygenase subunit alpha [Vibrio sp. CAIM 722]	Vibrio sp. CAIM 722	160	160	96%	2.00E-42	29.86%	434	WP_161158098.1
aromatic ring-hydroxylating dioxygenase subunit alpha [Vibrio viridaestus]	Vibrio viridaestus	147	147	96%	7.00E-38	27.73%	428	WP_124937905.1
Rieske 2Fe-2S domain-containing protein [Vibrio neptunius]	Vibrio neptunius	300	300	96%	2.00E-96	38.10%	399	WP_206371381.1
Rieske 2Fe-2S domain-containing protein [Vibrio neptunius]	Vibrio neptunius	300	300	96%	2.00E-96	38.35%	399	WP_045995176.1
Rieske 2Fe-2S domain-containing protein [Vibrio neptunius]	Vibrio neptunius	299	299	96%	4.00E-96	38.35%	399	WP_057373931.1
Rieske 2Fe-2S domain-containing protein [Vibrio pectenoides]	Vibrio pectenoides	295	295	96%	1.00E-94	37.84%	399	WP_171360116.1
aromatic ring-hydroxylating dioxygenase subunit alpha [Vibrio furnissii]	Vibrio furnissii	132	132	95%	5.00E-32	28.21%	453	WP_15816269.1
aromatic ring-hydroxylating dioxygenase subunit alpha [Vibrio]	Vibrio	131	131	95%	9.00E-32	28.21%	453	WP_05466680.1
Rieske 2Fe-2S domain-containing protein [Vibrio furnissii]	Vibrio furnissii	131	131	95%	9.00E-32	28.21%	453	WP_17252192.1
aromatic ring-hydroxylating dioxygenase subunit alpha [Vibrio furnissii]	Vibrio furnissii	129	129	95%	4.00E-31	27.97%	453	WP_004726039.1
aromatic ring-hydroxylating dioxygenase subunit alpha [Vibrio furnissii]	Vibrio furnissii	127	127	95%	4.00E-30	27.74%	453	WP_014205125.1
benzene 1,2-dioxygenase [Vibrio parahaemolyticus]	Vibrio parahaemolyticus	129	129	85%	7.00E-31	28.53%	462	KKF67655.1
anthranilate 1,2-dioxygenase large subunit [Vibrio crosseae]	Vibrio crosseae	100	100	85%	6.00E-21	24.35%	462	WP_048664359.1
anthranilate 1,2-dioxygenase large subunit [Vibrio crosseae]	Vibrio crosseae	100	100	85%	6.00E-21	24.35%	463	WP_125397386.1
anthranilate 1,2-dioxygenase large subunit [Vibrio crosseae]	Vibrio crosseae	100	100	85%	7.00E-21	24.42%	462	WP_057623771.1
anthranilate 1,2-dioxygenase large subunit [Vibrio crosseae]	Vibrio crosseae	100	100	85%	7.00E-21	24.67%	462	WP_048667507.1
anthranilate 1,2-dioxygenase large subunit [Vibrio]	Vibrio	100	100	85%	7.00E-21	24.35%	462	WP_048618002.1
Rieske 2Fe-2S domain-containing protein [Vibrio natriegens]	Vibrio natriegens	122	122	78%	1.00E-28	27.53%	458	WP_020334207.1
aromatic ring-hydroxylating dioxygenase subunit alpha [Vibrio toranzoniae]	Vibrio toranzoniae	90.9	90.9	64%	8.00E-16	25.36%	395	WP_08534133.1
aromatic ring-hydroxylating dioxygenase subunit alpha [Vibrio kanaloae]	Vibrio kanaloae	90.9	90.9	64%	1.00E-17	25.36%	395	WP_150877267.1
aromatic ring-hydroxylating dioxygenase subunit alpha [Vibrio toranzoniae]	Vibrio toranzoniae	89.7	89.7	64%	2.00E-17	25.00%	395	WP_161749287.1
aromatic ring-hydroxylating dioxygenase subunit alpha [Vibrio nereis]	Vibrio nereis	89.7	89.7	64%	2.00E-17	25.00%	395	WP_053394666.1
aromatic ring-hydroxylating dioxygenase subunit alpha [Vibrio natriegens]	Vibrio natriegens	89	89	64%	5.00E-17	24.64%	395	WP_020335442.1
aromatic ring-hydroxylating dioxygenase subunit alpha [Vibrio]	Vibrio	89	89	64%	5.00E-17	24.64%	395	WP_04548887.1
aromatic ring-hydroxylating dioxygenase subunit alpha [Vibrio natriegens]	Vibrio natriegens	88.2	88.2	64%	7.00E-17	24.64%	395	WP_17629250.1
aromatic ring-hydroxylating dioxygenase subunit alpha [Vibrio alginolyticus]	Vibrio alginolyticus	87.4	87.4	64%	1.00E-16	25.00%	397	EGQ7647142.1
aromatic ring-hydroxylating dioxygenase subunit alpha [Vibrio]	Vibrio	87.4	87.4	64%	1.00E-16	25.00%	395	WP_042521602.1
aromatic ring-hydroxylating dioxygenase subunit alpha [Vibrio diabolus]	Vibrio diabolus	86.3	86.3	64%	3.00E-16	24.64%	395	WP_167427702.1
aromatic ring-hydroxylating dioxygenase subunit alpha [Vibrio diabolus subgroup]	Vibrio diabolus subgroup	86.3	86.3	64%	3.00E-16	24.64%	395	WP_08534133.1
aromatic ring-hydroxylating dioxygenase subunit alpha [Vibrio alginolyticus]	Vibrio alginolyticus	86.3	86.3	64%	3.00E-16	24.64%	395	WP_22546230.1
aromatic ring-hydroxylating dioxygenase subunit alpha [Vibrio]	Vibrio	86.3	86.3	64%	3.00E-16	24.64%	395	WP_09352447.1
Phenylpropanoate dioxygenase and related ring-hydroxylating dioxygenases large terminal subunit [Vibrio diabolus]	Vibrio diabolus	86.3	86.3	64%	4.00E-16	24.64%	395	CDT84420.1
Rieske 2Fe-2S domain-containing protein [Vibrio alginolyticus]	Vibrio alginolyticus	86.3	86.3	64%	4.00E-16	24.29%	395	WP_213972879.1
aromatic ring-hydroxylating dioxygenase subunit alpha [Vibrio alginolyticus]	Vibrio alginolyticus	85.9	85.9	64%	4.00E-16	24.29%	395	WP_063365597.1
aromatic ring-hydroxylating dioxygenase subunit alpha [Vibrio alginolyticus]	Vibrio alginolyticus	85.9	85.9	64%	4.00E-16	24.29%	395	WP_191116089.1
2Fe-2S ferredoxin [Vibrio alginolyticus]	Vibrio alginolyticus	84.7	84.7	64%	5.00E-16	24.29%	311	PLX63815.1
aromatic ring-hydroxylating dioxygenase subunit alpha [Vibrio natriegens]	Vibrio natriegens	85.5	85.5	64%	7.00E-16	24.29%	395	WP_063015322.1
Rieske 2Fe-2S domain-containing protein [Vibrio alginolyticus]	Vibrio alginolyticus	85.1	85.1	64%	8.00E-16	24.37%	395	WP_213965089.1
aromatic ring-hydroxylating dioxygenase subunit alpha [Vibrio diabolus]	Vibrio diabolus	85.1	85.1	64%	9.00E-16	24.29%	395	WP_125397386.1
aromatic ring-hydroxylating dioxygenase subunit alpha [Vibrio kanaloae]	Vibrio kanaloae	84.7	84.7	64%	1.00E-15	24.29%	395	WP_130545790.1
Rieske 2Fe-2S domain-containing protein [Vibrio alginolyticus]	Vibrio alginolyticus	84.7	84.7	64%	1.00E-15	24.64%	395	WP_213891116.1
aromatic ring-hydroxylating dioxygenase subunit alpha [Vibrio alginolyticus]	Vibrio alginolyticus	84.7	84.7	64%	1.00E-15	24.29%	395	WP_005385883.1
aromatic ring-hydroxylating dioxygenase subunit alpha [Vibrio harveyi group]	Vibrio harveyi group	84.7	84.7	64%	1.00E-15	24.29%	395	WP_053037899.1
aromatic ring-hydroxylating dioxygenase subunit alpha [Vibrio harveyi group]	Vibrio harveyi group	84.7	84.7	64%	1.00E-15	24.29%	395	WP_053037899.1
aromatic ring-hydroxylating dioxygenase subunit alpha [Vibrio]	Vibrio	84.7	84.7	64%	1.00E-15	24.29%	395	WP_104973070.1
aromatic ring-hydroxylating dioxygenase subunit alpha [Vibrio alginolyticus]	Vibrio alginolyticus	84.7	84.7	64%	1.00E-15	24.29%	395	WP_225455584.1
aromatic ring-hydroxylating dioxygenase subunit alpha [Vibrio]	Vibrio	84.7	84.7	64%	1.00E-15	24.29%	397	EGR2324398.1
aromatic ring-hydroxylating dioxygenase subunit alpha [Vibrio diabolus]	Vibrio diabolus	84.7	84.7	64%	1.00E-15	24.29%	395	WP_134666108.1
aromatic ring-hydroxylating dioxygenase subunit alpha [Vibrio]	Vibrio	84.7	84.7	64%	1.00E-15	24.29%	395	WP_063015322.1
aromatic ring-hydroxylating dioxygenase subunit alpha [Vibrio kanaloae]	Vibrio kanaloae	89.7	89.7	64%	2.00E-17	26.23%	423	MB1348146.1
aromatic ring-hydroxylating dioxygenase subunit alpha [Vibrio alginolyticus]	Vibrio alginolyticus	85.9	85.9	56%	5.00E-16	25.41%	395	EID0031799.1
aromatic ring-hydroxylating dioxygenase subunit alpha [Vibrio alginolyticus]	Vibrio alginolyticus	85.5	85.5	56%	6.00E-16	25.41%	395	WP_053038411.1
aromatic ring-hydroxylating dioxygenase subunit alpha [Vibrio alginolyticus]	Vibrio alginolyticus	85.1	85.1	56%	9.00E-16	25.41%	395	EI1283971.1
aromatic ring-hydroxylating dioxygenase subunit alpha [Vibrio alginolyticus]	Vibrio alginolyticus	84.7	84.7	56%	1.00E-15	25.41%	395	WP_225495767.1
GlcA glycine betaine demethylase subunit A [Vibrio sp. ICM 18904]	Vibrio sp. ICM 18904	84.3	84.3	52%	1.00E-15	26.52%	346	GAJ71506.1
Rieske 2Fe-2S domain-containing protein [Vibrio natriegens]	Vibrio natriegens	124	124	51%	6.00E-29	34.09%	458	WP_062597743.1
Rieske 2Fe-2S domain-containing protein [Vibrio natriegens]	Vibrio natriegens	124	124	51%	6.00E-29	34.09%	458	WP_06300940.1
Rieske 2Fe-2S domain-containing protein [Vibrio sp. EY3]	Vibrio sp. EY3	122	122	51%	1.00E-28	33.64%	458	WP_014233847.1
Rieske 2Fe-2S domain-containing protein [Vibrio natriegens]	Vibrio natriegens	122	122	51%	1.00E-28	33.64%	458	WP_020333022.1
Rieske 2Fe-2S domain-containing protein [Vibrio alginolyticus]	Vibrio alginolyticus	120	120	51%	2.00E-29	36.70%	236	WP_225468170.1
unnamed protein product [Vibrio parahaemolyticus]	Vibrio parahaemolyticus	115	115	51%	1.00E-27	35.78%	248	WP_226057740.1
anthranilate 1,2-dioxygenase large subunit [Vibrio alginolyticus]	Vibrio alginolyticus	113	113	49%	9.00E-27	34.60%	261	KPM94080.1
Rieske 2Fe-2S domain-containing protein [Vibrio alginolyticus]	Vibrio alginolyticus	113	113	49%	1.00E-26	34.60%	262	WP_196363400.1
aromatic ring-hydroxylating dioxygenase subunit alpha [Vibrio zhigeli]	Vibrio zhigeli	96.7	96.7	49%	1.00E-19	28.64%	421	MB123014963.1
aromatic ring-hydroxylating dioxygenase subunit alpha [Vibrio ruber]	Vibrio ruber	104	104	49%	3.00E-22	30.45%	422	WP_077322826.1
aromatic ring-hydroxylating dioxygenase subunit alpha [Vibrio]	Vibrio	102	102	49%	1.00E-21	29.25%	419	WP_014234565.1
aromatic ring-hydroxylating dioxygenase subunit alpha [Vibrio natriegens]	Vibrio natriegens	102	102	49%	1.00E-21	29.25%	419	WP_063038011.1
aromatic ring-hydroxylating dioxygenase subunit alpha [Vibrio natriegens]	Vibrio natriegens	102	102	49%	1.00E-21	29.25%	419	WP_063031314.1
aromatic ring-hydroxylating dioxygenase subunit alpha [Vibrio natriegens]	Vibrio natriegens	102	102	49%	1.00E-21	29.25%	419	WP_17252169.1
aromatic ring-hydroxylating dioxygenase subunit alpha [Vibrio mangrovei]	Vibrio mangrovei	102	102	49%	1.00E-21	29.72%	424	WP_087479140.1
aromatic ring-hydroxylating dioxygenase subunit alpha [Vibrio spartinae]	Vibrio spartinae	102	102	49%	2.00E-21	29.72%	402	WP_228449027.1
aromatic ring-hydroxylating dioxygenase subunit alpha [Vibrio spartinae]	Vibrio spartinae	102	102	49%	2.00E-21	29.72%	422	WP_074372616.1
aromatic ring-hydroxylating dioxygenase subunit alpha [Vibrio gazogenes]	Vibrio gazogenes	102	102	49%	2.00E-21	29.72%	422	WP_072957579.1
aromatic ring-hydroxylating dioxygenase subunit alpha [Vibrio gazogenes]	Vibrio gazogenes	100	100	49%	4.00E-21	29.72%	422	WP_088133077.1
aromatic ring-hydroxylating dioxygenase subunit alpha [Vibrio xiamenensis]	Vibrio xiamenensis	100	100	49%	5.00E-21	28.77%	426	WP_093277965.1
aromatic ring-hydroxylating dioxygenase subunit alpha [Vibrio]	Vibrio	97.1	97.1	49%	8.00E-20	28.77%	419	WP_161156908.1
aromatic ring-hydroxylating dioxygenase subunit alpha [Vibrio viridaestus]	Vibrio viridaestus	107	107	48%	3.00E-23	31.10%	421	WP_124938518.1
aromatic ring-hydroxylating dioxygenase subunit alpha [Vibrio vulnificus]	Vibrio vulnificus	106	106	48%	7.00E-23	31.22%	433	TDL91992.1
aromatic ring-hydroxylating dioxygenase subunit alpha [Vibrio fluvialis]	Vibrio fluvialis	103	103	48%	7.00E-22	29.67%	423	MB1796736.1
aromatic ring-hydroxylating dioxygenase subunit alpha [Vibrio sp. E4404]	Vibrio sp. E4404	102	102	48%	1.00E-21	29.19%	422	WP_109319542.1
aromatic ring-hydroxylating dioxygenase subunit alpha [Vibrio fluvialis]	Vibrio fluvialis	102	102	48%	2.00E-21	29.19%	423	MBY8036178.1
aromatic ring-hydroxylating dioxygenase subunit alpha [Vibrio fluvialis]	Vibrio fluvialis	102	102	48%	2.00E-21	29.19%	423	MBY7785331.1
aromatic ring-hydroxylating dioxygenase subunit alpha [Vibrio fluvialis]	Vibrio fluvialis	101	101	48%	2.00E-21	29.19%	408	WP_226976343.1
aromatic ring-hydroxylating dioxygenase subunit alpha [Vibrio fluvialis]	Vibrio fluvialis	101	101	48%	2.00E-21	29.19%	423	MB14363260.1
aromatic ring-hydroxylating dioxygenase subunit alpha [Vibrio fluvialis]	Vibrio fluvialis	101	101	48%	2.00E-21	29.19%	423	WP_104965392.1
aromatic ring-hydroxylating dioxygenase subunit alpha [Vibrio fluvialis]	Vibrio fluvialis	101	101	48%	3.00E-21	29.19%	423	MBY799699.1
aromatic ring-hydroxylating dioxygenase subunit alpha [unclassified Vibrio]	unclassified Vibrio	101	101	48%	4.00E-21	29.19%	422	WP_136485708.1
aromatic ring-hydroxylating dioxygenase subunit alpha [Vibrio fluvialis]	Vibrio fluvialis	100	100	48%	5.00E-21	28.71%	423	MBY7973875.1
aromatic ring-hydroxylating dioxygenase subunit alpha [Vibrio fluvialis]	Vibrio fluvialis	100	100	48%	9.00E-21	28.71%	423	MB1348146.1
aromatic ring-hydroxylating dioxygenase subunit alpha [Vibrio mytili]	Vibrio mytili	97.1	97.1	48%	1.00E-19	27.		

7 Acknowledgments

I would like to take this opportunity to thank all those people who have made a special contribution to the success of Ph.D. through their support. First and foremost, I would like to mention my supervisor Prof Birte Höcker. I would especially like to thank her for her calmness and composure in critical phases of this project, her always available advice and support. But especially for the freedom she gave me to develop my project independently.

I would also like to thank Teresa Menzel, whom I enjoyed working with very much and who contributed a lot to our joint projects with her energy. A special mention also goes to Andreas Gagsteiger, to whom I owe a great deal of credit for our joint projects thanks to his hard work. Further, I would also like to thank the other members of the chair for their help and feedback on so many occasions and for participating in a variety of social activities that have made my time in particular so worthwhile.

And last but not least, my very special thanks go to my family and friends who have supported me tirelessly and put up with both my moods during frustrating periods and those full of scientific euphoria.

I am sincerely grateful for the contribution of all the people named here and those I cannot mention by name.

Legal Acknowledgments

Figure 4 “Typical schema for plastic entering the environment” and Figure 5 “Schematic representation of a spherulite” were created with Biorender.com.

Figure 2 “Example for mismanaged waste in coastal areas”. Photo by Antoine GIRET on Unsplash (unsplash.com/photos/7_TSzqJms4w)

8 References

- (1) Andrady, A. L.; Rajapakse, N. Additives and Chemicals in Plastics. In *Hazardous Chemicals Associated with Plastics in the Marine Environment*; Takada, H., Karapanagioti, H. K., Eds.; The Handbook of Environmental Chemistry; Springer International Publishing: Cham, 2019; pp 1–17. https://doi.org/10.1007/698_2016_124.
- (2) Hahladakis, J. N.; Velis, C. A.; Weber, R.; Iacovidou, E.; Purnell, P. An Overview of Chemical Additives Present in Plastics: Migration, Release, Fate and Environmental Impact during Their Use, Disposal and Recycling. *Journal of Hazardous Materials* **2018**, *344*, 179–199. <https://doi.org/10.1016/j.jhazmat.2017.10.014>.
- (3) Andrady, A. L.; Neal, M. A. Applications and Societal Benefits of Plastics. *Philosophical Transactions of the Royal Society B: Biological Sciences* **2009**, *364* (1526), 1977–1984. <https://doi.org/10.1098/rstb.2008.0304>.
- (4) Freinkel, S. A Brief History of Plastic's Conquest of the World <https://www.scientificamerican.com/article/a-brief-history-of-plastic-world-conquest/> (accessed 2021 -10 -19).
- (5) Crespy, D.; Bozonnet, M.; Meier, M. 100 Years of Bakelite, the Material of a 1000 Uses. *Angewandte Chemie International Edition* **2008**, *47* (18), 3322–3328. <https://doi.org/10.1002/anie.200704281>.
- (6) Bakelite First Synthetic Plastic - National Historic Chemical Landmark <https://www.acs.org/content/acs/en/education/whatischemistry/landmarks/bakelite.html> (accessed 2021 -10 -19).
- (7) Braun, D. PVC — Origin, Growth, and Future. *Journal of Vinyl and Additive Technology* **2001**, *7* (4), 168–176. <https://doi.org/10.1002/vnl.10288>.
- (8) Meikle, J. L. *American Plastic: A Cultural History*; Rutgers University: New Brunswick [NJ], 1997.
- (9) Geyer, R. A Brief History of Plastics. In *Mare Plasticum - The Plastic Sea: Combatting Plastic Pollution Through Science and Art*; Streit-Bianchi, M., Cimadevila, M., Trettnak, W., Eds.; Springer International Publishing: Cham, 2020; pp 31–47. https://doi.org/10.1007/978-3-030-38945-1_2.
- (10) Plastics Europe. Global plastic production 1950-2020 <https://www.statista.com/statistics/282732/global-production-of-plastics-since-1950/> (accessed 2021 -10 -19).
- (11) Carpenter, E. J.; Smith, K. L. Plastics on the Sargasso Sea Surface. *Science* **1972**, *175* (4027), 1240–1241. <https://doi.org/10.1126/science.175.4027.1240>.
- (12) Geyer, R.; Jambeck, J. R.; Law, K. L. Production, Use, and Fate of All Plastics Ever Made. *Science Advances* **3** (7), e1700782. <https://doi.org/10.1126/sciadv.1700782>.
- (13) Thompson, R. C.; Olsen, Y.; Mitchell, R. P.; Davis, A.; Rowland, S. J.; John, A. W. G.; McGonigle, D.; Russell, A. E. Lost at Sea: Where Is All the Plastic? *Science* **2004**, *304* (5672), 838–838. <https://doi.org/10.1126/science.1094559>.
- (14) Li, P.; Wang, X.; Su, M.; Zou, X.; Duan, L.; Zhang, H. Characteristics of Plastic Pollution in the Environment: A Review. *Bull Environ Contam Toxicol* **2021**, *107* (4), 577–584. <https://doi.org/10.1007/s00128-020-02820-1>.
- (15) Plastics Europe. PlasticsEurope - the facts 2020 https://www.plasticseurope.org/download_file/force/4829/319 (accessed 2021 -10 -20).
- (16) Sharma, A.; Aloysius, V.; Visvanathan, C. Recovery of Plastics from Dumpsites and Landfills to Prevent Marine Plastic Pollution in Thailand. *Waste Dispos. Sustain. Energy* **2019**, *1* (4), 237–249. <https://doi.org/10.1007/s42768-019-00027-7>.

- (17) Bishop, G.; Styles, D.; Lens, P. N. L. Recycling of European Plastic Is a Pathway for Plastic Debris in the Ocean. *Environment International* **2020**, *142*, 105893. <https://doi.org/10.1016/j.envint.2020.105893>.
- (18) Lechthaler, S.; Waldschläger, K.; Stauch, G.; Schüttrumpf, H. The Way of Macroplastic through the Environment. *Environments* **2020**, *7* (10), 73. <https://doi.org/10.3390/environments7100073>.
- (19) Briassoulis, D.; Babou, E.; Hiskakis, M.; Scarascia, G.; Picuno, P.; Guarde, D.; Dejean, C. Review, Mapping and Analysis of the Agricultural Plastic Waste Generation and Consolidation in Europe. *Waste Manage. Res.* **2013**, *31* (12), 1262–1278. <https://doi.org/10.1177/0734242X13507968>.
- (20) Okoffo, E. D.; O'Brien, S.; O'Brien, J. W.; Tschärke, B. J.; Thomas, K. V. Wastewater Treatment Plants as a Source of Plastics in the Environment: A Review of Occurrence, Methods for Identification, Quantification and Fate. *Environ. Sci.: Water Res. Technol.* **2019**, *5* (11), 1908–1931. <https://doi.org/10.1039/C9EW00428A>.
- (21) Braun, M.; Mail, M.; Heyse, R.; Amelung, W. Plastic in Compost: Prevalence and Potential Input into Agricultural and Horticultural Soils. *Sci. Total Environ.* **2021**, *760*, 143335. <https://doi.org/10.1016/j.scitotenv.2020.143335>.
- (22) Macfadyen, G.; Huntington, T.; Cappell, R. *Abandoned, Lost or Otherwise Discarded Fishing Gear*; FAO fisheries and aquaculture technical paper; United Nations Environment Programme : Food and Agriculture Organization of the United Nations: Rome, 2009.
- (23) Turner, A.; Williams, T.; Pitchford, T. Transport, Weathering and Pollution of Plastic from Container Losses at Sea: Observations from a Spillage of Inkjet Cartridges in the North Atlantic Ocean. *Environ. Pollut.* **2021**, *284*, 117131. <https://doi.org/10.1016/j.envpol.2021.117131>.
- (24) Thiel, M.; Luna-Jorquera, G.; Álvarez-Varas, R.; Gallardo, C.; Hinojosa, I. A.; Luna, N.; Miranda-Urbina, D.; Morales, N.; Ory, N.; Pacheco, A. S.; Portflitt-Toro, M.; Zavalaga, C. Impacts of Marine Plastic Pollution From Continental Coasts to Subtropical Gyres—Fish, Seabirds, and Other Vertebrates in the SE Pacific. *Frontiers in Marine Science* **2018**, *5*, 238. <https://doi.org/10.3389/fmars.2018.00238>.
- (25) Gall, S. C.; Thompson, R. C. The Impact of Debris on Marine Life. *Marine Pollution Bulletin* **2015**, *92* (1), 170–179. <https://doi.org/10.1016/j.marpolbul.2014.12.041>.
- (26) Gregory, M. R. Environmental Implications of Plastic Debris in Marine Settings—Entanglement, Ingestion, Smothering, Hangers-on, Hitch-Hiking and Alien Invasions. *Philosophical Transactions of the Royal Society B: Biological Sciences* **2009**, *364* (1526), 2013–2025. <https://doi.org/10.1098/rstb.2008.0265>.
- (27) Chamas, A.; Moon, H.; Zheng, J.; Qiu, Y.; Tabassum, T.; Jang, J. H.; Abu-Omar, M.; Scott, S. L.; Suh, S. Degradation Rates of Plastics in the Environment. *ACS Sustainable Chemistry & Engineering* **2020**. <https://doi.org/10.1021/acssuschemeng.9b06635>.
- (28) Choy, C. A.; Robison, B. H.; Gagne, T. O.; Erwin, B.; Firl, E.; Halden, R. U.; Hamilton, J. A.; Katija, K.; Lisin, S. E.; Rolsky, C.; S. Van Houtan, K. The Vertical Distribution and Biological Transport of Marine Microplastics across the Epipelagic and Mesopelagic Water Column. *Sci Rep* **2019**, *9* (1), 7843. <https://doi.org/10.1038/s41598-019-44117-2>.
- (29) Meides, N.; Menzel, T.; Poetzschner, B.; Löder, M. G. J.; Mansfeld, U.; Strohriegl, P.; Altstaedt, V.; Senker, J. Reconstructing the Environmental Degradation of Polystyrene by Accelerated Weathering. *Environ. Sci. Technol.* **2021**, *55* (12), 7930–7938. <https://doi.org/10.1021/acs.est.0c07718>.

- (30) Zhang, K.; Hamidian, A. H.; Tubić, A.; Zhang, Y.; Fang, J. K. H.; Wu, C.; Lam, P. K. S. Understanding Plastic Degradation and Microplastic Formation in the Environment: A Review. *Environmental Pollution* **2021**, *274*, 116554. <https://doi.org/10.1016/j.envpol.2021.116554>.
- (31) Arhant, M.; Le Gall, M.; Le Gac, P.-Y.; Davies, P. Impact of Hydrolytic Degradation on Mechanical Properties of PET - Towards an Understanding of Microplastics Formation. *Polymer Degradation and Stability* **2019**, *161*, 175–182. <https://doi.org/10.1016/j.polymdegradstab.2019.01.021>.
- (32) Gewert, B.; M. Plassmann, M.; MacLeod, M. Pathways for Degradation of Plastic Polymers Floating in the Marine Environment. *Environmental Science: Processes & Impacts* **2015**, *17* (9), 1513–1521. <https://doi.org/10.1039/C5EM00207A>.
- (33) Sang, T.; Wallis, C. J.; Hill, G.; Britovsek, G. J. P. Polyethylene Terephthalate Degradation under Natural and Accelerated Weathering Conditions. *European Polymer Journal* **2020**, *136*, 109873. <https://doi.org/10.1016/j.eurpolymj.2020.109873>.
- (34) Hurley, C. R.; Leggett, G. J. Quantitative Investigation of the Photodegradation of Polyethylene Terephthalate Film by Friction Force Microscopy, Contact-Angle Goniometry, and X-Ray Photoelectron Spectroscopy. *ACS Appl. Mater. Interfaces* **2009**, *1* (8), 1688–1697. <https://doi.org/10.1021/am900250q>.
- (35) Day, M.; Wiles, D. M. Photochemical Degradation of Poly(Ethylene Terephthalate). III. Determination of Decomposition Products and Reaction Mechanism. *Journal of Applied Polymer Science* **1972**, *16* (1), 203–215. <https://doi.org/10.1002/app.1972.070160118>.
- (36) Falkenstein, P.; Gräsing, D.; Bielytskyi, P.; Zimmermann, W.; Matysik, J.; Wei, R.; Song, C. UV Pretreatment Impairs the Enzymatic Degradation of Polyethylene Terephthalate. *Frontiers in Microbiology* **2020**, *11*, 689. <https://doi.org/10.3389/fmicb.2020.00689>.
- (37) Ryan, P. G.; Moore, C. J.; van Franeker, J. A.; Moloney, C. L. Monitoring the Abundance of Plastic Debris in the Marine Environment. *Philosophical Transactions of the Royal Society B: Biological Sciences* **2009**, *364* (1526), 1999–2012. <https://doi.org/10.1098/rstb.2008.0207>.
- (38) Andrady, A. L. Persistence of Plastic Litter in the Oceans. In *Marine Anthropogenic Litter*; Bergmann, M., Gutow, L., Klages, M., Eds.; Springer International Publishing: Cham, 2015; pp 57–72. https://doi.org/10.1007/978-3-319-16510-3_3.
- (39) Akdogan, Z.; Guven, B. Microplastics in the Environment: A Critical Review of Current Understanding and Identification of Future Research Needs. *Environmental Pollution* **2019**, *254*, 113011. <https://doi.org/10.1016/j.envpol.2019.113011>.
- (40) Weinstein, J. E.; Crocker, B. K.; Gray, A. D. From Macroplastic to Microplastic: Degradation of High-Density Polyethylene, Polypropylene, and Polystyrene in a Salt Marsh Habitat. *Environmental Toxicology and Chemistry* **2016**, *35* (7), 1632–1640. <https://doi.org/10.1002/etc.3432>.
- (41) Syberg, K.; Khan, F. R.; Selck, H.; Palmqvist, A.; Banta, G. T.; Daley, J.; Sano, L.; Duhaime, M. B. Microplastics: Addressing Ecological Risk through Lessons Learned. *Environmental Toxicology and Chemistry* **2015**, *34* (5), 945–953. <https://doi.org/10.1002/etc.2914>.
- (42) Boucher, J.; Friot, D. *Primary Microplastics in the Oceans: A Global Evaluation of Sources*; IUCN International Union for Conservation of Nature, 2017. <https://doi.org/10.2305/IUCN.CH.2017.01.en>.
- (43) De Falco, F.; Di Pace, E.; Cocca, M.; Avella, M. The Contribution of Washing Processes of Synthetic Clothes to Microplastic Pollution. *Sci Rep* **2019**, *9* (1), 6633. <https://doi.org/10.1038/s41598-019-43023-x>.

- (44) European Parliament. Microplastics: sources, effects and solutions | Ref.: 20181116STO19217
https://www.europarl.europa.eu/pdfs/news/expert/2018/11/story/20181116STO19217/20181116STO19217_en.pdf (accessed 2021 -10 -27).
- (45) Lebreton, L.; Slat, B.; Ferrari, F.; Sainte-Rose, B.; Aitken, J.; Marthouse, R.; Hajbane, S.; Cunsolo, S.; Schwarz, A.; Levivier, A.; Noble, K.; Debeljak, P.; Maral, H.; Schoeneich-Argent, R.; Brambini, R.; Reisser, J. Evidence That the Great Pacific Garbage Patch Is Rapidly Accumulating Plastic. *Sci Rep* **2018**, *8* (1), 4666. <https://doi.org/10.1038/s41598-018-22939-w>.
- (46) Bläsing, M.; Amelung, W. Plastics in Soil: Analytical Methods and Possible Sources. *Science of The Total Environment* **2018**, *612*, 422–435. <https://doi.org/10.1016/j.scitotenv.2017.08.086>.
- (47) van Emmerik, T.; Schwarz, A. Plastic Debris in Rivers. *WIREs Water* **2020**, *7* (1), e1398. <https://doi.org/10.1002/wat2.1398>.
- (48) Vermeiren, P.; Muñoz, C. C.; Ikejima, K. Sources and Sinks of Plastic Debris in Estuaries: A Conceptual Model Integrating Biological, Physical and Chemical Distribution Mechanisms. *Marine Pollution Bulletin* **2016**, *113* (1), 7–16. <https://doi.org/10.1016/j.marpolbul.2016.10.002>.
- (49) Näkki, P.; Setälä, O.; Lehtiniemi, M. Seafloor Sediments as Microplastic Sinks in the Northern Baltic Sea – Negligible Upward Transport of Buried Microplastics by Bioturbation. *Environmental Pollution* **2019**, *249*, 74–81. <https://doi.org/10.1016/j.envpol.2019.02.099>.
- (50) Lloret, J.; Pedrosa-Pamies, R.; Vandal, N.; Rorty, R.; Ritchie, M.; McGuire, C.; Chenoweth, K.; Valiela, I. Salt Marsh Sediments Act as Sinks for Microplastics and Reveal Effects of Current and Historical Land Use Changes. *Environmental Advances* **2021**, *4*, 100060. <https://doi.org/10.1016/j.envadv.2021.100060>.
- (51) Lambert, S.; Wagner, M. Microplastics Are Contaminants of Emerging Concern in Freshwater Environments: An Overview. In *Freshwater Microplastics*; Wagner, M., Lambert, S., Eds.; The Handbook of Environmental Chemistry; Springer International Publishing: Cham, 2018; Vol. 58, pp 1–23. https://doi.org/10.1007/978-3-319-61615-5_1.
- (52) Horton, A. A.; Walton, A.; Spurgeon, D. J.; Lahive, E.; Svendsen, C. Microplastics in Freshwater and Terrestrial Environments: Evaluating the Current Understanding to Identify the Knowledge Gaps and Future Research Priorities. *Science of The Total Environment* **2017**, *586*, 127–141. <https://doi.org/10.1016/j.scitotenv.2017.01.190>.
- (53) González-Pleiter, M.; Edo, C.; Aguilera, Á.; Viúdez-Moreiras, D.; Pulido-Reyes, G.; González-Toril, E.; Osuna, S.; de Diego-Castilla, G.; Leganés, F.; Fernández-Piñas, F.; Rosal, R. Occurrence and Transport of Microplastics Sampled within and above the Planetary Boundary Layer. *Science of The Total Environment* **2021**, *761*, 143213. <https://doi.org/10.1016/j.scitotenv.2020.143213>.
- (54) Zhang, H. Transport of Microplastics in Coastal Seas. *Estuarine, Coastal and Shelf Science* **2017**, *199*, 74–86. <https://doi.org/10.1016/j.ecss.2017.09.032>.
- (55) Petersen, F.; Hubbart, J. A. The Occurrence and Transport of Microplastics: The State of the Science. *Science of The Total Environment* **2021**, *758*, 143936. <https://doi.org/10.1016/j.scitotenv.2020.143936>.
- (56) Munari, C.; Infantini, V.; Scoponi, M.; Rastelli, E.; Corinaldesi, C.; Mistri, M. Microplastics in the Sediments of Terra Nova Bay (Ross Sea, Antarctica). *Marine Pollution Bulletin* **2017**, *122* (1), 161–165. <https://doi.org/10.1016/j.marpolbul.2017.06.039>.

- (57) Allen, S.; Allen, D.; Phoenix, V. R.; Le Roux, G.; Durántez Jiménez, P.; Simonneau, A.; Binet, S.; Galop, D. Atmospheric Transport and Deposition of Microplastics in a Remote Mountain Catchment. *Nat. Geosci.* **2019**, *12* (5), 339–344. <https://doi.org/10.1038/s41561-019-0335-5>.
- (58) Galloway, T. S.; Cole, M.; Lewis, C. Interactions of Microplastic Debris throughout the Marine Ecosystem. *Nat Ecol Evol* **2017**, *1* (5), 1–8. <https://doi.org/10.1038/s41559-017-0116>.
- (59) Prokić, M. D.; Radovanović, T. B.; Gavrić, J. P.; Faggio, C. Ecotoxicological Effects of Microplastics: Examination of Biomarkers, Current State and Future Perspectives. *TrAC Trends in Analytical Chemistry* **2019**, *111*, 37–46. <https://doi.org/10.1016/j.trac.2018.12.001>.
- (60) Wright, S. L.; Thompson, R. C.; Galloway, T. S. The Physical Impacts of Microplastics on Marine Organisms: A Review. *Environ Pollut* **2013**, *178*, 483–492. <https://doi.org/10.1016/j.envpol.2013.02.031>.
- (61) Campanale, C.; Massarelli, C.; Savino, I.; Locaputo, V.; Uricchio, V. F. A Detailed Review Study on Potential Effects of Microplastics and Additives of Concern on Human Health. *International Journal of Environmental Research and Public Health* **2020**, *17* (4), 1212. <https://doi.org/10.3390/ijerph17041212>.
- (62) Marn, N.; Jusup, M.; Kooijman, S. A. L. M.; Klanjscek, T. Quantifying Impacts of Plastic Debris on Marine Wildlife Identifies Ecological Breakpoints. *Ecology Letters* **2020**, *23* (10), 1479–1487. <https://doi.org/10.1111/ele.13574>.
- (63) Cox, K. D.; Covernton, G. A.; Davies, H. L.; Dower, J. F.; Juanes, F.; Dudas, S. E. Human Consumption of Microplastics. *Environ. Sci. Technol.* **2019**, *53* (12), 7068–7074. <https://doi.org/10.1021/acs.est.9b01517>.
- (64) Xu, M.; Halimu, G.; Zhang, Q.; Song, Y.; Fu, X.; Li, Y.; Li, Y.; Zhang, H. Internalization and Toxicity: A Preliminary Study of Effects of Nanoplastic Particles on Human Lung Epithelial Cell. *Science of The Total Environment* **2019**, *694*, 133794. <https://doi.org/10.1016/j.scitotenv.2019.133794>.
- (65) Brennecke, D.; Duarte, B.; Paiva, F.; Caçador, I.; Canning-Clode, J. Microplastics as Vector for Heavy Metal Contamination from the Marine Environment. *Estuarine, Coastal and Shelf Science* **2016**, *178*, 189–195. <https://doi.org/10.1016/j.ecss.2015.12.003>.
- (66) Liu, S.; Shi, J.; Wang, J.; Dai, Y.; Li, H.; Li, J.; Liu, X.; Chen, X.; Wang, Z.; Zhang, P. Interactions Between Microplastics and Heavy Metals in Aquatic Environments: A Review. *Frontiers in Microbiology* **2021**, *12*, 730. <https://doi.org/10.3389/fmicb.2021.652520>.
- (67) Rodrigues, J. P.; Duarte, A. C.; Santos-Echeandía, J.; Rocha-Santos, T. Significance of Interactions between Microplastics and POPs in the Marine Environment: A Critical Overview. *TrAC Trends in Analytical Chemistry* **2019**, *111*, 252–260. <https://doi.org/10.1016/j.trac.2018.11.038>.
- (68) Gkoutselis, G.; Rohrbach, S.; Harjes, J.; Obst, M.; Brachmann, A.; Horn, M. A.; Rambold, G. Microplastics Accumulate Fungal Pathogens in Terrestrial Ecosystems. *Sci Rep* **2021**, *11* (1), 13214. <https://doi.org/10.1038/s41598-021-92405-7>.
- (69) Kirstein, I. V.; Kirmizi, S.; Wichels, A.; Garin-Fernandez, A.; Eler, R.; Löder, M.; Gerds, G. Dangerous Hitchhikers? Evidence for Potentially Pathogenic *Vibrio* Spp. on Microplastic Particles. *Marine Environmental Research* **2016**, *120*, 1–8. <https://doi.org/10.1016/j.marenvres.2016.07.004>.
- (70) Xu, J.; Cui, Z.; Nie, K.; Cao, H.; Jiang, M.; Xu, H.; Tan, T.; Liu, L. A Quantum Mechanism Study of the C-C Bond Cleavage to Predict the Bio-Catalytic Polyethylene Degradation. *Frontiers in Microbiology* **2019**, *10*, 489. <https://doi.org/10.3389/fmicb.2019.00489>.

- (71) Guengerich, F. P.; Yoshimoto, F. K. Formation and Cleavage of C–C Bonds by Enzymatic Oxidation–Reduction Reactions. *Chem. Rev.* **2018**, *118* (14), 6573–6655. <https://doi.org/10.1021/acs.chemrev.8b00031>.
- (72) Zoghiami, A.; Paës, G. Lignocellulosic Biomass: Understanding Recalcitrance and Predicting Hydrolysis. *Front Chem* **2019**, *7*, 874. <https://doi.org/10.3389/fchem.2019.00874>.
- (73) Hall, M.; Bansal, P.; Lee, J. H.; Realff, M. J.; Bommarius, A. S. Cellulose Crystallinity – a Key Predictor of the Enzymatic Hydrolysis Rate. *The FEBS Journal* **2010**, *277* (6), 1571–1582. <https://doi.org/10.1111/j.1742-4658.2010.07585.x>.
- (74) Sidar, A.; Albuquerque, E. D.; Voshol, G. P.; Ram, A. F. J.; Vijgenboom, E.; Punt, P. J. Carbohydrate Binding Modules: Diversity of Domain Architecture in Amylases and Cellulases From Filamentous Microorganisms. *Frontiers in Bioengineering and Biotechnology* **2020**, *8*, 871. <https://doi.org/10.3389/fbioe.2020.00871>.
- (75) Bakan, B.; Marion, D. Assembly of the Cutin Polyester: From Cells to Extracellular Cell Walls. *Plants (Basel)* **2017**, *6* (4), 57. <https://doi.org/10.3390/plants6040057>.
- (76) Physical, Thermal, and Mechanical Properties of Polymers. In *Biosurfaces*; John Wiley & Sons, Ltd, 2014; pp 329–344. <https://doi.org/10.1002/9781118950623.app1>.
- (77) Mohanan, N.; Montazer, Z.; Sharma, P. K.; Levin, D. B. Microbial and Enzymatic Degradation of Synthetic Plastics. *Frontiers in Microbiology* **2020**, *11*, 2837. <https://doi.org/10.3389/fmicb.2020.580709>.
- (78) Jiang, S.; Su, T.; Zhao, J.; Wang, Z. Isolation, Identification, and Characterization of Polystyrene-Degrading Bacteria From the Gut of *Galleria Mellonella* (Lepidoptera: Pyralidae) Larvae. *Frontiers in Bioengineering and Biotechnology* **2021**, *9*, 746. <https://doi.org/10.3389/fbioe.2021.736062>.
- (79) Cassone, B. J.; Grove, H. C.; Elebute, O.; Villanueva, S. M. P.; LeMoine, C. M. R. Role of the Intestinal Microbiome in Low-Density Polyethylene Degradation by Caterpillar Larvae of the Greater Wax Moth, *Galleria Mellonella*. *Proceedings of the Royal Society B: Biological Sciences* **2020**, *287* (1922), 20200112. <https://doi.org/10.1098/rspb.2020.0112>.
- (80) Magnin, A.; Pollet, E.; Avérous, L. Chapter Fifteen - Characterization of the Enzymatic Degradation of Polyurethanes. In *Methods in Enzymology*; Weber, G., Bornscheuer, U. T., Wei, R., Eds.; Enzymatic Plastic Degradation; Academic Press, 2021; Vol. 648, pp 317–336. <https://doi.org/10.1016/bs.mie.2020.12.011>.
- (81) Ignat, L.; Ignat, M.; Ciobanu, C.; Doroftei, F.; Popa, V. I. Effects of Flax Lignin Addition on Enzymatic Oxidation of Poly(Ethylene Adipate) Urethanes. *Industrial Crops and Products* **2011**, *34* (1), 1017–1028. <https://doi.org/10.1016/j.indcrop.2011.03.010>.
- (82) Hauff, S.; Chefetz, B.; Shechter, M.; Vetter, W. Determination of Hydroxylated Fatty Acids from the Biopolymer of Tomato Cutin and Their Fate during Incubation in Soil. *Phytochemical Analysis* **2010**, *21* (6), 582–589. <https://doi.org/10.1002/pca.1238>.
- (83) SHISHIYAMA, J.; ARAKI, F.; AKAI, S. Studies on Cutin-Esterase II. Characteristics of Cutin-Esterase from *Botrytis Cinerea* and Its Activity on Tomato-Cutin. *Plant and Cell Physiology* **1970**, *11* (6), 937–945. <https://doi.org/10.1093/oxfordjournals.pcp.a074585>.
- (84) Kolattukudy, P. E.; Podila, G. K.; Mohan, R. Molecular Basis of the Early Events in Plant–Fungus Interaction. *Genome* **1989**, *31* (1), 342–349. <https://doi.org/10.1139/g89-052>.
- (85) Chen, S.; Su, L.; Chen, J.; Wu, J. Cutinase: Characteristics, Preparation, and Application. *Biotechnology Advances* **2013**, *31* (8), 1754–1767. <https://doi.org/10.1016/j.biotechadv.2013.09.005>.

- (86) Martinez, C.; De Geus, P.; Lauwereys, M.; Matthyssens, G.; Cambillau, C. Fusarium Solani Cutinase Is a Lipolytic Enzyme with a Catalytic Serine Accessible to Solvent. *Nature* **1992**, *356* (6370), 615–618. <https://doi.org/10.1038/356615a0>.
- (87) Ollis, D. L.; Cheah, E.; Cygler, M.; Dijkstra, B.; Frolow, F.; Franken, S. M.; Harel, M.; Remington, S. J.; Silman, I.; Schrag, J. The Alpha/Beta Hydrolase Fold. *Protein Eng* **1992**, *5* (3), 197–211. <https://doi.org/10.1093/protein/5.3.197>.
- (88) Khan, F. I.; Lan, D.; Durrani, R.; Huan, W.; Zhao, Z.; Wang, Y. The Lid Domain in Lipases: Structural and Functional Determinant of Enzymatic Properties. *Frontiers in Bioengineering and Biotechnology* **2017**, *5*, 16. <https://doi.org/10.3389/fbioe.2017.00016>.
- (89) Nikolaivits, E.; Kanelli, M.; Dimarogona, M.; Topakas, E. A Middle-Aged Enzyme Still in Its Prime: Recent Advances in the Field of Cutinases. *Catalysts* **2018**, *8* (12), 612. <https://doi.org/10.3390/catal8120612>.
- (90) Kawai, F.; Kawabata, T.; Oda, M. Current State and Perspectives Related to the Polyethylene Terephthalate Hydrolases Available for Biorecycling. *ACS Sustainable Chem. Eng.* **2020**, *8* (24), 8894–8908. <https://doi.org/10.1021/acssuschemeng.0c01638>.
- (91) Kawai, F.; Kawabata, T.; Oda, M. Current Knowledge on Enzymatic PET Degradation and Its Possible Application to Waste Stream Management and Other Fields. *Appl Microbiol Biotechnol* **2019**, *103* (11), 4253–4268. <https://doi.org/10.1007/s00253-019-09717-y>.
- (92) Kim, H. R.; Song, W. S. Optimization of Papain Treatment for Improving the Hydrophilicity of Polyester Fabrics. *Fibers Polym* **2010**, *11* (1), 67–71. <https://doi.org/10.1007/s12221-010-0067-z>.
- (93) Zimmermann, W.; Billig, S. Enzymes for the Biofunctionalization of Poly(Ethylene Terephthalate). In *Biofunctionalization of Polymers and their Applications*; Nyanhongo, G. S., Steiner, W., Gübitz, G., Eds.; Advances in Biochemical Engineering / Biotechnology; Springer: Berlin, Heidelberg, 2011; pp 97–120. https://doi.org/10.1007/10_2010_87.
- (94) Demirel, B.; Yaraş, A.; Elçiçek, H. Crystallization Behavior of PET Materials. *BAUN J Inst Sci* **2016**, *13* (1), 26–35.
- (95) Jabarin, S. A.; Lofgren, E. A. Effects of Water Absorption on Physical Properties and Degree of Molecular Orientation of Poly (Ethylene Terephthalate). *Polymer Engineering & Science* **1986**, *26* (9), 620–625. <https://doi.org/10.1002/pen.760260907>.
- (96) Kawai, F.; Oda, M.; Tamashiro, T.; Waku, T.; Tanaka, N.; Yamamoto, M.; Mizushima, H.; Miyakawa, T.; Tanokura, M. A Novel Ca²⁺-Activated, Thermostabilized Polyesterase Capable of Hydrolyzing Polyethylene Terephthalate from *Saccharomonospora Viridis* AHK190. *Appl Microbiol Biotechnol* **2014**, *98* (24), 10053–10064. <https://doi.org/10.1007/s00253-014-5860-y>.
- (97) Tournier, V.; Topham, C. M.; Gilles, A.; David, B.; Folgoas, C.; Moya-Leclair, E.; Kamionka, E.; Desrousseaux, M.-L.; Texier, H.; Gavalda, S.; Cot, M.; Guémard, E.; Dalibey, M.; Nomme, J.; Cioci, G.; Barbe, S.; Chateau, M.; André, I.; Duquesne, S.; Marty, A. An Engineered PET Depolymerase to Break down and Recycle Plastic Bottles. *Nature* **2020**, *580* (7802), 216–219. <https://doi.org/10.1038/s41586-020-2149-4>.
- (98) Maurya, A.; Bhattacharya, A.; Khare, S. K. Enzymatic Remediation of Polyethylene Terephthalate (PET)–Based Polymers for Effective Management of Plastic Wastes: An Overview. *Frontiers in Bioengineering and Biotechnology* **2020**, *8*, 1332. <https://doi.org/10.3389/fbioe.2020.602325>.

- (99) Müller, R.-J.; Schrader, H.; Profe, J.; Dresler, K.; Deckwer, W.-D. Enzymatic Degradation of Poly(Ethylene Terephthalate): Rapid Hydrolyse Using a Hydrolase from *T. Fusca*. *Macromolecular Rapid Communications* **2005**, *26* (17), 1400–1405. <https://doi.org/10.1002/marc.200500410>.
- (100) Bhatti, A. A.; Haq, S.; Bhat, R. A. Actinomycetes Benefaction Role in Soil and Plant Health. *Microb Pathog* **2017**, *111*, 458–467. <https://doi.org/10.1016/j.micpath.2017.09.036>.
- (101) Herrero Acero, E.; Ribitsch, D.; Steinkellner, G.; Gruber, K.; Greimel, K.; Eiteljoerg, I.; Trotscha, E.; Wei, R.; Zimmermann, W.; Zinn, M.; Cavaco-Paulo, A.; Freddi, G.; Schwab, H.; Guebitz, G. Enzymatic Surface Hydrolysis of PET: Effect of Structural Diversity on Kinetic Properties of Cutinases from *Thermobifida*. *Macromolecules* **2011**, *44* (12), 4632–4640. <https://doi.org/10.1021/ma200949p>.
- (102) Then, J.; Wei, R.; Oeser, T.; Barth, M.; Belisário-Ferrari, M. R.; Schmidt, J.; Zimmermann, W. Ca²⁺ and Mg²⁺ Binding Site Engineering Increases the Degradation of Polyethylene Terephthalate Films by Polyester Hydrolases from *Thermobifida Fusca*. *Biotechnology Journal* **2015**, *10* (4), 592–598. <https://doi.org/10.1002/biot.201400620>.
- (103) Wei, R.; Oeser, T.; Schmidt, J.; Meier, R.; Barth, M.; Then, J.; Zimmermann, W. Engineered Bacterial Polyester Hydrolases Efficiently Degrade Polyethylene Terephthalate Due to Relieved Product Inhibition. *Biotechnology and Bioengineering* **2016**, *113* (8), 1658–1665. <https://doi.org/10.1002/bit.25941>.
- (104) Sulaiman, S.; Yamato, S.; Kanaya, E.; Kim, J.-J.; Koga, Y.; Takano, K.; Kanaya, S. Isolation of a Novel Cutinase Homolog with Polyethylene Terephthalate-Degrading Activity from Leaf-Branch Compost by Using a Metagenomic Approach. *Appl Environ Microbiol* **2012**, *78* (5), 1556–1562. <https://doi.org/10.1128/AEM.06725-11>.
- (105) Sulaiman, S.; You, D.-J.; Kanaya, E.; Koga, Y.; Kanaya, S. Crystal Structure and Thermodynamic and Kinetic Stability of Metagenome-Derived LC-Cutinase. *Biochemistry* **2014**, *53* (11), 1858–1869. <https://doi.org/10.1021/bi401561p>.
- (106) Shirke, A. N.; White, C.; Englaender, J. A.; Zwarycz, A.; Butterfoss, G. L.; Linhardt, R. J.; Gross, R. A. Stabilizing Leaf and Branch Compost Cutinase (LCC) with Glycosylation: Mechanism and Effect on PET Hydrolysis. *Biochemistry* **2018**, *57* (7), 1190–1200. <https://doi.org/10.1021/acs.biochem.7b01189>.
- (107) Yoshida, S.; Hiraga, K.; Takehana, T.; Taniguchi, I.; Yamaji, H.; Maeda, Y.; Toyohara, K.; Miyamoto, K.; Kimura, Y.; Oda, K. A Bacterium That Degrades and Assimilates Poly(Ethylene Terephthalate). *Science* **2016**, *351* (6278), 1196–1199. <https://doi.org/10.1126/science.aad6359>.
- (108) Austin, H. P.; Allen, M. D.; Donohoe, B. S.; Rorrer, N. A.; Kearns, F. L.; Silveira, R. L.; Pollard, B. C.; Dominick, G.; Duman, R.; Omari, K. E.; Mykhaylyk, V.; Wagner, A.; Michener, W. E.; Amore, A.; Skaf, M. S.; Crowley, M. F.; Thorne, A. W.; Johnson, C. W.; Woodcock, H. L.; McGeehan, J. E.; Beckham, G. T. Characterization and Engineering of a Plastic-Degrading Aromatic Polyesterase. *PNAS* **2018**, *115* (19), E4350–E4357. <https://doi.org/10.1073/pnas.1718804115>.
- (109) Liu, B.; He, L.; Wang, L.; Li, T.; Li, C.; Liu, H.; Luo, Y.; Bao, R. Protein Crystallography and Site-Direct Mutagenesis Analysis of the Poly(Ethylene Terephthalate) Hydrolase PETase from *Ideonella Sakaiensis*. *ChemBioChem* **2018**, *19* (14), 1471–1475. <https://doi.org/10.1002/cbic.201800097>.
- (110) Joo, S.; Cho, I. J.; Seo, H.; Son, H. F.; Sagong, H.-Y.; Shin, T. J.; Choi, S. Y.; Lee, S. Y.; Kim, K.-J. Structural Insight into Molecular Mechanism of Poly(Ethylene Terephthalate) Degradation. *Nat Commun* **2018**, *9* (1), 382. <https://doi.org/10.1038/s41467-018-02881-1>.

- (111) Chen, C.-C.; Han, X.; Ko, T.-P.; Liu, W.; Guo, R.-T. Structural Studies Reveal the Molecular Mechanism of PETase. *The FEBS Journal* **2018**, *285* (20), 3717–3723. <https://doi.org/10.1111/febs.14612>.
- (112) Fecker, T.; Galaz-Davison, P.; Engelberger, F.; Narui, Y.; Sotomayor, M.; Parra, L. P.; Ramírez-Sarmiento, C. A. Active Site Flexibility as a Hallmark for Efficient PET Degradation by *I. Sakaiensis* PETase. *Biophysical Journal* **2018**, *114* (6), 1302–1312. <https://doi.org/10.1016/j.bpj.2018.02.005>.
- (113) Han, X.; Liu, W.; Huang, J.-W.; Ma, J.; Zheng, Y.; Ko, T.-P.; Xu, L.; Cheng, Y.-S.; Chen, C.-C.; Guo, R.-T. Structural Insight into Catalytic Mechanism of PET Hydrolase. *Nat Commun* **2017**, *8* (1), 2106. <https://doi.org/10.1038/s41467-017-02255-z>.
- (114) Madeira, F.; Park, Y. M.; Lee, J.; Buso, N.; Gur, T.; Madhusoodanan, N.; Basutkar, P.; Tivey, A. R. N.; Potter, S. C.; Finn, R. D.; Lopez, R. The EMBL-EBI Search and Sequence Analysis Tools APIs in 2019. *Nucleic Acids Res* **2019**, *47* (W1), W636–W641. <https://doi.org/10.1093/nar/gkz268>.
- (115) Letunic, I.; Bork, P. Interactive Tree Of Life (ITOL) v5: An Online Tool for Phylogenetic Tree Display and Annotation. *Nucleic Acids Research* **2021**, *49* (W1), W293–W296. <https://doi.org/10.1093/nar/gkab301>.
- (116) Magalhães, R. P.; Cunha, J. M.; Sousa, S. F. Perspectives on the Role of Enzymatic Biocatalysis for the Degradation of Plastic PET. *International Journal of Molecular Sciences* **2021**, *22* (20), 11257. <https://doi.org/10.3390/ijms222011257>.
- (117) Wei, R.; Song, C.; Gräsing, D.; Schneider, T.; Bielytskyi, P.; Böttcher, D.; Matysik, J.; Bornscheuer, U. T.; Zimmermann, W. Conformational Fitting of a Flexible Oligomeric Substrate Does Not Explain the Enzymatic PET Degradation. *Nat Commun* **2019**, *10* (1), 5581. <https://doi.org/10.1038/s41467-019-13492-9>.
- (118) Jerves, C.; Neves, R. P. P.; Ramos, M. J.; da Silva, S.; Fernandes, P. A. Reaction Mechanism of the PET Degrading Enzyme PETase Studied with DFT/MM Molecular Dynamics Simulations. *ACS Catal.* **2021**, *11* (18), 11626–11638. <https://doi.org/10.1021/acscatal.1c03700>.
- (119) Son, H. F.; Cho, I. J.; Joo, S.; Seo, H.; Sagong, H.-Y.; Choi, S. Y.; Lee, S. Y.; Kim, K.-J. Rational Protein Engineering of Thermo-Stable PETase from *Ideonella Sakaiensis* for Highly Efficient PET Degradation. *ACS Catal.* **2019**, *9* (4), 3519–3526. <https://doi.org/10.1021/acscatal.9b00568>.
- (120) Son, H. F.; Joo, S.; Seo, H.; Sagong, H.-Y.; Lee, S. H.; Hong, H.; Kim, K.-J. Structural Bioinformatics-Based Protein Engineering of Thermo-Stable PETase from *Ideonella Sakaiensis*. *Enzyme Microb Technol* **2020**, *141*, 109656. <https://doi.org/10.1016/j.enzmictec.2020.109656>.
- (121) Cui, Y.; Chen, Y.; Liu, X.; Dong, S.; Tian, Y.; Qiao, Y.; Mitra, R.; Han, J.; Li, C.; Han, X.; Liu, W.; Chen, Q.; Wei, W.; Wang, X.; Du, W.; Tang, S.; Xiang, H.; Liu, H.; Liang, Y.; Houk, K. N.; Wu, B. Computational Redesign of a PETase for Plastic Biodegradation under Ambient Condition by the GRAPE Strategy. *ACS Catal.* **2021**, *11* (3), 1340–1350. <https://doi.org/10.1021/acscatal.0c05126>.
- (122) Knott, B. C.; Erickson, E.; Allen, M. D.; Gado, J. E.; Graham, R.; Kearns, F. L.; Pardo, I.; Topuzlu, E.; Anderson, J. J.; Austin, H. P.; Dominick, G.; Johnson, C. W.; Rorrer, N. A.; Szostkiewicz, C. J.; Copié, V.; Payne, C. M.; Woodcock, H. L.; Donohoe, B. S.; Beckham, G. T.; McGeehan, J. E. Characterization and Engineering of a Two-Enzyme System for Plastics Depolymerization. *PNAS* **2020**, *117* (41), 25476–25485. <https://doi.org/10.1073/pnas.2006753117>.
- (123) Moog, D.; Schmitt, J.; Senger, J.; Zarzycki, J.; Rexer, K.-H.; Linne, U.; Erb, T.; Maier, U. G. Using a Marine Microalga as a Chassis for Polyethylene Terephthalate (PET) Degradation. *Microbial Cell Factories* **2019**, *18* (1), 171. <https://doi.org/10.1186/s12934-019-1220-z>.

- (124) Siracusa, V.; Blanco, I. Bio-Polyethylene (Bio-PE), Bio-Polypropylene (Bio-PP) and Bio-Poly(Ethylene Terephthalate) (Bio-PET): Recent Developments in Bio-Based Polymers Analogous to Petroleum-Derived Ones for Packaging and Engineering Applications. *Polymers* **2020**, *12* (8), 1641. <https://doi.org/10.3390/polym12081641>.
- (125) He, H.; Liu, B.; Xue, B.; Zhang, H. Study on Structure and Properties of Biodegradable PLA/PBAT/Organic-Modified MMT Nanocomposites. *Journal of Thermoplastic Composite Materials* **2019**, 0892705719890907. <https://doi.org/10.1177/0892705719890907>.
- (126) Nakajima, H.; Dijkstra, P.; Loos, K. The Recent Developments in Biobased Polymers toward General and Engineering Applications: Polymers That Are Upgraded from Biodegradable Polymers, Analogous to Petroleum-Derived Polymers, and Newly Developed. *Polymers* **2017**, *9* (10), 523. <https://doi.org/10.3390/polym9100523>.
- (127) Danso, D.; Schmeisser, C.; Chow, J.; Zimmermann, W.; Wei, R.; Leggewie, C.; Li, X.; Hazen, T.; Streit, W. R. New Insights into the Function and Global Distribution of Polyethylene Terephthalate (PET)-Degrading Bacteria and Enzymes in Marine and Terrestrial Metagenomes. *Appl Environ Microbiol* **2018**, *84* (8), e02773-17. <https://doi.org/10.1128/AEM.02773-17>.
- (128) Weigert, S.; Gagsteiger, A.; Menzel, T.; Höcker, B. A Versatile Assay Platform for Enzymatic Poly(Ethylene-Terephthalate) Degradation. *Protein Engineering, Design and Selection* **2021**, *34*, gzab022. <https://doi.org/10.1093/protein/gzab022>.
- (129) Wei, R.; Oeser, T.; Billig, S.; Zimmermann, W. A High-Throughput Assay for Enzymatic Polyester Hydrolysis Activity by Fluorimetric Detection. *Biotechnol J* **2012**, *7* (12), 1517–1521. <https://doi.org/10.1002/biot.201200119>.
- (130) Wang, S.; Zhang, Y.; He, J.; Jia, X.; Lin, J.; Li, M.; Wang, Q. Molecular Analyses of Bacterioplankton Communities with Highly Abundant *Vibrio* Clades: A Case Study in Bohai Sea Coastal Waters. *J. Ocean. Limnol.* **2019**, *37* (5), 1638–1648. <https://doi.org/10.1007/s00343-019-8210-1>.
- (131) Lovell, C. R. Ecological Fitness and Virulence Features of *Vibrio Parahaemolyticus* in Estuarine Environments. *Appl Microbiol Biotechnol* **2017**, *101* (5), 1781–1794. <https://doi.org/10.1007/s00253-017-8096-9>.
- (132) Keszy, K.; Labrenz, M.; Scales, B. S.; Kreikemeyer, B.; Oberbeckmann, S. *Vibrio* Colonization Is Highly Dynamic in Early Microplastic-Associated Biofilms as Well as on Field-Collected Microplastics. *Microorganisms* **2021**, *9* (1), 76. <https://doi.org/10.3390/microorganisms9010076>.
- (133) Menzel, T.; Weigert, S.; Gagsteiger, A.; Eich, Y.; Sittl, S.; Papastavrou, G.; Ruckdäschel, H.; Altstädt, V.; Höcker, B. Impact of Enzymatic Degradation on the Material Properties of Poly(Ethylene Terephthalate). *Polymers* **2021**, *13* (22), 3885. <https://doi.org/10.3390/polym13223885>.

Eidesstattliche Versicherung

(§ 8 Satz 2 Nr. 3 PromO Fakultät)

Hiermit versichere ich eidesstattlich, dass ich die Arbeit selbstständig verfasst und keine anderen als die von mir angegebenen Quellen und Hilfsmittel benutzt habe (vgl. Art. 64 Abs. 1 Satz 6 BayHSchG).

(§ 8 Satz 2 Nr. 3 PromO Fakultät)

Hiermit erkläre ich, dass ich die Dissertation nicht bereits zur Erlangung eines akademischen Grades eingereicht habe und dass ich nicht bereits diese oder eine gleichartige Doktorprüfung endgültig nicht bestanden habe.

(§ 8 Satz 2 Nr. 4 PromO Fakultät)

Hiermit erkläre ich, dass ich Hilfe von gewerblichen Promotionsberatern bzw. –vermittlern oder ähnlichen Dienstleistern weder bisher in Anspruch genommen habe noch künftig in Anspruch nehmen werde.

(§ 8 Satz 2 Nr. 7 PromO Fakultät)

Hiermit erkläre ich mein Einverständnis, dass die elektronische Fassung der Dissertation unter Wahrung meiner Urheberrechte und des Datenschutzes einer gesonderten Überprüfung unterzogen werden kann.

(§ 8 Satz 2 Nr. 8 PromO Fakultät)

Hiermit erkläre ich mein Einverständnis, dass bei Verdacht wissenschaftlichen Fehlverhaltens Ermittlungen durch universitätsinterne Organe der wissenschaftlichen Selbstkontrolle stattfinden können.

Bayreuth, 19.01.2022

Ort, Datum,

Unterschrift